NTNU

Norwegian University of
Science and Technology

Finite Element Analysis of Coupled Thermo-Hydro-Mechanical Processes in Fully Saturated, Partially Frozen Soils

Hooman Rostami

Geotechnics and Geohazards
Submission date: June 2017
Supervisor: Gustav Grimstad, IBM
Co-supervisor: Seyed Ali Ghoreishian Amiri, IBM
Steinar Nordal, IBM

Norwegian University of Science and Technology
Department of Civil and Environmental Engineering

NORGES TEKNISK-
NATURVITENSKAPELIGE UNIVERSITET
INSTITUTT FOR BYGG OG MILJØTEKNIKK

Thesis Title: Finite Element Analysis of Coupled Thermo-Hydro-Mechanical Processes in Fully Saturated, Partially Frozen Soils	**Date:** 11.06.2017 **Number of pages:** 101
	Master Thesis x

Name: Hooman Rostami

Professor in charge/supervisor: Gustav Grimstad (NTNU); and Laura Tonni (UniBo)

Other external professional contacts/supervisors: Seyed Ali Ghoreishian Amiri (NTNU) and Steinar Nordal (NTNU)

Abstract:

Interest in permafrost, or seasonally frozen ground, has been increasing over the last decades. Nearly 24% of the northern hemisphere, is covered with permafrost. Humankind's need for energy and raw materials has pushed technology to operate on these frozen grounds. Construction and operation of infrastructures, such as roads, pipelines, and tunnels on these areas mean engineers have to deal with frozen soil. In addition, with climate change, permafrost warming and subsequent thawing can trigger or accelerate natural hazards, like rockfalls and debris flows. Furthermore, there is a growing interest in artificial ground freezing for stopping groundwater flow into the construction sites, for example in tunnels, and also for strengthening soil mass to improve stability.

There are fundamental differences between frozen soil and unfrozen soil, such as frost heave, thaw settlement, cryogenic suction which yearn for a new body of knowledge in this area. Saturated frozen soil is a mixture of soil grain, ice and unfrozen water. Thermo-hydro-mechanical interaction between different phases of such a mixture is the cause of strengthening of the frozen soil and its volume expansion during freezing. Also, the behavior of frozen soil depends on temperature and confining pressure.

A new constitutive model called Elastoplastic Frozen Soil Model, which is based on Modified Cam Clay Model, was developed at NTNU to represent the behavior of frozen soils. The model uses two-stress state concept and is able to represent fundamental and crucial behaviors of frozen soil, such as ice segregation phenomenon, thawing consolidation and thaw settlement, and strength weakening due to pressure.

This model has been validated before and here in this thesis, boundary value problems were run to show the validity and capability of the model to correctly represent the real BVPs. A large-scale laboratory experiment, which was run in the 80s and the 90s in Canada, was chosen as the BVPs. In this experiment, a chilled pipe was causing heave in a frost-susceptible soil. This BVPs were successfully modeled and simulated and they showed a good correspondence between numerical simulation and experimental results. The temperature contour plot and heave was compared and good corresponding between numerical simulation and experimental results were obtained.

Keywords:

1. Frozen Soil
2. Constitutive Model
3. THM Analysis
4. Frost Heave

Hooman Rostami

NTNU – Trondheim
Norwegian University of
Science and Technology

Faculty of Engineering Science and Technology
Department of Civil and Env. Engineering
Geotechnical Division

MSc Thesis

TBA4900 – Geotechnical Engineering

June 2017

By

Hooman Rostami

Title: Finite element analysis of coupled thermal-hydro-mechanical analysis of fully saturated, partially frozen soils

Background

Over the past few decades, surge for finding new raw material sources has increased likelihood of facing permafrost grounds. Permafrost grounds cover 24% of the northern hemisphere and these lands cause unique situations and challenges to geotechnical engineers, such as frost action and frost heave, thaw settlement and weakening, and permafrost degradation. These challenges are caused by unique features of frozen soils which common soil constitutive models cannot describe. These features, mainly, are ice segregation phenomenon, thawing consolidation and thaw settlement, and strength weakening due to pressure melting.

Problem Formulation

For capturing these behaviors, a new constitutive model, called "Elastoplastic Frozen Soil Model" has been proposed at geotechnical division of NTNU. This constitutive model has been previously written as a User Defined Soil Model for the FE program *Plaxis 2D*. In this work, this model firstly will be explained and explored; it will be shown how this model in essence has the ability to capture different behaviors of frozen soil. Then, boundary value problem will be run to test the validity and robustness of the model and to see if the model can replicate the results of a large-scale laboratory experiment.

Trondheim, June 2017

FOR GUSTAV GRIMSTAD
STEINAR NORDAL

Gustav Grimstad
Professor
Geotechnical division of NTNU

Preface

The work presented in this mater thesis is part of my MSc degree in *"Ingegneria per l'Ambiente e il Territorio"* curriculum of *"Earth Resource Engineering"* at University of Bologna (UniBo). This thesis was conducted in collaboration with Norwegian University of Science and Technology (NTNU), during my Erasmus+ exchange studies. It was carried out at NTNU system as TBA4900 Geotechnical Engineering MSc thesis, worth 30 ECTS, in Spring of 2016/17 from 14.01.2017 to 11.06.2017. The primary work was done in Geotechnical Engineering Division of NTNU where daily work took place. Main supervisors at the department were S.A. Ghoreishian Amiri and G. Grmistad, with co-supervision of S. Nordal. My supervisor in charge at University of Bologna was Laura Tonni from Department of Civil, Chemical, Environmental, and Materials Engineering, DICAM. This report and an oral defence at University of Bologna will be equal to 18 ECTS of "Research A" and "Research B" at University of Bologna.

Trondheim, June 2017

Hooman Rostami

Acknowledgment

I would first like to express my sincere gratitude to my daily thesis advisor, Dr. Seyed Ali Ghoreishian Amiri for his support, guidance, and mentorship. He helped me through the moments that I thought "*it doesn't work! It will never work!*". He helped a lot with both doing the research and writing the manuscript.

Next, I want to thank my supervisors, Gustav Grimstad at NTNU and Laura Tonni from UniBo. My discussions with Gustav was always helpful and informative. He was always patient and interested in helping me with my problems. In addition, I want to express my gratitude to Steinar Nordal for his trust, who initially accepted me to do my thesis at Geotechnical Division of NTNU. I always enjoyed my discussions with him; they are always interesting, informative and thought-provoking. Besides, I want to thank Gudmund R. Eiksund and Mohammad Ali H. Ashrafi for the conversation that I had with them. All the people from Geotechnical Division were helpful and friendly and their doors were always open for all of us. A true *Thank you* for all of them!

Also, I want to thank Professor Ezio Mesini and Stefano Gandolfi from the University of Bologna for providing me with the opportunity to study in Norway. This opportunity made my master program truly international.

I am also grateful for the colleagues and friends at geotechnical engineering division with whom I shared my frustrations and difficult moments: Toma, Marius, Kristian, Stian, and Johannes. My friends who made me not feel like the "crazy one in the room"; Christa and David. Also, special thanks to Arghavan for her proof-readings. Also, with a special mention to Zita and Evelien for their nice gestures during this time; friends in Bologna, Sina, Sarvenaz, and Filippo; friends back home, Mehrdad and Mehran.

Lastly, I express my very profound gratitude to my parents and my brother, for their support and understanding during my studies abroad.

H.R.

Abstract

Interest in permafrost, or seasonally frozen ground, has been increasing over the last decades. Nearly 24% of the northern hemisphere, is covered with permafrost. Humankind's need for energy and raw materials has pushed technology to operate on these frozen grounds. Construction and operation of infrastructures, such as roads, pipelines, and tunnels on these areas mean engineers have to deal with frozen soil. In addition, with climate change, permafrost warming and subsequent thawing can trigger or accelerate natural hazards, like rockfalls and debris flows. Furthermore, there is a growing interest in artificial ground freezing for stopping groundwater flow into the construction sites, for example in tunnels, and also for strengthening soil mass to improve stability.

There are fundamental differences between frozen soil and unfrozen soil, such as frost heave, thaw settlement, cryogenic suction which yearn for a new body of knowledge in this area. Saturated frozen soil is a mixture of soil grain, ice and unfrozen water. Thermo-hydro-mechanical interaction between different phases of such a mixture is the cause of strengthening of the frozen soil and its volume expansion during freezing. Also, the behavior of frozen soil depends on temperature and confining pressure.

A new constitutive model called Elastoplastic Frozen Soil Model, which is based on Modified Cam Clay Model, was developed at *NTNU* to represent the behavior of frozen soils. The model uses two-stress state concept and is able to represent fundamental and crucial behaviors of frozen soil, such as ice segregation phenomenon, thawing consolidation and thaw settlement, and strength weakening due to pressure.

This model has been validated before and here in this thesis, boundary value problems were run to show the validity and capability of the model to correctly represent the real BVPs. A large-scale laboratory experiment, which was run in the 80s and the 90s in Canada, was chosen as the BVPs. In this experiment, a chilled pipe was causing heave in a frost-susceptible soil. This BVPs were successfully modeled and simulated and they showed a good correspondence between numerical simulation and experimental results. The temperature contour plot and heave was compared and good corresponding between numerical simulation and experimental results were obtained.

Contents

List of Tables

List of Figures

Chapter 1

Introduction

1.1 Background

Engineering practices in frozen grounds have increased since past decades. Types of frozen soils that engineers encounter can be categorized into two different compartments, 1) naturally-occurring frozen ground 2) artificial frozen soils. In the northern hemisphere, about 24% of land is occupied by permafrost (Zhang et al., 2003) (A map of the northern hemisphere and southern hemisphere can be seen in Figure 1.1). Also, according to Gisnås et al., in Scandinavia, about 56 percent of Norway, and 35 percent of Sweden is covered with permafrost (a map can be seen in Figure 1.2) and according to Boeckli et al. (2012), around $3353 km^2$ of Italian Alps is covered with permafrost (a map of distribution of permafrost of the Alps in different countries is depicted in Figure 1.3) .

Since past decades, the increase in humankind's demand has pushed technology to extract raw materials and energy from permafrosted areas. Hence, construction of structures and infrastructures, such as highways, pipelines, and tunnels in cold regions has increased. On the other hand, using artificial ground freezing (AGF) is growing because of advancement in ground freezing technology. Freezing is a useful method to be used as temporary groundwater control in difficult condition. Not only freezing can help to watertight the soil, it also helps it to increase its strength.

Dealing with frozen soil is a new challenge because of nature of frozen soil (more in Chapter 2). Some of the unique engineering challenges that are faced when it comes to dealing with frozen soil are:

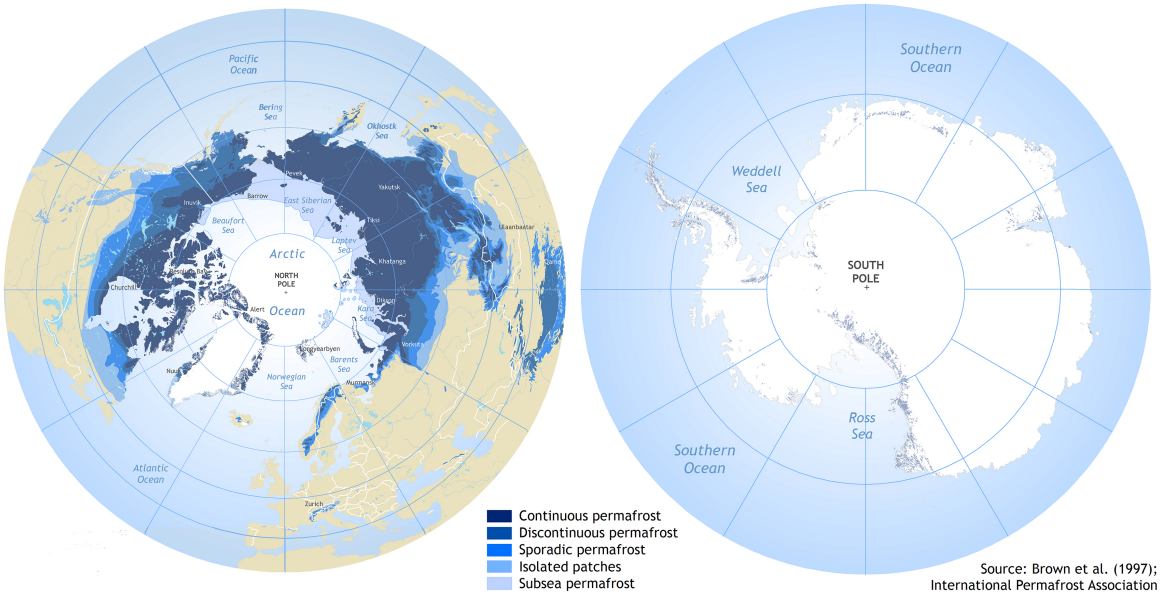

Figure 1.1: Permafrost map of northern hemisphere and southern hemisphere (from Brown et al. (1997))

1.1.1 Frost Action

Frost action is the weathering caused by cycles of freezing and thawing. This phenomenon usually happens more in climates with seasonal freezing, where the temperature can go below and above 0°C. It can cause damages to infrastructures, such a broken cables, broken pipelines, heaved pipelines (Figure 1.4c), cracked pavements (Figure 1.4a), jacked up foundations (Figure 1.4b) and tilted structures.

1.1.2 Frost Heave

Frost heave is the upward displacement caused when soil mixture has a temperature below freezing point and pore water starts to freeze and as it freezes, it sucks in water to the frozen fringe (this process will be looked more in depth in Chapter 2). Frost heave is a major source of damage to transportation infrastructures, such as roads, pipelines, and railways. In the United States alone, over two billion dollars is spent annually on repairing frost heave damages to roads (DiMillio (1999)). A picture of a road that has frost heaved can be seen in Figure 1.5.

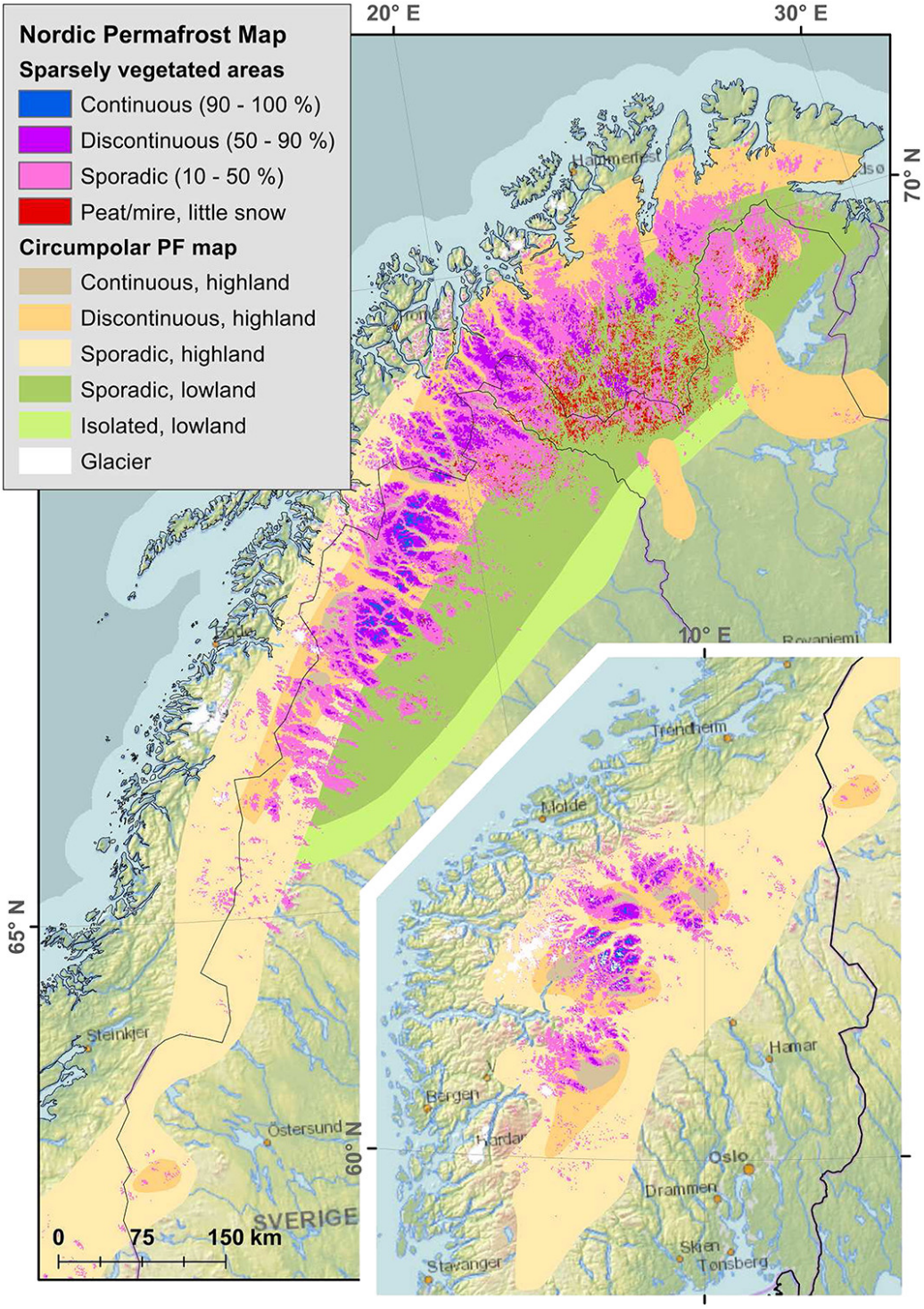

Figure 1.2: Permafrost map of Scandinavian Peninsula (from Gisnås et al.)

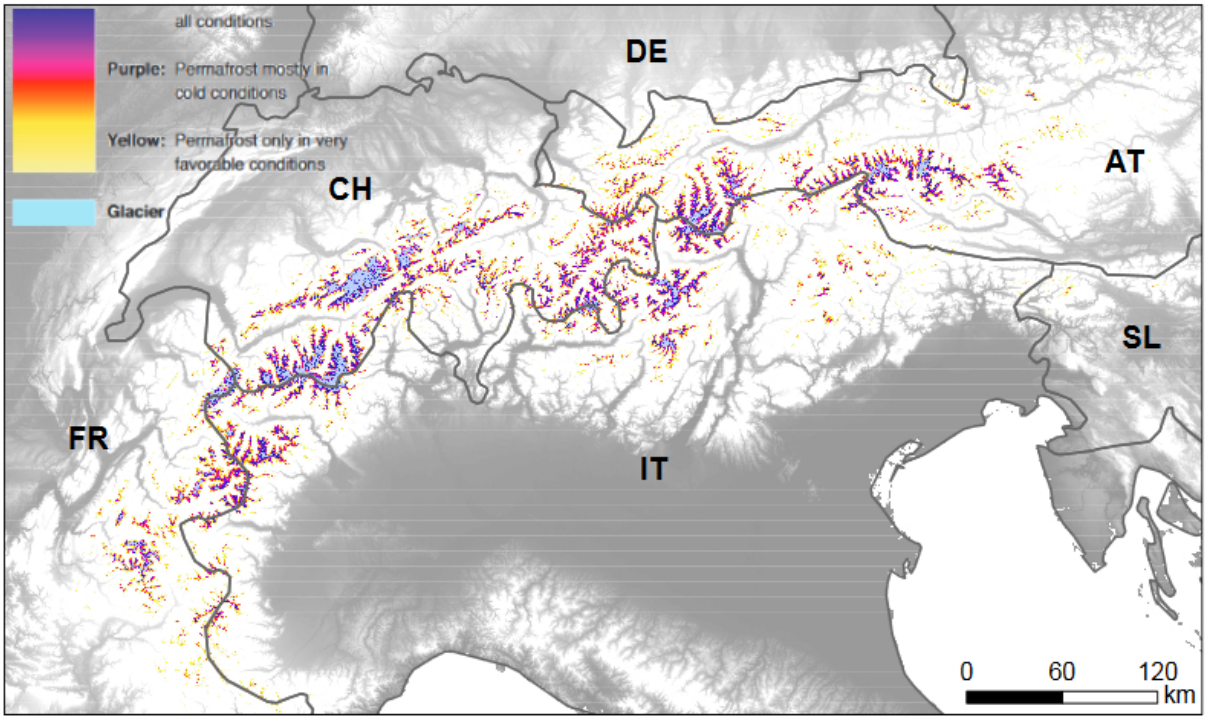

Figure 1.3: Alpine Permafrost Index Map (APIM) of European Alps (from Boeckli et al. (2012))

(a) Cracked pavement due to frost heave in a city street in Yukon, Canada (from Dore and Zubeck (2008))

(b) Jacked up foundation in a building in Antarctica (*Neumayer Station III*) (from Tin et al. (2010))

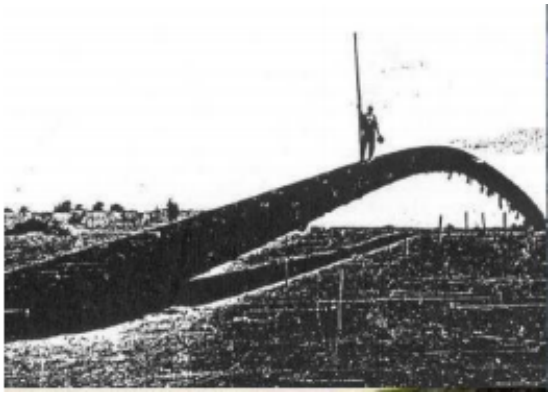

(c) Pipeline heave out of the ground (from Peppin and Style (2013))

Figure 1.4: Damages caused to infrastructures by frost action

Figure 1.5: Frost heave damaged a road (from DiMillio (1999))

1.1.3 Thaw Settlement

As the temperature of the saturated soil drops, pore-water starts transforming into ice; in addition, unfrozen water will move toward the frozen crystals to form ice lenses, which are bands of pure ice in the soil structure (more on that in Chapter 2). In other words, upon freezing, there will be a volume expansion due to this unfrozen water migration.

When ice starts to melt, and soil thaws, the soil starts to get used to new void ratio equilibrium (Andersland and Ladanyi (2004)). This excessive melted ice will start to dissipate. Either self-weight of soil matrix or external force will make water to move and since the freezing process has destroyed soil matrix, the soil might not consolidate back all the amount that it has heaved. This difference between the amount of thawing and heaving will accentuate when the freeze/thaw cycle happen over and over again (Xie et al., 2015). This cycles can reduce cohesion and strength of soil matrix.

1.1.4 Thaw Weakening

When the temperature of seasonal permafrost starts to increase, ice in frozen, frost-susceptible soil starts to thaw. If this newly melted water can not drain to lower layers, since there is still frozen soil below it that hinder its movement, an excess pressure starts to develop which reduces the soil strength and active layer start to lose its bearing capacity. This process is called thaw weakening. According to Dudeja (2011), the likelihood of occurrence of thaw weakening depends on frost-susceptibility of soil, its permeability, its underlying layer and its drainage conditions, and rate of thawing.

1.1.5 Permafrost Degradation

Permafrost degradation is the phenomenon where areal extent or thickness of permafrost decreases. Many low-latitude mountainous regions of Europe are just a few degrees below permafrost degree and a slight increase in temperature, can increase the depth of summer thawing and consequently, it can cause permafrost degradation. According to Harris (2005), there is a likely correlation between increased magnitude and frequency of mountain slope instability with permafrost degradation. This is exemplified by the 1987 *Val Pola* landslide case, in the Italian Alps, which according to Crosta et al. (2004), for this case, permafrost degradation is thought to be one of the decisive factors. Furthermore, Noetzli et al. (2003) shows that permafrost is probably one of the determining element for a group of 20 large alpine collapses.

1.1.6 Artificial Ground Freezing

Artificial ground freezing of soil mass has been used as the method to control water flow and strengthen the soil structure for over a century. Frozen ground has higher strength; thus it can offer ground support; the frozen soil has almost zero permeability; thus it is water tight and can stop high water inflow to construction (for example, like tunnels). This method works reasonably good in practice, but there are potential problems related to how soil matrix will react to thawing and how it will settle.

1.2 Motivation

For understanding all these phenomena, a good body knowledge of the mechanical and thermal behavior of frozen soil is necessary. Then for modeling structures in or on soil mass, a sound, valid and coherent constitutive model is necessary (constitutive models relates stresses to strains). There are a couple of constitutive models out there, but they all have their strength and weaknesses. Here, newly developed elastoplastic frozen soil model, developed by geotechnical engineering division of NTNU, will be used to represent the behavior of frozen soil (more on the behavior of this model and its strengths and limitations in chapter 4). For validation, verification and increasing robustness of every new constitutive model, boundary value problems have to be run to test these factors. In this work, two BVPs were run successfully which shows validity and robustness of the model.

1.3 Objectives

1. Presenting the "Elastic Plastic Frozen Soil Model" for saturated condition and a relatively conclusive literature review of all the other models.
2. Testing currently implemented model, which is implemented as a user-defined model in the FE program Plaxis, by:
   (a) Simulating boundary value problems and compare the results with experimental data
   (b) In a real boundary value problem and comparing results with measurements
3. Finally, modifying the model in the case of discrepancies (in such case repeat no. 2).

1.4 Limitations

The elastoplastic model, as will be explained in Chapter 4, is for fully saturated situations; it also is rate-independent and does not take into account salinity. The rate-dependant version of the model is available (Ghoreishian Amiri et al. (2016a)), so future development of the model can be incorporating salinity effect and water-air unsaturation. For validation part, which is the work of this thesis, another boundary value problem, like the Zhang and Kushwaha (1998) experiment can be done to show robustness and ability of the model. More importantly, simulation of thawing should be finished. Another suggestion would be to have sensitivity analysis on parameters.

1.5 Structure of the Report

- **Chapter 1** - Introduction
  - In this chapter, a background to the general scheme of work is presented. Motivation, objective and limitation of the work have been presented.
- **Chapter 2** - Theoretical Background
  - In this chapter, a theoretical background to thermo-mechanical behavior of frozen soil has been presented.
- **Chapter 3** - Methods
  - Here, method used to run the BVP simulation is presented.

- **Chapter 4** - Elastoplastic Frozen Soil Model
  - Here, the elastoplastic model is presented; explanation on how it works and how it can simulate the behavior of soil is discussed as well.
- **Chapter 5** - Boundary Value Problems
  - In this chapter, boundary value problem that have been run was presented.
- **Chapter 6** - Summary
  - Summary and conclusion of the work, discussion of the results and limitation and recommendation for future work is presented here.

Chapter 2

Literature Review

Soil mass below bulk water freezing point undergoes some structural changes. This necessitates a precise study of characteristics of the frozen soil. As the pore-water start to freeze, ice will act as the binding element between soil grains. In addition, the soil will suck in unfrozen water into freezing fringe and pores will start to expand. These behaviors will be discussed in this chapter. Moreover, an overview of how soil will behave under cooling, how it will change and how frozen soil will behave under mechanical and thermal loading with different ice percentage, will be discussed. At the end, an overview of the constitutive models which have been developed so far to capture these behaviors will be presented.

2.1 Temperature Effect

Unlike bulk water where all of it freezes after reaching bulk freezing temperature, water in soil pores does not freeze after reaching this point. As seen in Figure 2.1, pore water will not start freezing at T_f but at T_{sc} which a bit lower. This is because of formation of ice nuclei and the increase of temperature after that point is due to release of ice heat latency. After that, free water freezes and release of ice latent heat will slow down the process. This curve will change based on mineral composition, specific surface area of the soil grains, nature of the fluid in the pores. So, for each soil as temperature decreases, unfrozen water content, the amount of unfrozen water to the amount of ice and water in pores, will change differently. In other words, each soil will have different unfrozen water content curve. An example of it can be seen in Figure 2.2.

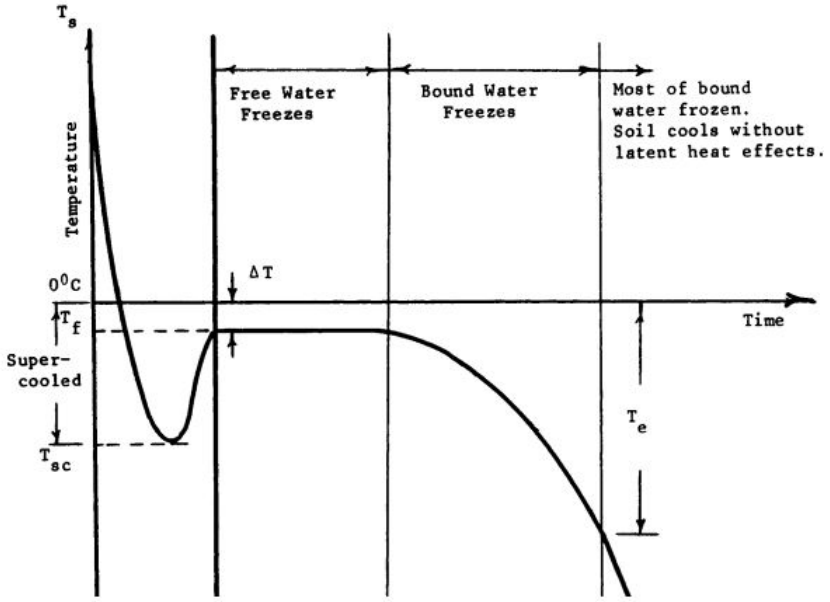

Figure 2.1: Cooling curve for soil and water mixture (from Andersland and Ladanyi (2004))

2.1.1 Permeability

As temperature of soil decreases, the pore-water freezes and this means that there is a reduced space that water can travel in. Laboratory tests show that as temperature decreases and pores start to be occupied by ice, hydraulic conductivity decreases (see Figure 2.3).

2.2 Mechanical Behavior

In this section, mechanical behavior of soil and the parameters which affect it, will be discussed. Cryogenic suction, ice content, temperature, confining pressure are factors that, besides usual factors like soil type, will affect how frozen soil will behave. Beside these factors, salinity and strain rate will affect the behavior of frozen soils but their incorporation is out of the scope of this work.

2.2.1 Cryogenic Suction

As said in Section 2.1, there will be unfrozen water even in temperature below the bulk freezing point. According to Wettlaufer and M. Grae Worster (2006), there are two types of mechanisms which control the behavior of frozen soil. These two are “curvature-induced premelting" and “interfacial premelting", which are illustrated in Figure 2.4. Curvature-induced premelting, as a result of the surface tension of water trapped inbetween soil particles, creates super-cooled

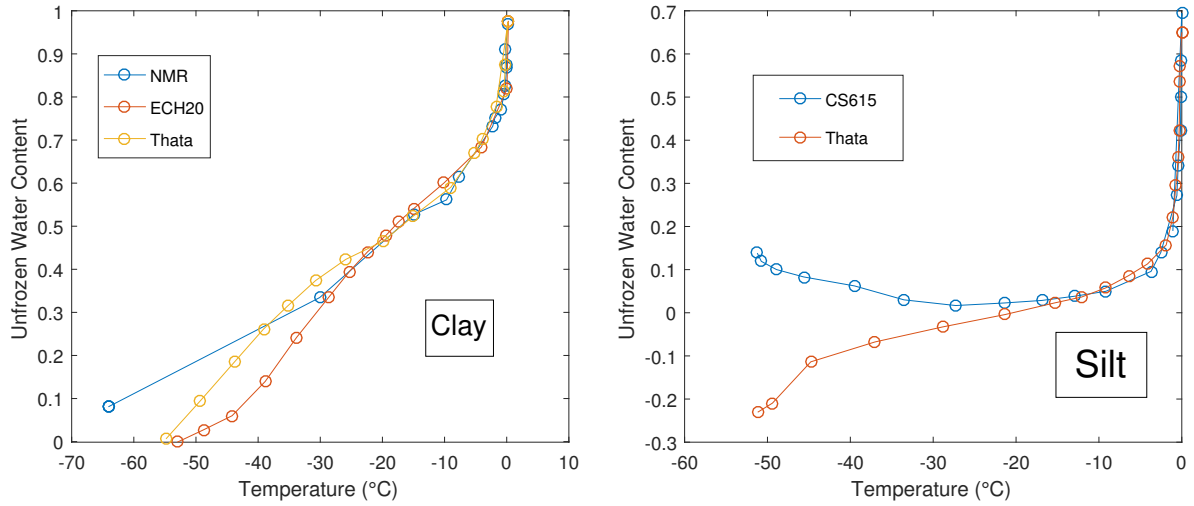

(a) Clay (b) Silt

Figure 2.2: Unfrozen Water content for different soils (adapted from Yoshikawa and Overduin (2005))

pore water, according to Gibbs-Thomson law, which creates something similar to the capillary suction which bonds grain together. Taber (1929) and Taber (1930) long ago has shown that as soil pore-water freezes, water migrates to the freezing area. (this is the reason for frost heave which was mentioned in Section 1.1.2). This mechanism is usually more likely to be dominant in low ice contents, which results in increasing of soil strength. On the other hand, interfacial premelting creates a thin unfrozen water film which separates ice from soil grains. This mechanics results in repulsive forces between ice and soil grains which try to produce a more-widen gap between ice and soil grains by sucking in more water. These repulsive forces between soil and ice grains will cause grain segregation. In addition, segregated grains mean low contact between grain, i.e. lower strength. This mechanism is more active in higher ice contents.

2.2.2 Ice Content

Experimental works demonstrate that at lower ice contents, by increasing ice content, strength of sample increases which can be explained by “curvature- induced premelting” mechanisms. As mentioned before, this mechanism is more active in lower ice contents and it causes a suction in soil mixture and this suction bonds grains together which translate into a higher effective stress for soil mixture. Conversely, in higher ice contents, by increasing ice content, the compressive strength of soil will decrease. This phenomenon is caused mainly by “interfacial premelting" mechanism, which is more influential at that point and it causes grain segregation which means that the grains will be pushed away from each other, and ice lenses will start to form, which means soil grains’ interaction will be destroyed, which begets a lower compressive

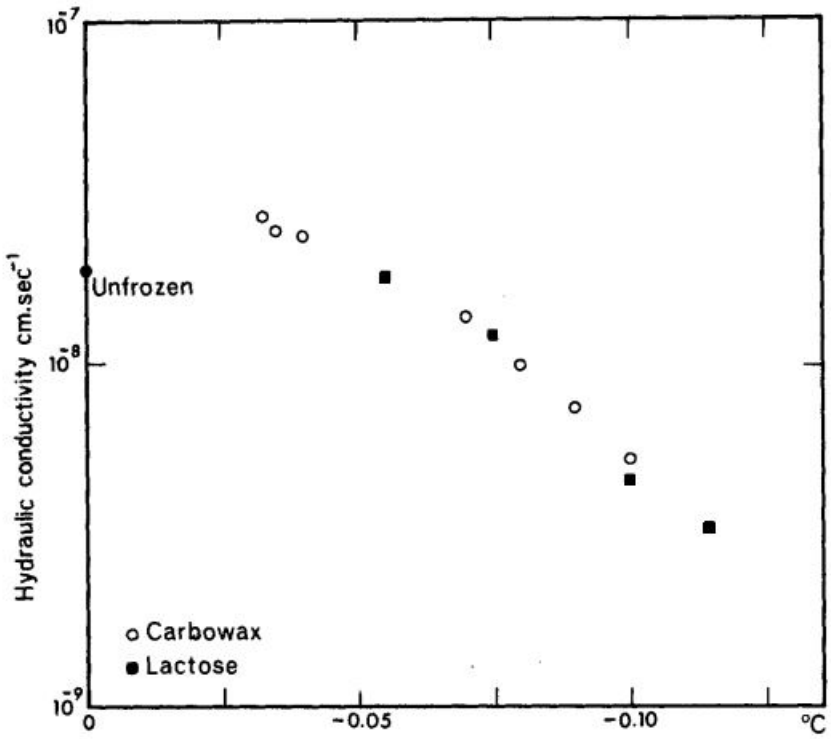

Figure 2.3: Hydraulic Conductivity in temperature variation for Leda clay sample (from Burt and Williams (1976))

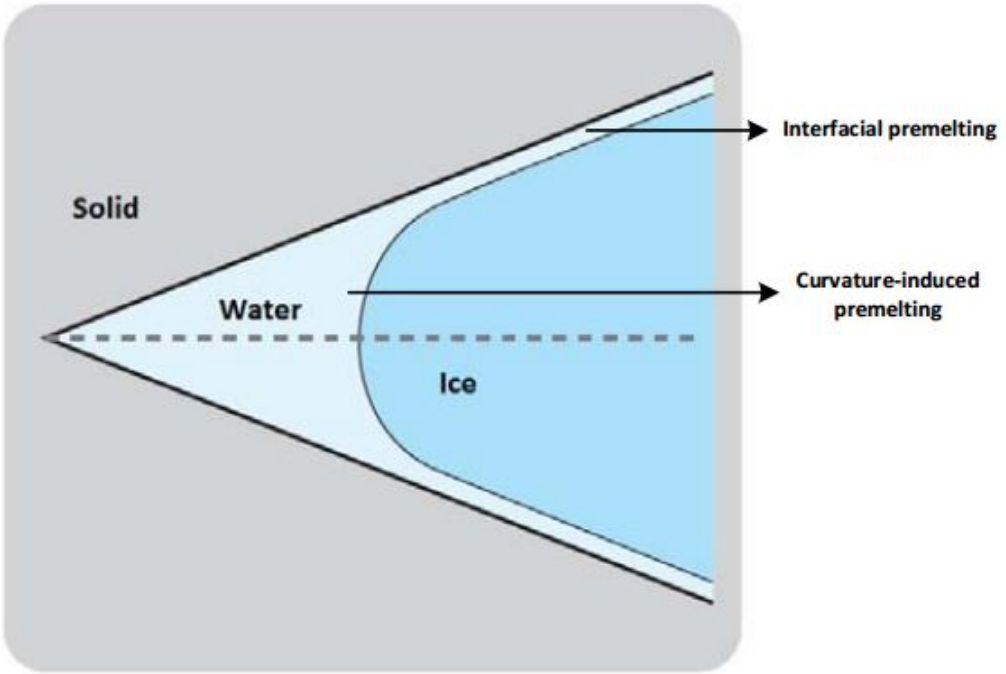

Figure 2.4: "curvature-induced premelting" and "interfacial premelting" during intrusion of ice into a wedge-shape wet preferential solid (adapted from Wettlaufer and M. Grae Worster (2006))

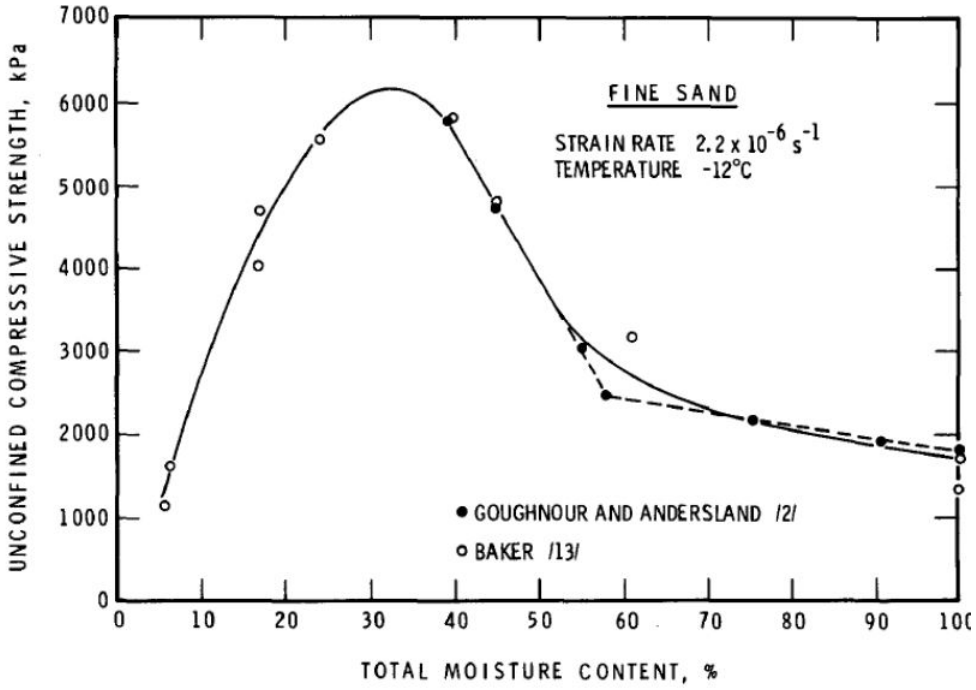

Figure 2.5: Effect of total moisture content on unconfined compressive strength of a frozen sand at a constant strain rate and temperature (from Zhou (2014))

strength in soil mixture. This behavior is shown in Figure 2.5.

2.2.3 Temperature

Many laboratory results have shown that temperature is one of the most important factors which affect the mechanical properties of frozen soils (Xie et al. (2014); Bragg and Andersland (1981); Youssef (1986)). As seen in Section 2.2.2, ice content, which is a function of temperature, impacts the mechanical properties of soil by either pushing or bonding grains together. Yuanming et al. (2010) shows at a constant confining pressure, with the decrease in temperature, soil mixture will act stiffer. As seen in Figure 2.6, stress-strain curve of frozen soil experiences three stages:

1. initially there is an elastic response, where the curve is almost a linear line and this means that there is little or no plastic strains developed in the mixture.
2. After a point, plastic deformations kick in
3. At the end, softening will happen where the slopes of stress-strain curves are negative.

As seen in the figure, for both confining pressures, by decreasing temperature, elastic response will act stiffer. Also, by decreasing temperature, soil mixture will act more brittle.

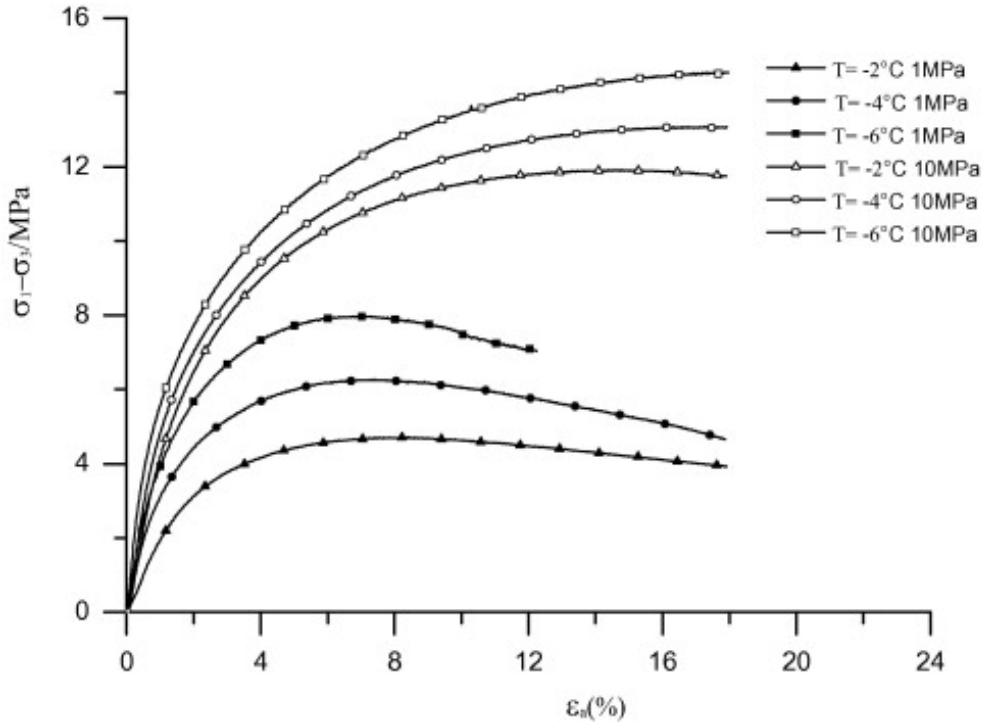

Figure 2.6: Stress-strain curves of frozen soil at two confining pressure with different temperatures (from Yuanming et al. (2010))

Yamamoto and Springman (2014) observe similar behavior.

2.2.4 Confining Pressure

Effect of confining pressure on frozen soils' mechanical behaviors has been reported in many scientific papers (Parameswaran and Jones (1981); Chamberlain et al. (1972); Arenson and Springman (2005); Sinitsyn and Løset (2011)). At lower confining pressures, frozen soil, similarly to the unfrozen soil, shows higher strength by increasing of confining pressure. This phenomenon can be seen in Figure 2.7, in which by increasing of confining pressure at a constant temperature, soil starts to show a stiffer elastic response and a higher peak shear stress. As confining pressure increases, after a point, increasing confining pressure will decrease maximum shear stress. In other words, after a point, confining pressure will start to pressure melt ice. After that point, an increase of confining pressure will pressure melt more of ice content until it melts all the ice and it reaches a value close to fully fluid-saturated situation. If confining pressure continues to increase even more after this point, there will be no more ice to pressure melt, so increase in confining pressure, just like fully saturated situation, will start to increase peak shear strength of soil.

These behaviors can be seen in Figure 2.8. Two different soils, a tilt, named WLT and a sand, named OWS, was tested. In OWS sand, an increase in strength in the *Region I* is obvious.

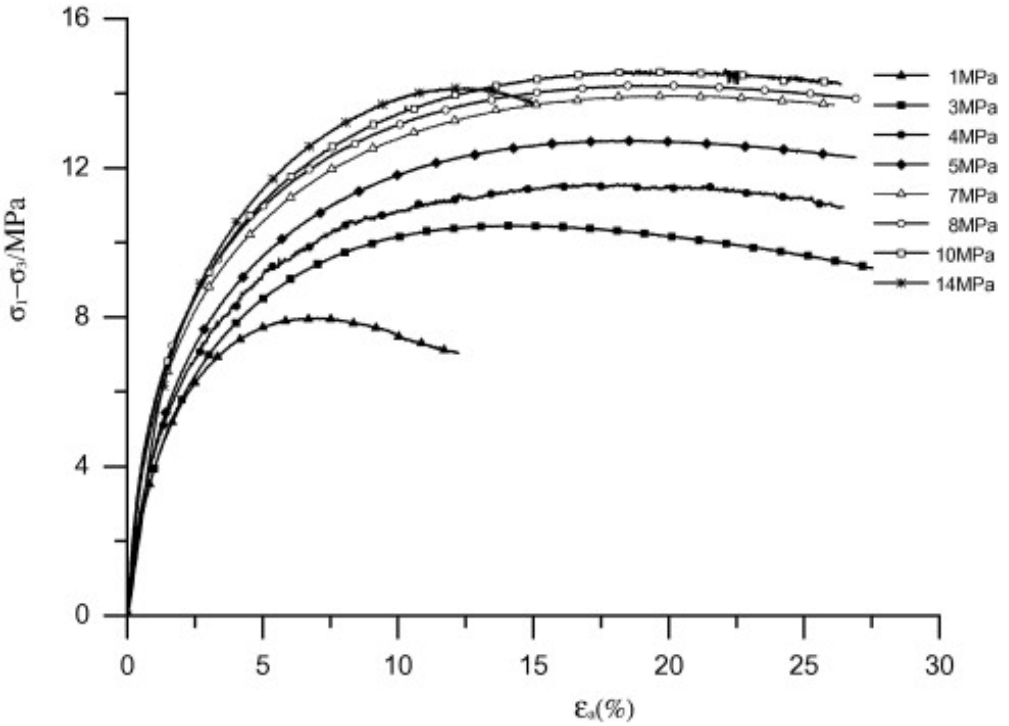

Figure 2.7: Stress-strain curves of frozen soil at different at -6°C confining pressures (from Yuanming et al. (2010))

This is due to inter-particle friction and particle interlocking. For glacial tilt of WLT, there is no significant increase in strength with an increase of confining pressure. *Region II* can be seen for both soils. As said before, this the part that a reduction in soil strength with an increase of confining pressure will be seen. Then, there is *Region III* where soil strength will start to increase again with an increase in confining pressure.

2.3 Current Constitutive Models

As mentioned until now, there is a fundamental difference between behavior of unfrozen and frozen soil. Hence, specific modifications and elaborations of common constitutive models are required in order to capture these unique different behaviors. A *constitutive equation* or *constitutive relation* is a set of relations which relates forces or stresses to deformations or strains. Stress state variables are used to define constitutive relations, hence to define mechanical behavior. There have been quite a few models which tried to model the frozen soil behavior. A brief discussion will be given on each model's, or group of models', features and shortcomings.

Unlike fully saturated unfrozen soil, in frozen soil effective stress is not enough to describe the soil mass. Most of models developed for describing frozen soil behavior have adopted total-stress-based models (Ladanyi (1972); Selvadurai et al. (1999); Arenson and Springman (2005);

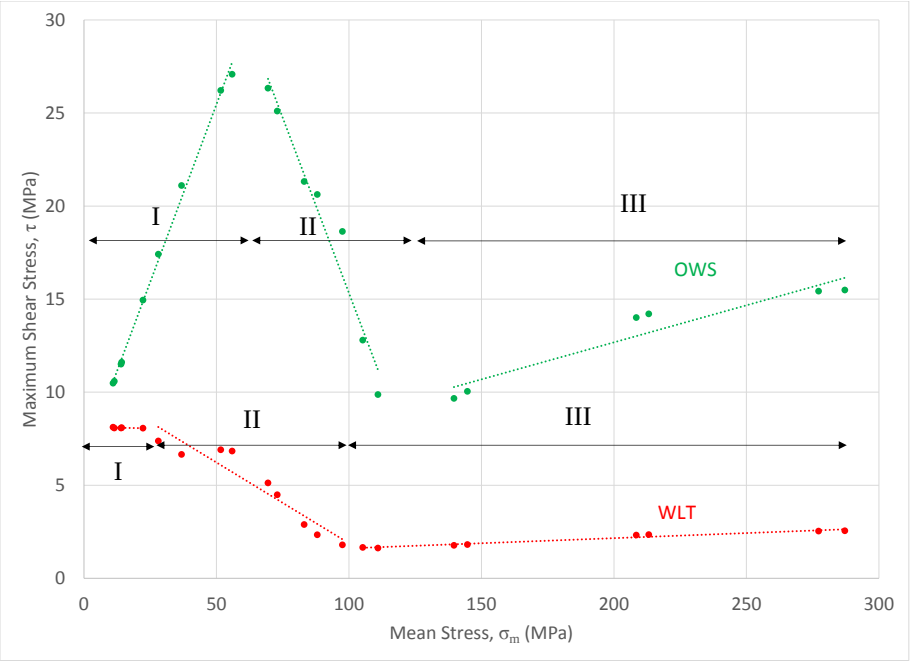

Figure 2.8: Variation of peak shear stress with different confining stresses (adapted from (Chamberlain et al., 1972))

Lai et al. (2008); Zhu et al. (2010); Yuanming et al. (2010)). Even though this approach can simulate soil behavior due to external mechanical loads, it could not simulate thermal-loading-only situations, namely simulating deformation under a freezing/thawing test. In other words, these models are not able to calculate deformations under variation of only ice content and temperature. In addition, unfrozen water will make difficulties for describing total stresses.

There is also another approach where it tries to use only a Bishop-type effective stress as stress state variable. This approach has been used by some researchers to simulate behavior of frozen soil (Thomas et al. (2009); Nicolsky et al. (2008); Li et al. (2008); Nixon (1991)). Like unsaturated soil mechanics, a different definition of pore pressure is used in these models. Nicolsky et al. (2008) and Li et al. (2008) used a combination of frozen water pressure and unfrozen water pressure in partially frozen and fully frozen soils. On the other hand, Thomas et al. (2009) and Nixon (1991) preferred to have only water pressure in partially frozen state and ice pressure in the fully frozen state.

Alternatively, Nishimura et al. (2009) proposed using two-stress variables, which was developed originally by Alonso et al. (1990) for Barcelona Basic Model (BBM). BBM is developed for unsaturated soil and it uses suction and net stress (excess of total stress over suction) as stress state variables. Nishimura et al. (2009) extend BBM by redefining “net stress” (as the excess of

total stress over ice pressure) and “cryogenic suction” as the two stress state variables. In their model, as soil freezes, cryogenic suction increases and ice pressure increases and that results in zero or negative net mean stress, which fails the soil matrix in tension and this ends up in soil grain segregation and an increase in void ratio and a softer behavior in soil. In the unfrozen state, the model reduces to simple Cam Clay model. Since grain segregation is caused by the tensile failure, by using net stress in the unfrozen state, the soil will always dilate upon shearing which is not the case in reality. Zhou (2014) has a similar model where he uses “temperature” instead of “cryogenic suction” as one of the stress state variables. He uses a strength upscaling procedure to account ice content and temperature in failure criterion.

Zhang and Michalowski (2015) uses classical “effective stress” and “pore ice ratio”, defined as the ratio of the volume of ice to the volume of solid particles, as stress state variables. This model gives unrealistically high effective confining pressure for the time that unfrozen water content is very small.

Chapter 3

Methods

In this thesis, finite element method is used as a simulation tool. The Finite Element Method (FEM) or referred to as Finite Element Analysis (FEA), is a numerical method for solving problems in the different field of engineering and computational physics. This method is not an exact method but gives a good approximate solution to some of the problems that there is no closed-form solution. FEM is used in geotechnical engineering similarly to structural engineering. *Displacement method* is usually used, where for mechanical analysis forces and loads are applied to a structure or soil body and then their response in terms of deformations and displacements is obtained. For hydro and thermal analyses, heat flux or fluid flow is analogous to the force and temperature and head or pore-pressure to displacement. Here, FE program specifically written for geotechnical application, called *Plaxis* is used. Since the focus of this work is not to present or explain how FE methods and *Plaxis* in particular works, only a brief introduction to it will be given (for more information look at Brinkgreve et al. (2017) and Zienkiewicz et al. (2005)).

3.1 Main Principles

In finite element method, soil body is divided into elements and an approximate description of the behavior of each element is developed and then all of these elements are joined together by a numerical and mathematical integration process which adds up the behavior of each element into the behavior of whole soil body. *Plaxis 2D* usually use 6 or 15 nodal point triangular elements, but here 6 nodal point element is used.

According to Nordal (2016) every modern FEM program follows following operations:

1. **Element modelling**, using element stiffness matrix, a set of equations for each element is defined.

2. **Global modelling**, where stiff matrices for all elements is assembled into global stiffness matrix. Also, an incremental load vector is found.

3. **Equation solving**, where a global displacement increment is found from load increment, by solving the global equation.

4. **Stress Evaluation**, whereby using global displacement strain, the increment in each element is found, which then used to find stress in each element.

5. **Testing for numerical accuracy**, where load increment is adjusted (if necessary) by adding more iterations. If too high unbalanced forces are in the elements, a new strain increment is given and step 3 onward must be repeated.

6. **Updating results**, where incremental stresses and strains are added to form final ones.

7. **Calculation of new load increment**, where a new load increment is applied and steps two onward are repeated. These increments are added until specified external load or failure is reached.

Since this analysis is a coupled thermo-hydro-mechanical analysis, step 3, equation solving, is an interaction of all three loads (as seen in Figure 3.1).

Noted that one of most important part in step 4, at least for geotechnical engineering, is defining the constitutive model, which defines the stress-strain relationship. In this work, the main focus is on this part and hereafter no further explanation of how FE software or how the method itself work will not be given. Furthermore, in the Chapter 4, the new constitutive model will be explained in detail. But first, a short description of constitutive models will be given.

3.1.1 Constitutive Model

In essence, a constitutive model is a set of algebraic, differential and integral equations relating stress and strain tensor together. Usually, simple models, like Mohr-Coulomb is used in geotechnical engineering for modeling simple behaviors. As pointed out in Chapter 2, the frozen soil has a very complicated nature and the presence of frozen water impacts its mechanical behavior. Conventional models do not account for phase change of water to ice upon freezing and its effect on soil behavior. Hence, this yearns for a specific constitutive model other than conventional models. A new constitutive model will be presented in Chapter 4.

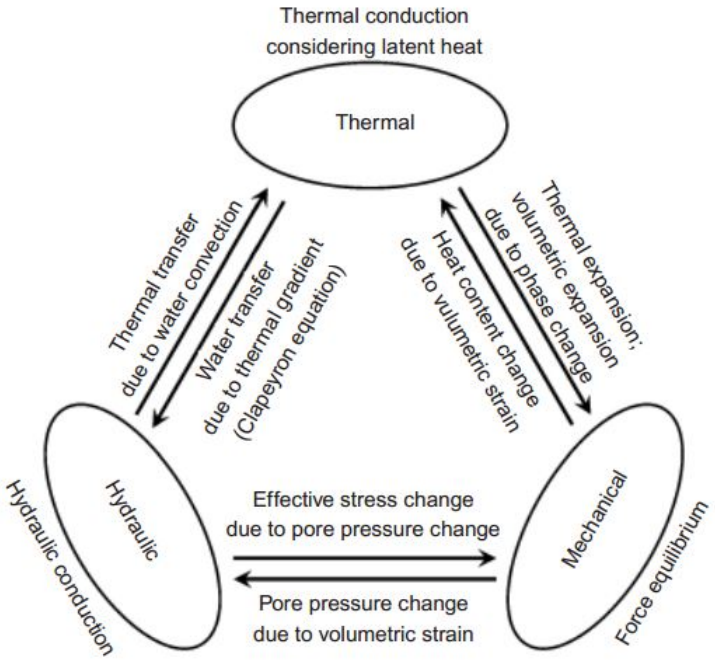

Figure 3.1: Thermo-hydro-mechanical interaction mechanism in frozen soil (from Thomas et al. (2009))

3.2 Computing Unit

A PC with 64-bit version of Windows 10, with Intel i7 2.8 GHz processor, 16 GB of RAM, was used to run the simulations.

Chapter 4

Elastoplastic Frozen Soil model

Elastoplastic Frozen Soil model was developed by Ghoreishian Amiri et al. (2016c). The basis of this thesis is on this constitutive model. In the following chapter, main features and characteristics of the model are explained. The relationship with every feature of the model and physics of frozen soil is explained for showing difference and robustness of this model in comparison to others. In this model, for simplicity, no gaseous phase or dissolved salt is considered, which mean that soil matrix is comprised of ice, unfrozen water, and soil grains. Besides, the model is strain-rate independent. Model is based on Modified Cam-Clay (MCC) and in addition, uses two-stress state concept. This model is able to represent fundamental and crucial behaviors of frozen soil, such as ice segregation phenomenon, thawing consolidation and thaw settlement, and strength weakening due to pressure melting.

4.1 The Constitutive Model

In the model developed by Ghoreishian Amiri et al. (2016c), stress state variables are "solid state stress", σ^* and "cryogenic suction", S_c. These two are explained in more detail in following sections.

Solid Phase Stress

As mentioned in Section 2.2.1, as temperature decreases and pore-water freezes, the soil will become stronger which is the result of soil grains getting cemented together. In other words, ice bonds soil grains together. In reality, if a soil, with both soil grains and ice, is loaded, ice grains can take shear stresses as well. Consequently, in this model, it is supposed that ice can

be loaded as well. Since for this model both soil and ice grains can take shear stresses, solid phase stress will contain both soil and ice grains stresses. Finally, "solid phase stress" can be defined. Solid phase stress is the sum of stresses in both ice and soil grains minus the pressure of the unfrozen part of water. This means that:

$$\sigma^* = \sigma - S_{uw} p_w I \tag{4.1}$$

where σ^* is the solid state stress, σ is the sum of ice and soil grain stress, S_{uw} is unfrozen water content, p_w is the water pressure and I is the unit tensor.

Cryogenic Suction

Mathematically, Cryogenic suction, or cryosuction, is the difference between ice pressure and water pressure and it is defined as follow:

$$S_c = p_i - p_w \tag{4.2}$$

where S_c is cryogenic suction, p_w and p_i are water and ice phase pressure, respectively. Cryogenic suction can be calculated using Clausius-Clapeyron relation as basic of equilibrium between ice and unfrozen water phases,

$$S_c = p_i - p_w \approx -\rho_i L \frac{T}{T_f} \tag{4.3}$$

where ρ_i is the density of ice, L is latent heat of fusion, T is the temperature of the system on the Kelvin scale and T_f is the freezing–thawing temperature of water–ice system at the given pressure. T_f is calculated by following formula:

$$T_f = T_{f,ref} \left(\frac{p_i}{-p_{0,ref}} + 1 \right)^{\frac{1}{\alpha}} \tag{4.4}$$

where $T_{f,ref}$ is the reference freezing-thawing temperature, usually 273.16 K, $p_{0,ref}$ is the corresponding reference pressure to the reference temperature, usually $p_{0,ref}$=-395 MPa and α is a constant, commonly between 7 and 9. It should be noted that cryogenic suction is accounting temperature effect by ice content and solid stress is taking unfrozen water into account.

4.1.1 Unfrozen Water Content

As discussed in Section 2.1, there is a particular temperature-unfrozen water content curve for each soil. In this model, unfrozen water content, S_{uw}, is a function of cryogenic suction, and

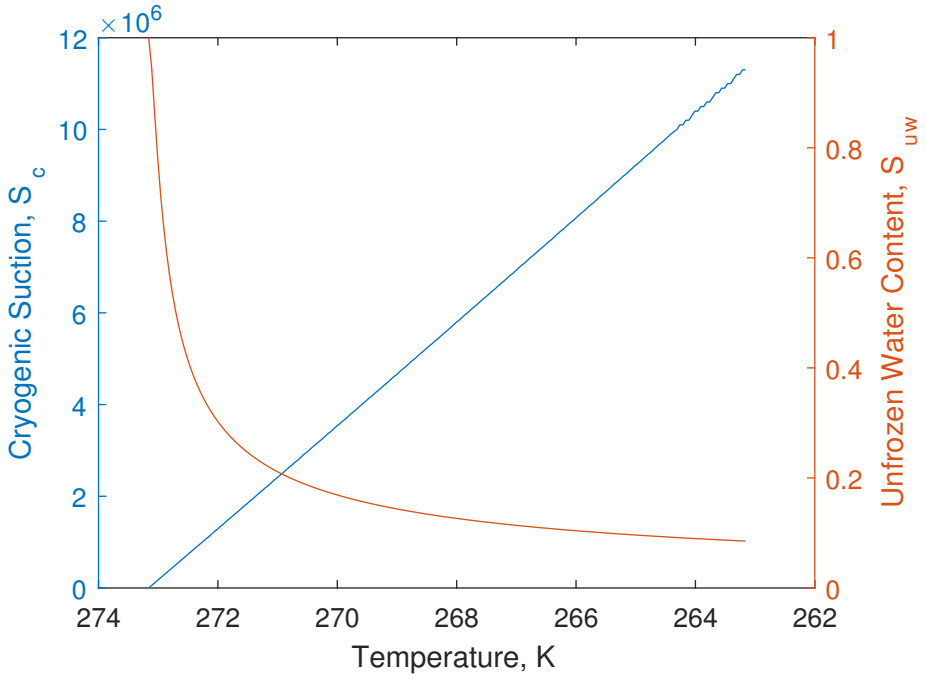

Figure 4.1: unfrozen water content and cryogenic suction variation with temperature decrease

two constants, namely ρ_r and λ_r. These two constants are for fitting unfrozen water curve with laboratory data. The function which was used, can be seen in Equation 4.5. In addition, for showing how cryogenic suction and unfrozen water content will change with temperature variation, they are plotted in Figure 4.1.

$$S_{uw} = \left[1 + \left(\frac{S_c}{\rho_r}\right)^{\frac{1}{1-\lambda_r}}\right]^{-\lambda_r} \tag{4.5}$$

4.2 Strain Decomposition

Alike any model, decomposition of the strain increment, $d\epsilon$, has to be defined. If the strain is inside yield surface, it will result in elastic strain, if it is passing current yield surface, it will result in plastic strain and push the yield surface to the final point of the stress increment vector caused by corresponding incremental strain. This plastic strain is caused by These will be represented in the first letter of subscript of the decomposed strain as, m and s, respectively. Moreover, elastic and plastic deformation, which will be represented in second letter of subscript of the decomposed strain as, e and p, respectively. Hence, decomposition of strain will be as following:

$$d\epsilon = d\epsilon^{me} + d\epsilon^{se} + d\epsilon^{mp} + d\epsilon^{sp} \tag{4.6}$$

4.3 Elastic Response

The elastic response will be comprised of elastic response of mechanical loading and cryogenic suction variation. For the mechanical response, it is supposed that solid phase is a mixture of soil grains and frozen water. Hence, elastic parameters will differ based on ice saturation degree. When pore water is unfrozen, the mixture has unfrozen soil properties, and when it completely freezes, it has frozen soil properties. Consequently, as soil starts to freeze and moves from unfrozen state to frozen state, mixture will be in a state where elastic parameters come from a weighted sum of frozen and unfrozen states, where weight of frozen parameter will be ice saturation, S_i, and weight of unfrozen parameter will be $(1 - S_i)$. Consequently, bulk modulus, K, and shear modulus, G, will be equal to:

$$G = (1 - S_i)G_0 + \frac{S_i E_f}{2(1 + \nu_f)} \tag{4.7}$$

$$K = (1 - S_i)\frac{(1 + e)p^*_{y0}}{\kappa_0} + \frac{S_i E_f}{3(1 - 2\nu_f)} \tag{4.8}$$

where K and G are bulk and shear modulus of soil and ice mixture, S_i is ice saturation, which is volume of frozen water to sum of frozen and unfrozen water, G_0 is unfrozen shear modulus, E_f and ν_f are Young modulus and Poisson ratio of frozen soil, respectively, p^*_{y0} is the preconsolidation stress of unfrozen soil. As shown by Petrovic (2003), ice has a temperature dependant behavior and for accounting that, E_f is supposed to be temperature dependent:

$$E_f = E_{f,ref} - E_{f,inc}(T - T_{ref}) \tag{4.9}$$

where $E_{f,ref}$ is the E_f at the reference temperature, T_{ref}, T is temperature at Kelvin scale and $E_{f,inc}$ is the rate of E_f change with temperature. Now by having mechanical elastic parameters, mechanical elastic strain can be defined as follow:

$$d\epsilon^{me} = \begin{bmatrix} d\epsilon^{me}_p \\ d\epsilon^{me}_q \end{bmatrix} = \begin{bmatrix} \frac{1}{K} & 0 \\ 0 & \frac{1}{3G} \end{bmatrix} \begin{bmatrix} dp^* \\ dq^* \end{bmatrix} = D^{-1} d\sigma^* \tag{4.10}$$

where p^* solid phase mean stress and q^* is solid phase deviatoric stress.

After mechanical elastic strain, elastic strain due to cryogenic suction variation should be explored. Change in suction value (below grain segregation threshold) can cause elastic deformation which is equal to:

$$d\epsilon^{se} = \frac{\kappa_s}{3(1 + e)} \frac{dS_c}{S_c + p_{atm}} I \tag{4.11}$$

where κ_s is elastic swelling index due to cryogenic suction change, and p_{atm} is atmospheric pressure.

Now by having both mechanical and suction elastic strain, elastic strain can be defined as:

$$d\epsilon_p^e = \frac{1}{K} dp^* + \frac{\kappa_s}{3(1+e)} \frac{dS_c}{S_c + p_{atm}} \tag{4.12}$$

$$d\epsilon_q^e = \frac{1}{3G} dq^* \tag{4.13}$$

4.4 Yield Surfaces

The model aims to represent soil behavior from the fully unfrozen state up to fully frozen state and every ice saturation degree in-between. Hence, at unfrozen state, where cryogenic suction is equal to zero, the model reduces to Cam Clay model. For unfrozen contents other than zero, the soil will be a mixture of unfrozen water, ice and soil grains.

In order to take curvature-induced pre-melting effects which increases the strength of soil mixture by bonding soil grains together, yield surface will get bigger by increasing in the cryogenic suction value. This phenomenon is shown in loading collapse (LC) curve where preconsolidation stress, p_y^* increases by increase of cryogenic suction. As said before, ice bonds soil grain together and gives it compressive strength; it also gives soil mixture ability to take tension as well. Hence, there is an ice tension line (ITL) which represents soil ability to take tensile stress with cryogenic suction.

These three curves are shown in Figure 4.2. LC curve is defined as a function of cryogenic suction and its formula can be seen in Equation 4.16. ITL is, alike, a function of cryogenic suction and its formula can be seen in Equation 4.14.

$$p^* = -k_t S_c \tag{4.14}$$

where k_t is the parameter for accounting for increase in apparent cohesion due to increase in cryogenic suction.

The yield criterion of the solid phase, in each value of cryogenic suction, makes a yield surface. As said before, by increasing cryogenic suction, p_y^* will increase and yield surface will become bigger. If all of the yield surface from all of suctions until the grain segregation threshold point is accumulated, this creates the yield criterion curve and it will be defined as follow:

$$F_1 = \left(p^* - k_t S_c\right)\left[\left(p^* - k_t S_c\right) S_{uw}^m - \left(p_y^* - k_t S_c\right)\right] + \left(\frac{q*}{M}\right)^2 \tag{4.15}$$

where p_y^* is the partially frozen state preconsolidation stress, M is the tangent of the critical-

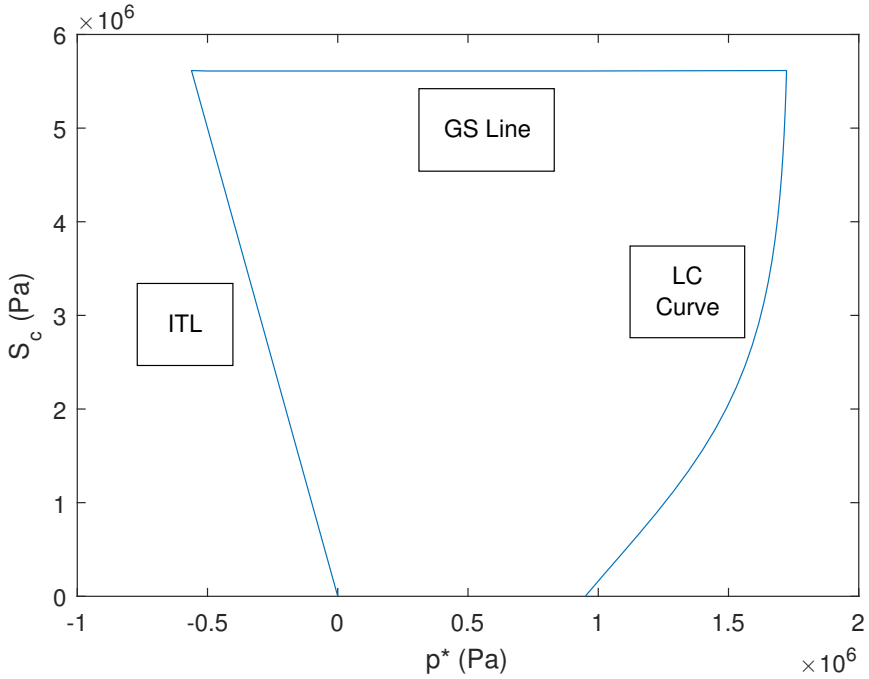

Figure 4.2: Loading collapse (LC) line, grain segregation (GS) line and ice tension line (ITL) in the $p^* - S_c$ plane

state line (CSL) and m is a yield parameter.

$$p_y^* = p_c^* \left(\frac{p_{y0}^*}{p_c^*} \right)^{\frac{\lambda_0 - \kappa}{\lambda - \kappa}} \tag{4.16}$$

where p_c^* is reference stress, κ is the MCC elastic swelling index of the soil mixtures, λ_0 is the unfrozen state MCC compression index and λ is the partially frozen state MMC compression index.

$$\kappa = \frac{1+e}{K} p_{y0}^* \tag{4.17}$$

$$\lambda = \lambda_0 \left[(1-r) exp(-\beta S_c) + r \right] \tag{4.18}$$

where r is a constant which depend on the maximum stiffness of the soil and β is a parameter which controls the rate of change in soil stiffness with cryogenic suction change.

It should be noted that it is supposed by an increase in cryogenic suction, soil compression index, λ will decrease, i.e. soil will become stiffer. On the other hand, MCC swelling index, κ, will stay constant.

As said before, as soil freezes, increase in ice percentage will mean that soil and ice mixture will start to show ice-way behavior; in other words, it will start to show perfect plastic behavior. For accounting this effect, two parameters, namely S_{uw} and m, are in yield criterion, Equation 4.15. In this model as soil freezes, or as S_{uw} decreases, the S_{uw}^m factor can change the shape of the ellipsoid. The way it works is that as temperature decreases and unfrozen water content

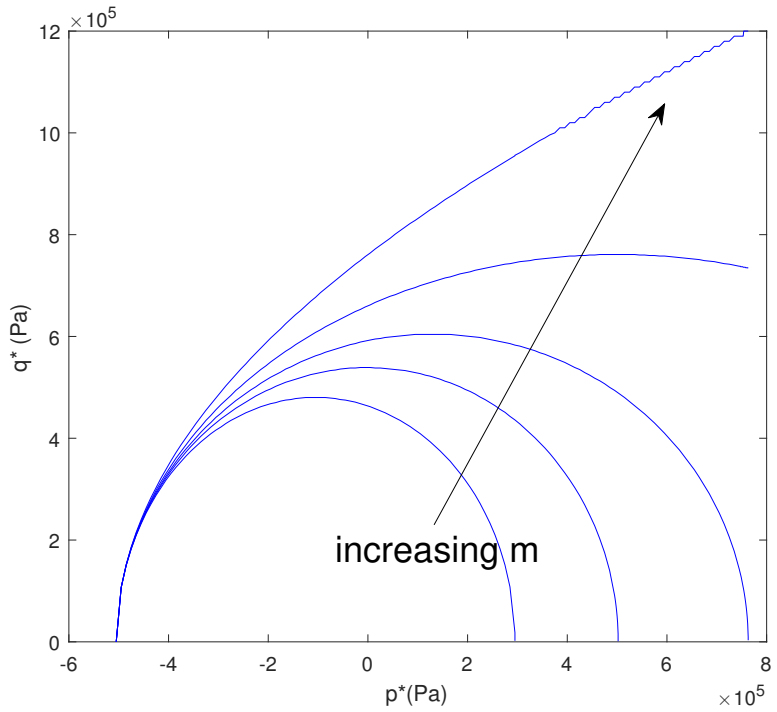

Figure 4.3: influence of parameter, m in the shape yield surface in $p^* - q^*$ plane for when S_{uw}=0.01 (adapted from Ghoreishian Amiri et al. (2016b))

decreases, depending on m, ellipsoid can expand into more plastic ice-like behavior Moreover, an increase in the value of parameter m, as seen in Figure 4.3, will expand ellipsoid in any given constant S_{uw}. Noted that when m is equal to 0, its minimum value, this expansion of ellipsoid is deactivated, and when m is equal to 1, its maximum value, it affects the shape the most.

As talked in Section 2.2.1, an increase in cryogenic suction at a point will lead to grain segregation (known commonly as ice segregation phenomenon). This phenomenon, as discussed in 2.2.1, is primarily controlled by interfacial premelting mechanics. For accounting this behavior of soil, The Grain Segregation, GS, yield criterion is defined as:

$$F_2 = S_c - \frac{S_{c,seg}}{S_{uw}} = 0 \tag{4.19}$$

Where $S_{c,seg}$ is the threshold vale of cryogenic suction which after this value ice segregation phenomenon will start. The grain segregation (GS) line shows this yield surface, and it can be seen, in 2D, in Figure 4.2 and in 3D space in Figure 4.4.

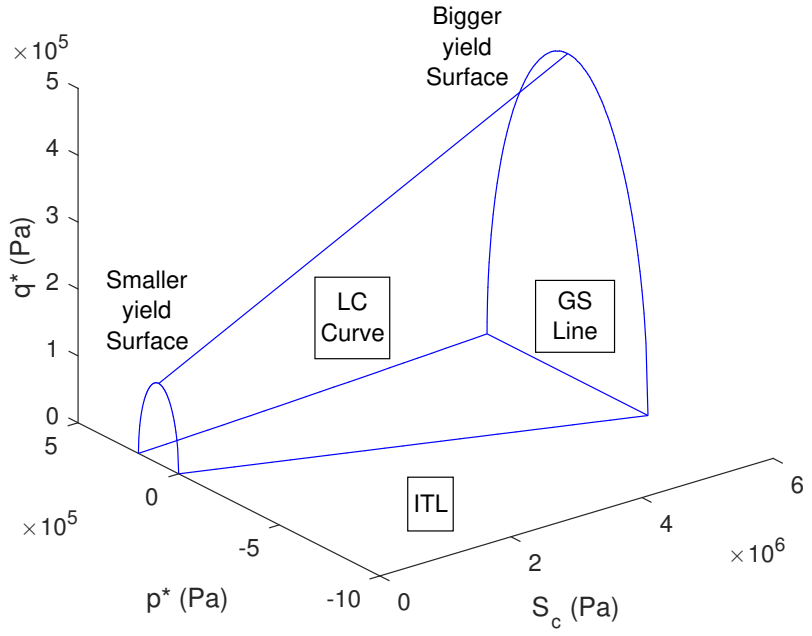

Figure 4.4: Three-dimensional depiction of the yield surface (with m=0)

4.5 Hardening Rules

Just like Modified Cam Clay (MCC) Model, the hardening rule relates plastic volume changes to the corresponding change in preconsolidation pressure. The elastic part of volume change shall be subtracted from total volume change. Hence we can say:

$$d\epsilon = d\epsilon^e + d\epsilon^p \qquad d\epsilon = \frac{\lambda}{1+e}\frac{dp_0^*}{p_0^*} \tag{4.20}$$

$$d\epsilon^e = \frac{\kappa}{1+e}\frac{dp^*}{p^*} \qquad d\epsilon^p = \frac{\lambda-\kappa}{1+e}\frac{dp_0^*}{p_0^*} \tag{4.21}$$

Having above equation in mind, it should be noted that the there is two yield curve, LC curve, and GS line. Movement of each yield surface causes plastic deformation. Hence:

$$d\epsilon_v^p = d\epsilon_v^{mp} + d\epsilon_v^{sp} \tag{4.22}$$

Just like MCC model, mechanical volumetric plastic deformations will be equal to:

$$d\epsilon_v^{mp} = \frac{\lambda-\kappa}{1+e}\frac{dp_y^*}{p_y^*} \tag{4.23}$$

Noted that in mechanical-only loading, if a soil specimen is loaded in an oedometer, a curve like Figure 4.5a will be obtained where at first soil will have a certain rate of change in specific

volume with load increase, called swelling index or κ, until preconsoidation point, then with a higher rate, namely compression index or λ, specific volume of soil will increase with an increase in load. Thermal-only loading will results in a similar curve in v-ln($S_c + P_{atm}$) plane (as seen in Figure 4.5b).

As said before, cryogenic suction will change soil void volume. In better words, this curve means that by variation in cryogenic suction, the void ratio will change and this curve shows how cryogenic suction increments relates to change in specific volume. At first, by increasing cryogenic suction, the specific volume will decrease with κ_s rate and after grain segregation threshold, $S_{c,seg}$, specific volume will increase with λ_s rate with the increase of cryogenic suction. As mentioned before, segregation increases void volume and this is the reason of change of direction of the line after segregation threshold point. After all of these, it can be said that cryogenic suction volumetric plastic deformations will be equal to:

$$d\epsilon_v^{sp} = -\frac{\lambda_s + \kappa_s}{1+e} \frac{dS_{c,seg}}{S_{c,seg} + P_{atm}} \tag{4.24}$$

If a stress increment moves outside of yield surface, plastic deformations will happen and yield surface will move according to the end pint of the stress increment. It supposed that thermal and mechanical loading are coupled together and affect one another. Hence, any plastic strain will move both surfaces. If there is a contractive strain, it means that soil will become stiffer, i.e. move to a higher p^*_{y0}, and LC curve will move outward, and this will push GSL to down. Plastic deformation means that soil particles are collapsing and volume of the void are decreasing, which means that there is less space for frozen water to act, which mean that ice segregation threshold will decrease. The corresponding change in the shape of the of yield surfaces can be seen in Figure 4.6. In other words, it can be said that a mechanical contractive plastic strain will move LC curve to right and GS line down.

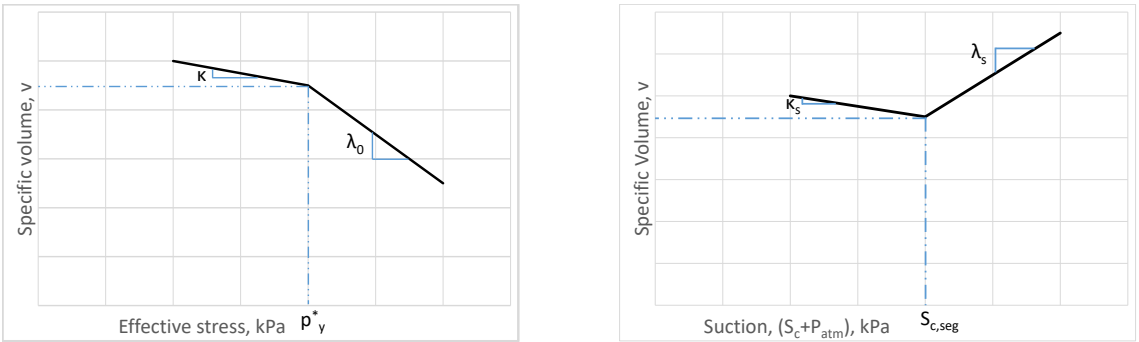

(a) mechanical compression (b) thermal cooling

Figure 4.5: Behavior of soil sample under isotropic loading

Conversely, a plastic dilation, either due to ice segregation or movement of LC curve to

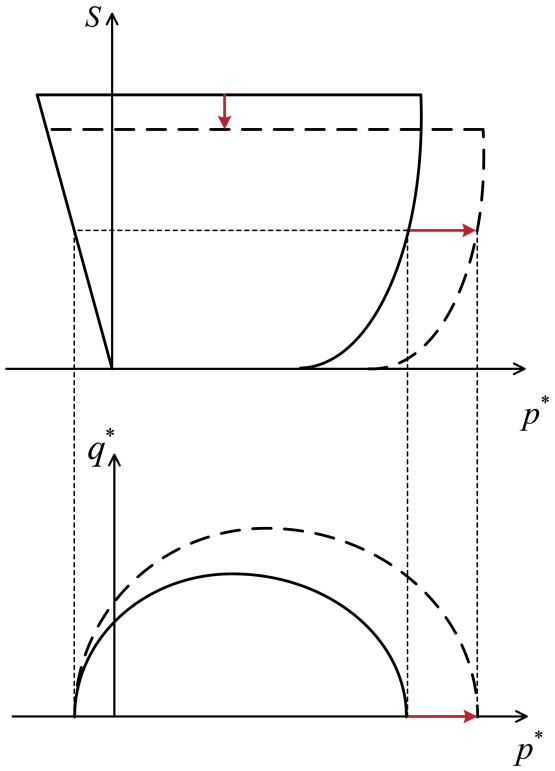

Figure 4.6: Evolution of yield surfaces due to plastic compression in (a) $p^* - S_c$ and (b) $p^* - q^*$ planes(from Ghoreishian Amiri et al. (2016c))

left, will mean that soil will dilate, and the increase in volume will mean that there will be more space and surface for ice to act upon, or in other words, ice segregation threshold will increase, or the GSL will be pushed upward. Moreover, like MCC model, by plastic dilation, yield surface will collapse and p^*_{y0} will decrease and soil will become softer, which means that an inward movement of LC curve will happen. The corresponding change in the shape of the yield surfaces can be seen in Figure 4.7.

Having in mind what has been said so far, hardening rule for LC curve will be written by rewriting Equation 4.23. If, similar equation for plastic deformation due to cryogenic suction variation is considered, it can be said that:

$$\frac{dp^*_{y0}}{p^*_{y0}} = \frac{1+e}{\lambda_0 - \kappa_0}(d\epsilon_v^{mp} + d\epsilon_v^{sp}) \tag{4.25}$$

Expanding above equation gives final equation. Hence, hardening rule for LC yield surface is as follow:

$$\frac{dp^*_{y0}}{p^*_{y0}} = \frac{1+e}{\lambda_0 - \kappa_0} d\epsilon_v^{mp} + \frac{1+e}{\lambda_0 - \kappa_0} d\epsilon_v^{sp} \tag{4.26}$$

Similarly, by rewriting Equation 4.24, hardening rule for GS line can be obtained. If a

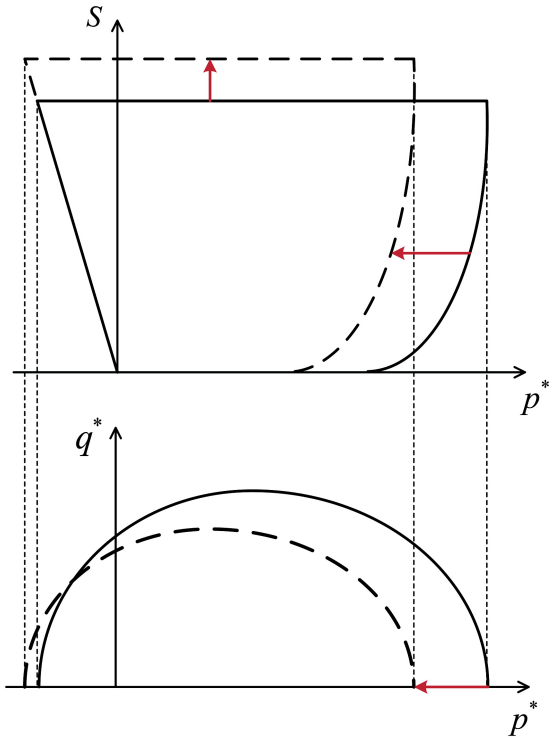

Figure 4.7: Evolution of yield due to ice segregation in (a) $p^* - S_c$ and (b) $p^* - q^*$ planes (from Ghoreishian Amiri et al. (2016c))

similar equation for mechanical plastic deformation is considered, it can be said:

$$\frac{dS_{c,seg}}{S_{c,seg} + p_{atm}} = -\frac{1+e}{\lambda_s + \kappa_s}(d\epsilon_v^{mp} + d\epsilon_v^{sp}) \tag{4.27}$$

$$\frac{dS_{c,seg}}{S_{c,seg} + p_{atm}} = -\frac{1+e}{\lambda_s + \kappa_s} d\epsilon_v^{sp} - \frac{1+e}{\lambda_s + \kappa_s}(1 - \frac{S_c}{S_{c,seg}}) d\epsilon_v^{mp} \tag{4.28}$$

4.6 Flow Rules

A non-associated flow, where another surface other than yield surface is defined as the plastic potential function, will be used for LC yield surface. Flow rule for LC curve can be seen in Equation 4.29. The plastic potential function, Q_1 is given in Equation 4.30. An associated flow rule was used for GS yield surface, which means that same yield surface was used as the plastic potential function. Flow rule for GS line can be seen in Equation 4.31.

$$d\epsilon^{mp} = d\lambda_1 \frac{\partial Q_1}{\partial \sigma^*} \tag{4.29}$$

$$Q_1 = S_{uw}^{\gamma}\left(p^* - \frac{p_y^* + k_t S_c}{2}\right)^2 + \left(\frac{q^*}{M}\right)^2 \tag{4.30}$$

$$d\epsilon^{sp} = -d\lambda_2 \frac{\partial F_2}{\partial S_c} I \tag{4.31}$$

4.7 Model Parameters

Currently there are 27 parameters in total required by the model(see Table 4.1). 17 parameters describe soil parameters; 5 parameters are describing state parameters initializing, and another 5 parameters describing ice and water parameters.

Table 4.1: Model Parameters

Parameter Type	Parameter	Description	Unit
Soil parameters	T_{ref}	Reference Temperature	K
	$E_{f,ref}$	Young's modulus of frozen soil at a reference temperature	N/m^2
	$E_{f,inc}$	Rate of change in Young's modulus with temperature	$N/m^2/K$
	ν_f	Frozen soil Poisson's ratio	-
	G_0	Unfrozen soil shear modulus	N/m^2
	κ_0	Unfrozen soil elastic swelling index	-
	p_c^*	Reference stress	N/m^2
	λ_0	Unfrozen soil compression index	-
	γ	Plastic potential parameter	-
	k_t	Rate of change in apparent cohesion with cryosuction	-
	M	Slope of the critical state line	-
	λ_s	Elasto-plastic compressibility coefficient for cryosuction variation	-
	κ_s	Elastic compressibility coefficient for cryosuction variation	-
	r	coefficient (related to the maximum soil stiffness)	-
	β	Rate of change in soil stiffness with cryosuction	m^2/N
	m	Yield parameter	-

	p_{atm}	Atmospheric pressure	N/m^2
Parameters for initializing state parameters	$(p^*_{y0})_{in}$	Initial unfrozen soil preconsolidation stress	N/m^2
	λ_r	Fitting parameter for unfrozen water saturation curve	-
	Y_{ref}	Reference depth for p^*_{y0}	m
	Δp^*_{y0}	Rate of change in p^*_{y0} with depth	$N/m^2/m$
	e_0	Initial void ratio	-
	$(S_{c,seg})_{in}$	Initial segregation threshold	N/m^2
ice and water parameters	ρ_r	Fitting parameter for unfrozen water saturation curve	N/m^2
	α	Ice thawing Pressure dependency parameter	-
	$T_{0,ref}$	Reference temperature	K
	$p_{0,ref}$	Reference pressure for ice thawing	N/m^2
	K_w	Water bulk modulus	N/m^2

Chapter 5

Boundary Value Problems

Jointed Canada-France Heave Facility

Caen frost heave facility was operated in form of a "large-scale" laboratory experiment in a facility in *Caen*, *France* by Canadian and French researchers. The incentive was to study how soil around a chilled pipe, which carries a cold liquefied gas, will behave. One of the issues with pipelines traversing soils in North of Canada is uneven frost heave. If pipeline is traversing permanent permafrost, where the ground is perennially frozen, pipe will not move vertically. Problem is that in seasonally frozen grounds, where soil freezes in winter and thaws in summer. If during freezing, soil around pipeline heaves, it will move pipeline with it upward and this will not cause a considerable problem by itself, but issue is when pipeline is traversing two types of soil and one type of soil is heaving more than the other. This situation can be seen in Figure 5.1, where chilled pipe is causing two different heaves in the two soil types which will lead to deflection and it might buckle the pipe. This was the incentive behind this joint Canadian-French research center to see how much frost-susceptible soil will heave. The non-frost susceptible soil, here sand, heaves very little, hence in this thesis, main work was focused on the modeling the frost susceptible soil, silt.

5.1 Project Description

This large-scale test facility was constructed at *Station de Gel* at *Le Centre de Geomorphologie* at *Caen*, *France* (Dallimore (1985)). The facility is a 18 m long, 8 m wide and 5 m high, where soil is built to 1.75 m high. All face sides are thermally and hydraulically closed, and bottom of the facility is adiabatic, but it is open hydraulically and water can come in; top side

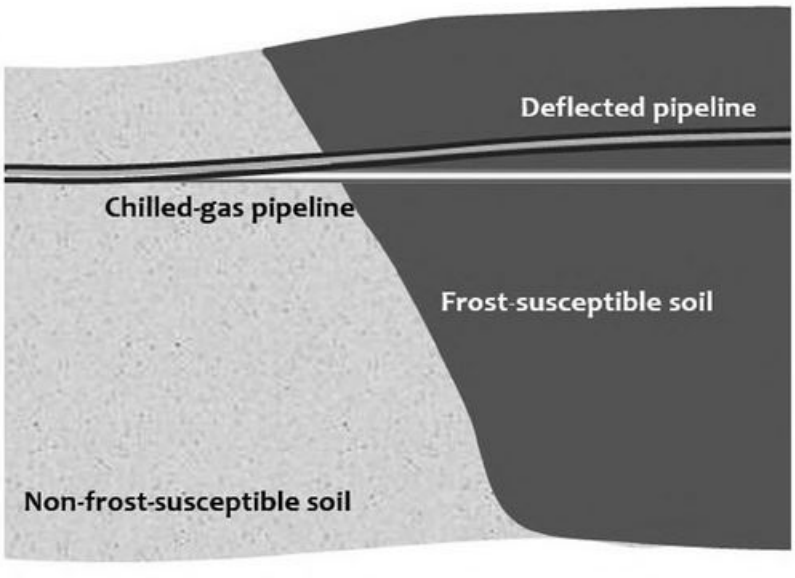

Figure 5.1: Differential heave in a chilled pipe traversing two types of soils (from Selvadurai and Suvorov (2016))

will be thermally loaded by ambient temperature but there will be no water come in from there (schematic view of the facility can be seen in Figure 5.2). Also, a steel pipeline with 5 mm wall thickness, 210 GPa elastic modulus, 27.3 cm diameter was buried 33 cm bellow surface. For creating the same situation as field, two soil with obviously different frost susceptibility was used. For highly frost susceptible soil the Caen silt was used and for low frost susceptible soil SNEC sand was used. There has been laboratory experiments on these two soils and the result of some of these laboratory experiments can be seen in Table 5.1 (for more details look at Dallimore (1985)).

Table 5.1: Caen Silt and SNEC sand measured parameters

	Parameters	
	Caen Silt	SNEC Sand
Permeability ($\frac{m}{s}$)	1.5×10^{-8}	1.5×10^{-5}
Particle Density ($\frac{g}{cm^3}$)	2.665	-
Young's Modulus (MPa)	11.2	20
Dry Density ($\frac{kN}{m^3}$)	15	18.5
Porosity (-)	0.4	–

5.2 Experiment Cycles

There has been two major cycle of freezing, first started in September of 1982 with four freezing and three thawing periods which lasted until May 1989. Second cycle of freezing and thawing periods was run between 1990 and 1993.

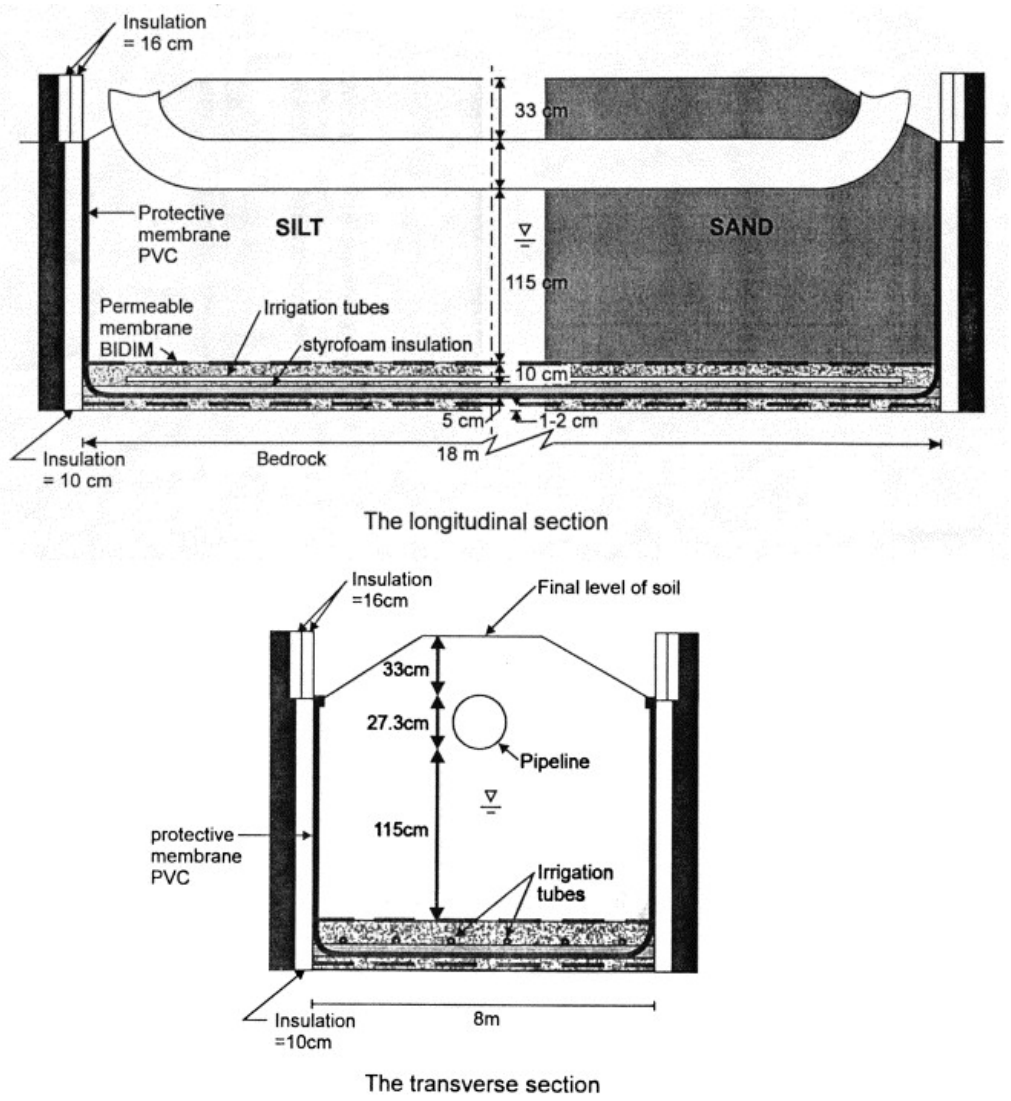

Figure 5.2: Schematic view of Caen test facility (from (Selvadurai et al., 1999))

5.2.1 First Cycle of Freezing

First cycle of freezing is comprised of four freezing periods and each, except the last one, is followed by thawing period. By cooling fans and by a constant flowing of a chilled fluid in pipe, the ambient temperature and pipe temperature, respectively, were kept constant at a desired temperature. Duration and temperature of each of these periods are mentioned in Table 5.2. Here, the main focus will be on the 3rd freezing step.

Table 5.2: Operation condition of site in first freezing cycle (After Williams et al. (1993))

	Event	Duration(Days)	Operation Condition	
			Ambient Temperature(°C)	Pipe Temperature(°C)
First Group of Experiments	1st Freeze	260	-0.75	-2
	1st Thaw	131	4	-2
	2nd Freeze	702	-0.75	-5
	2nd Thaw	136	4	ambient
	3rd Freeze	359	-0.75	-5
	3rd Thaw	85	4	ambient
	4th Freeze	507	-0.75	-5

5.2.1.1 Laboratory data

Only reported and available data for third cycle is the freezing step (Williams et al. (1993) and Williams et al.). No data is available from thawing step. Hence, only the freezing step, which run for 359 days, will be modeled. Heave data for four point on the surface in third freeze period was measured. A schematic view of site situation is given in Figure 5.3. It can be seen that there are 4 “sites” which their heave during the freezing time is measured. Also, it can be seen that how insulation and soil is in place. For simplicity only one half of symmetry line will be modelled.

5.2.1.2 Model Setup

As mentioned in Chapter 3, 2-dimensional FEM program, called *Plaxis 2D* will be used as a numerical tool. A medium mesh was used for whole soil body and a lower coarseness factor around pipe and top boundary was selected to increase accuracy where thermal load will be applied. In Figure 5.4 mesh and elements of the this BVP can be seen.

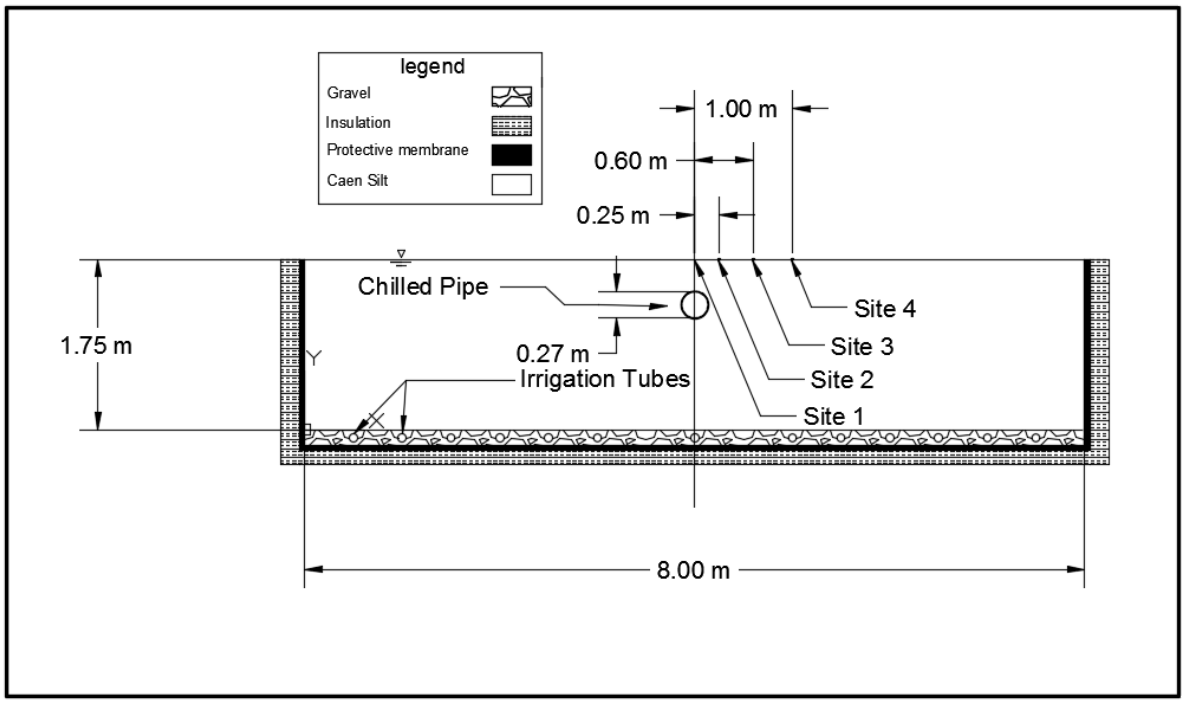

Figure 5.3: Schematic view of the section that will be modeled (Modified after Selvadurai et al. (1999))

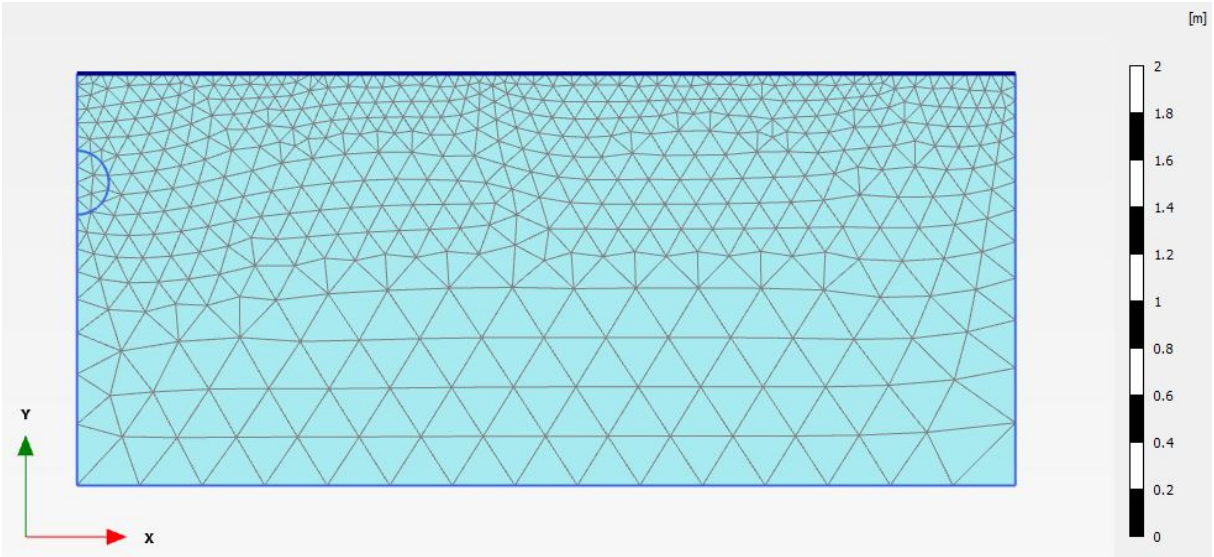

Figure 5.4: Meshing of the model in FE program

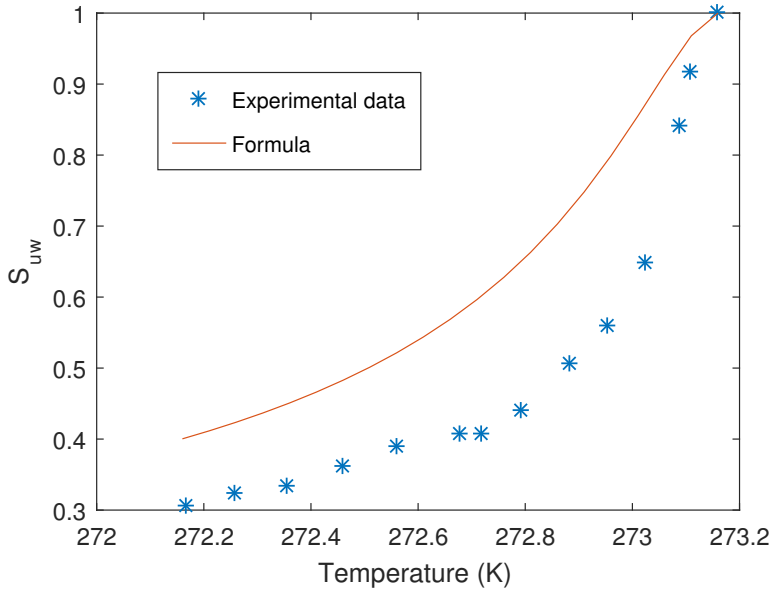

Figure 5.5: Volumetric unfrozen water content for Caen silt

5.2.1.3 Soil Parameters

For running the model, input parameters have to be given to *Plaxis* (as seen before in Table 4.1). Some of these parameters have been measured (as seen in Table 5.1) or they can be calculated indirectly, but rest of the parameters have to be back-calculated.

Beside data from Table 5.1, another lab experiment was unfrozen water content. Based on laboratory experiments, two fitting parameters for unfrozen water content curve for Equation 4.5 can be found. Fitted curve and lab data can be seen in Figure 5.5.

One group of input parameters are thermal parameters of water and ice phases. Here, standard values for water and ice were used (look at Table 5.3). In addition, there are general soil properties that are mostly measured except thermal parameters (Table 5.4). These parameters were back calculated by Bekele (2016) and by using those parameters, a good corresponding between numerical results and lab data can be seen (Figure 5.13).

For accounting the latent heat of ice, in “thermal” tab of soil properties, in “unfrozen content” part, a table has to be given using Equation 4.5 and two fitting parameters obtained. This table has different temperatures and their corresponding unfrozen water content.

5.2.1.4 Constitutive Model Parameters

In Table 5.5, “elastoplastic frozen soil” parameters can be seen. Some of these parameters are calculated from lab tests, and the rest are back calculated. In should be noted that K_w,

Table 5.3: Thermal parameters of water and ice phases

Parameters	Value	Parameters	Parameters
T_{ref} (K)	272.16	α_{water} (1/K)	0.21×10^{-3}
γ_{water} (N/m^3)	10×10^3	T_{water} (K)	277.16
c_{water} (J/kg/K)	4190	c_{ice} (J/kg/K)	2095
$\lambda_{s^1_{water}}$ (W/m/K)	0.6	$\lambda_{s^1_{ice}}$ (W/m/K)	2.2
L_{water} (J/kg)	344×10^3	α_{ice} (1/K)	0.05×10^{-3}

Table 5.4: Soil General Properties

Parameters	Value	Parameters	Value
General tabsheet			
Drainage	Drained	γ_{sat} (N/m^3)	15×10^3
γ_{unsat} (N/m^3)	15×10^3	e_0 (-)	0.66
Groundwater tabsheet			
k_x (m/s)	0.01×10^{-6}	k_y (m/s)	0.01×10^{-6}
Thermal tabsheet			
c_s (J/kg/K)	800	α_x (1/K)	0.04×10^{-3}
λ_s /W/m/K)	0.65	α_y (1/K)	0.04×10^{-3}
ρ_s (kg/m^3)	2650	α_z (1/K)	0.04×10^{-3}
Initial tabsheet			
$K_{0,x}$ (-)	0.9825	$K_{0,z}$ (-)	0.9825

bulk modulus of water, usually 2.2×10^9, is inserted a low value because the current version of FE program used, Plaxis 2016 version, does not take ice bulk modulus into account. So, in this way, the bulk modulus of water is manipulated to compensate this shortcoming of FE program. In addition, pipeline parameters are summarized in Table 5.6, which were measured. For Illustration, initial yield surface is plotted and it can be seen in Figure 5.6.

5.2.1.5 Hydraulic Model

For accounting the cryogenic suction in soil, under "groundwater" tab in soil model, "Van Genuchten" model was used (for more information look at Brinkgreve et al. (2017)). This model has three parameters which relates the saturation to the pressure head, ϕ_p by following formula:

$$S(\phi_p) = S_{res} + (S_{sat} - S_{res}) \left[1 + \left(g_a \, |\phi_p| \right)^{g_n} \right]^{g_c} \tag{5.1}$$

where S_{res} is a residual saturation which part of fluid that stays in the pore, even at high suction heads, S_{sat} is saturation degree under "saturated condition", g_a, g_n, and g_c are fitting parameters and ϕ_p, pressure head, is equal to:

$$\phi_p = \frac{p_w}{\gamma_w} \tag{5.2}$$

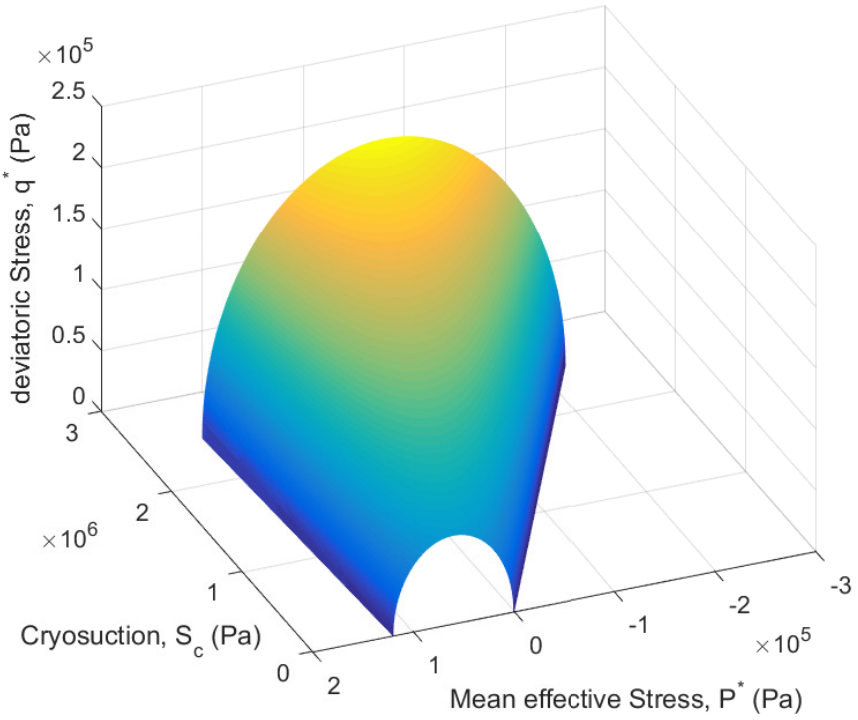

Figure 5.6: Initial yield surface for Caen Silt

Table 5.5: Caen BVP soil input frozen soil model's parameters

Parameters	Value	Parameters	Value
T_{ref} (K)	273.16	β (m^2/N)	0.08×10^{-6}
$E_{f,ref}$ (N/m^2)	50×10^6	λ_r (-)	0.3712
$E_{f,inc}$ (N/m^2/K)	10×10^6	ρ_r (N/m^2)	250×10^3
ν_f (-)	0.45	α (-)	9
G_0 (N/m^2)	4×10^6	T_{ref} (K)	273.16
κ_0 (-)	0.1	p_{ref} (N/m^2)	-395×10^6
p_c^* (N/m^2)	-40×10^3	m (-)	1
λ_0 (-)	0.45	p_{y0}^* (N/m^2)	-120×10^3
γ (-)	1	Y_{ref} (m)	0
k_t (-)	0.09	Δp_{y0}^* (N/m^2/m)	0
M (-)	1.2	e_0 (-)	0.66
λ_s (-)	0.85	$(S_{c,seg})_{in}$ (N/m^2)	250×10^3
κ_s (-)	5×10^{-3}	p_{atm} (N/m^2)	-100×10^3
r (-)	0.6	K_w (N/m^2)	10×10^6

Table 5.6: Pipeline Properties

Parameter	Value	Parameter	Value
Material Type	Elastic	EI (Nm^2/m)	2083
EA_1 (N/m)	1×10^9	w (N/m/m)	340

where, p_w is suction pore stress, γ_w is the unit weight of the pore fluid. As a reminder, in the "ELastoplastic Frozen soil" model, following formula shows unfrozen water content (this formula is written for the first time in Equation 4.5):

$$S_{uw} = \left[1 + \left(\frac{S_c}{\rho_r}\right)^{\frac{1}{1-\lambda_r}}\right]^{-\lambda_r} \tag{5.3}$$

Now, by comparing them one by one, it can be said that $S_{sat} = 1$, $g_a = \frac{\gamma_w}{\rho_r}$, $g_n = \frac{1}{1-\lambda_r}$ and $g_c = -\lambda_r$, S_{res} has to get a value close to 0, but a value of 0.02 is good enough.

Under Van Genuchten hydraulic model, relative permeability is defined as follow:

$$k_{rel}(S) = \ max\left[(S_e)^{g_l}\left(1 - \left[1 - S_e^{\left(\frac{g_n}{g_n-1}\right)}\right]^{\left(\frac{g_n-1}{g_n}\right)}\right)^2, 10^{-4}\right] \tag{5.4}$$

where, g_l is a fitting parameter and S_e, effective saturation, is equal to:

$$S_e \ = \ \frac{S - S_{res}}{S_{sat} - S_{res}} \tag{5.5}$$

By fitting the Equation 5.4 to laboratory data, g_l was found to be 0.5. The fitted curve and laboratory data can be seen in Figure 5.7. This trend of decreasing relative permeability with ice saturation increase is congruent with reality (refer to Section 2.1.1).

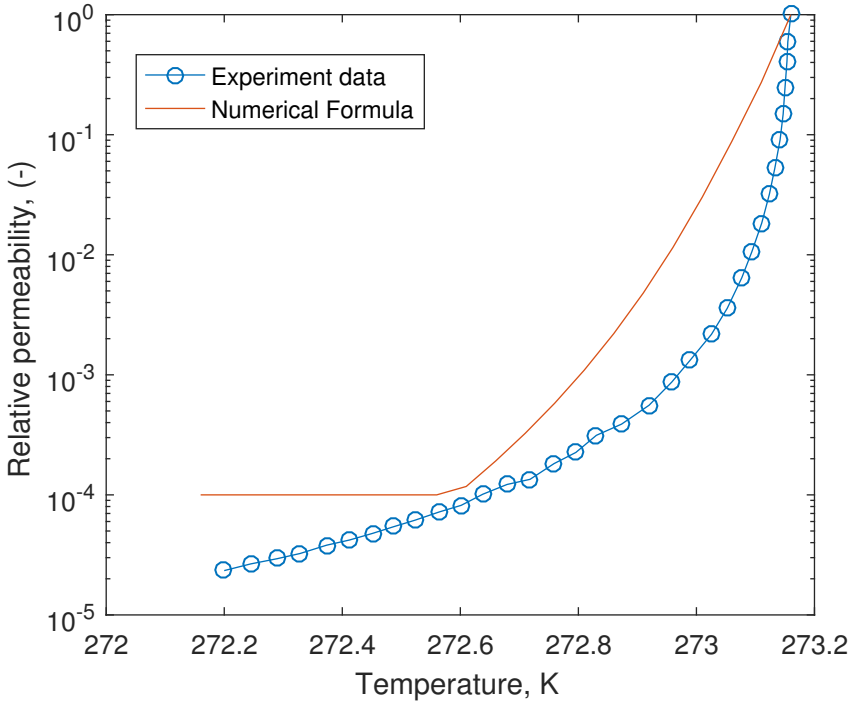

Figure 5.7: permeability of Caen Silt

5.2.1.6 Stages and Control Parameters

For running the simulation with these parameters, some stages with certain control parameters are needed. In Table 5.7, control parameters for this simulation and phases which were used can be seen. In “Initial” stage, stresses are distributed by K0 procedure (with supposing that pipe is not there and instead soil is in place); then in “construction” phase, pipe is “excavated” and pipeline is activated; in “cooling” phase, ambient temperature and and pipe temperature is lowered to experiment values, -5°C for pipe and -0.75°C for ambient; then in “time” phases, without any change in temperature, model was run for duration of the laboratory experiment. The reason that there is more than one “time” phase is that 359 days was such a long time for *Plaxis* to be run in only 10,000 steps, which is the maximum number of steps, so the time was dived up to couple of phases, without any changes in-between.

5.2.1.7 Simulation Results

Finally, after running the simulation, heave at site 1, 2, 3 and 4 can be seen in Figure 5.8, Figure 5.9, Figure 5.10, Figure 5.11, respectively. Moreover, movement of pipe can be seen in Figure 5.12. There is a good correspondence between model results and experiment data. Also, in Appendix B.1, evolution of heave in whole geometry of model is depicted. It can be seen that the point right above the center line of pipe is having the highest heave and heave reduces as moving far away from pipe.

Also, in Figure 5.13, counter plot of temperature can be seen. Result of Numerical calculation is in the background with color shadings, where highest temperature, with maximum of 275.6 K, depicted with warm colors and coldest temperature, is depicted with cool colors, with minimum of 268 K. Result of Experimental results are the black lines on the top of counter shadings (from Smith and Patterson (1989)). They are showing 273.16K isotherm in soil for different times. White line shows the frost line, where below this line there is no ice in pores, and this result belongs to 50th day of experiments which should be compared with first line. By comparing these two lines, it can be seen that there is a good correspondence between simulation and experiment. More plot of temperature distribution in different time steps is reported in Appendix B.3.

Table 5.7: Control Parameters of Caen BVP simulation

	General			Deformation Control Parameters				Numerical Control Parameters		
	Calculation type	Thermal Calculation type	Time interval	Max steps	Tolerated Error	Max load fraction per step	over-relaxation factor	Max Steps	Tolerated Error	over-relaxation factor
Initial	K0 Procedure	Steady State Thermal	0	1000	0.01	-	1.2	-	-	-
construction	Fully coupled flow-deformation	Use previous temperature	360×10^3	1000	0.01	0.5	1.2	1000	5×10^{-3}	1.5
Cooling	Fully coupled flow-deformation	Use previous temperature	36×10^3	10000	0.03	0.01	0.8	10000	5×10^{-3}	0.8
1st time effect	Fully coupled flow-deformation	Use previous temperature	3×10^6	10000	0.04	0.01	0.8	10000	5×10^{-3}	0.8
2nd time effect	Fully coupled flow-deformation	Use previous temperature	5×10^6	10000	0.04	0.01	0.8	10000	5×10^{-3}	0.8
3rd time effect	Fully coupled flow-deformation	Use previous temperature	13.03×10^6	10000	0.035	0.01	0.08	10000	5×10^{-3}	0.8
4th time effect	Fully coupled flow-deformation	Use previous temperature	14×10^6	10000	0.01	0.05	0.8	10000	5×10^{-3}	0.8
5th time effect	Fully coupled flow-deformation	Use previous temperature	3.73×10^6	10000	0.01	0.1	0.8	10000	5×10^{-3}	0.8

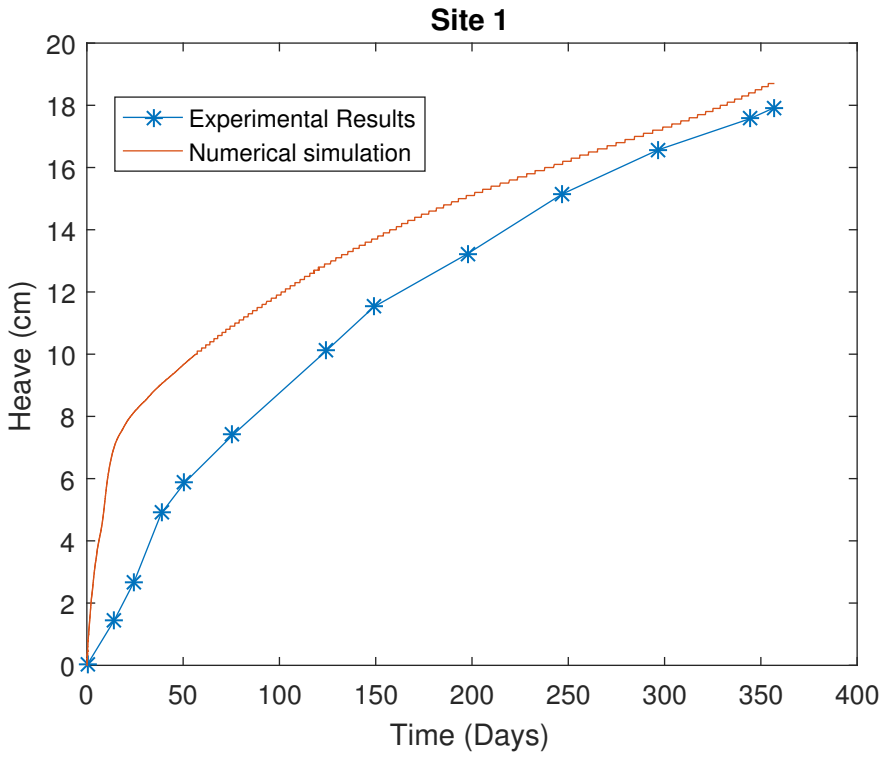

Figure 5.8: Heave at Site 1

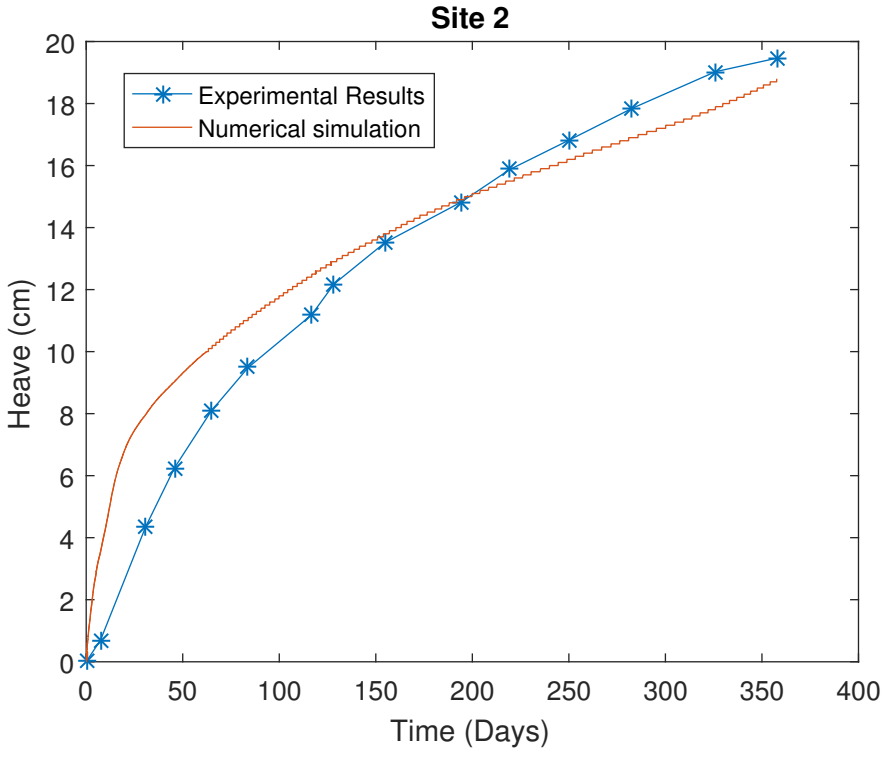

Figure 5.9: Heave at Site 2

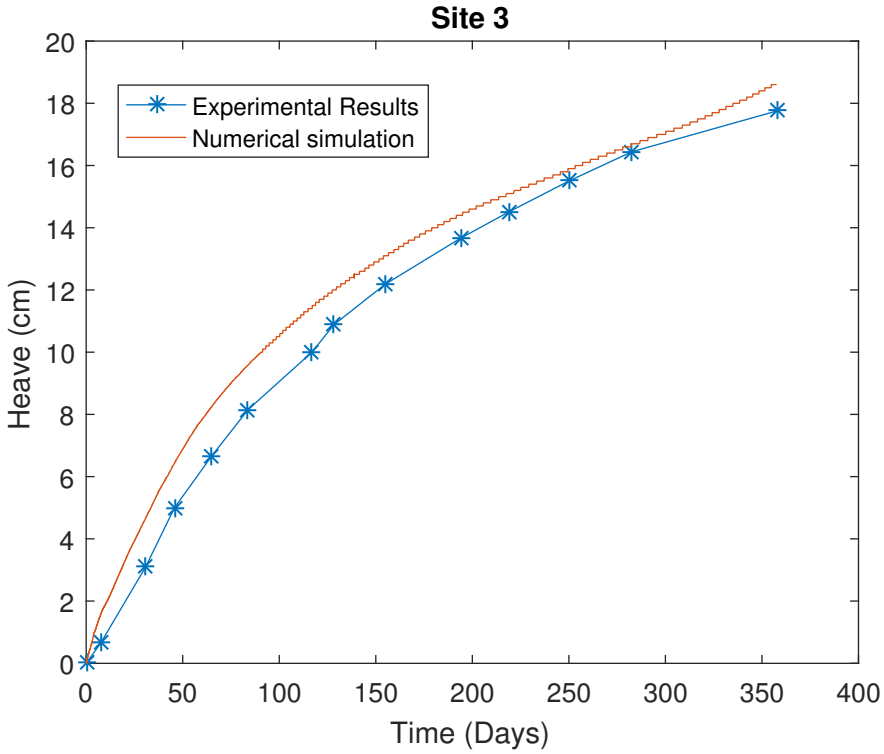

Figure 5.10: Heave at Site 3

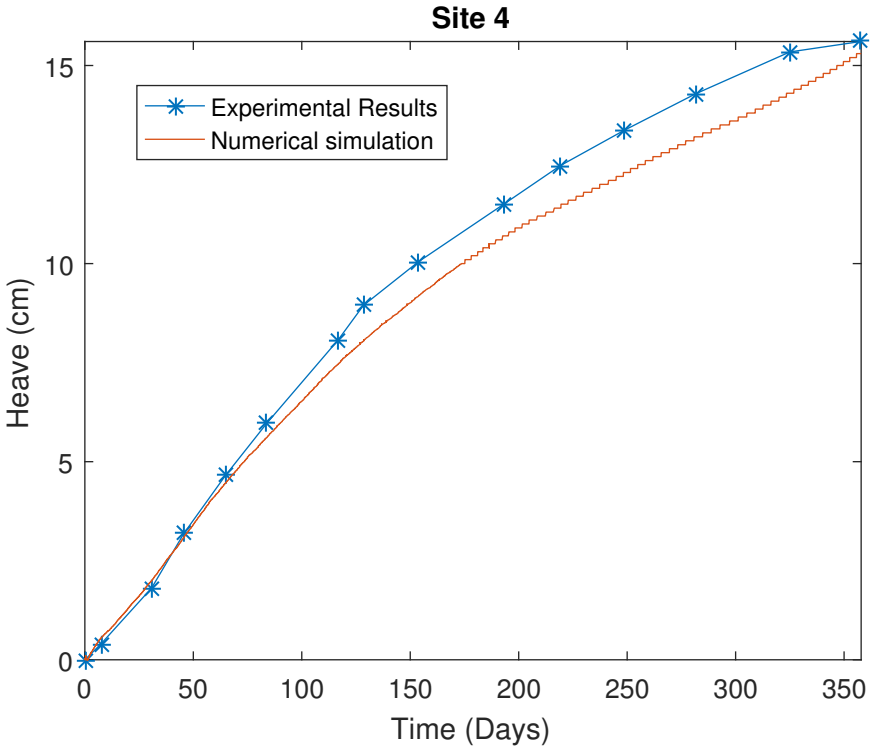

Figure 5.11: Heave at Site 4

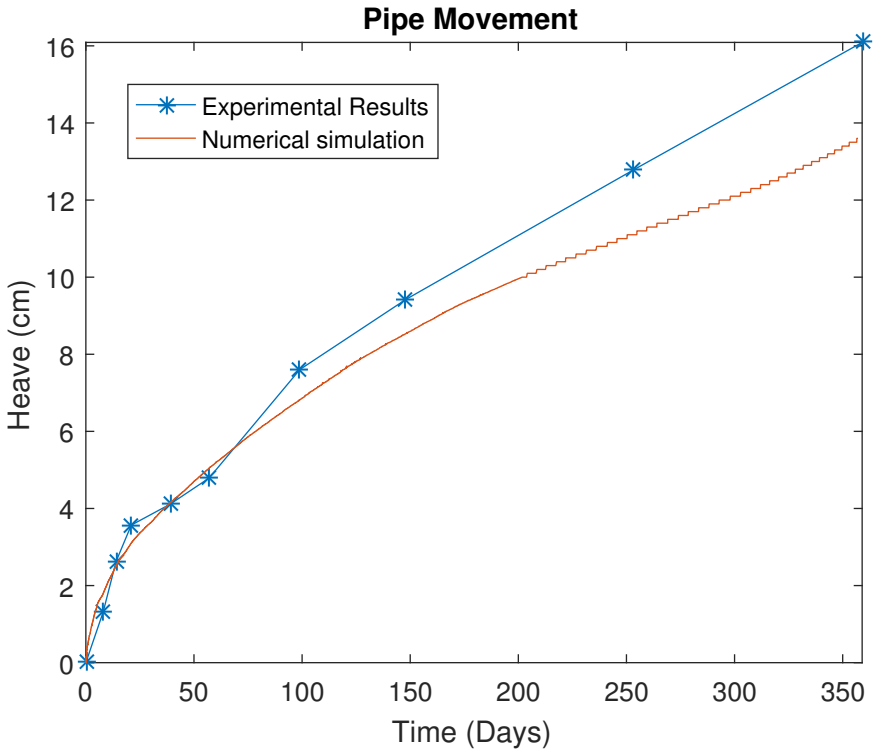

Figure 5.12: Pipe Movement

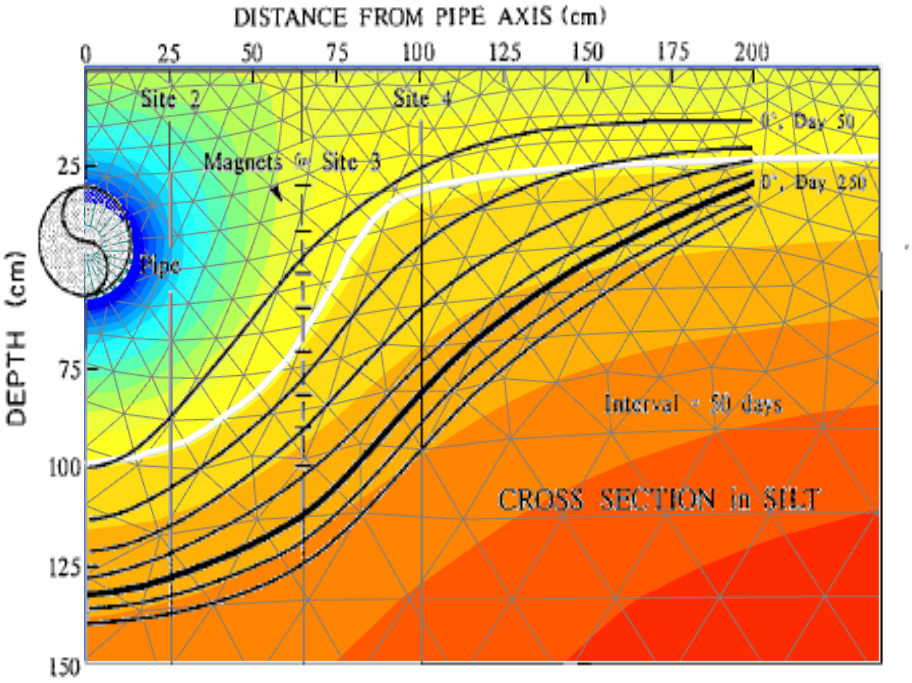

Figure 5.13: Temperature distribution of model vs measured 0°C isotherm after 50 days experimental results are represented with black lines (from Smith and Patterson (1989))

5.2.2 Second Cycle of Freezing

Second cycle of freezing and thawing was run between 1990 and 1993. This cycle had two groups of experiments. Details of first group can be seen in Table 5.8. Firstly, a freezing period was run for 270 days; then a 41 days of further chilling of pipe was done; then pipe temperature was increased and lastly ambient temperature was increased as well.

Table 5.8: Operation condition of site in second freezing cycle (After Williams et al. (1993))

	Event	Duration(Days)	Operation Condition		
			Pipe Temperature(°C)	Ambient Temperature(°C)	
				UF	PF
First Group	Pre-freezing	270	-	-	-8
	1st Freeze	215	-5	-0.75	-0.75
	Pipe chilling	41	-8.5	-0.75	-0.75
	Pipe relaxation	13	+5	-0.75	-0.75
	Thawing	101	+5	+5	-5

5.2.2.1 Laboratory Results

Even though the heave data was recorded for couple of point on the surface of experiment, the only available data was pipe movement. The structure of site is the same except height of trout was increased 30cm from bottom.

5.2.2.2 Model Setup

A medium mesh was used for whole soil body with lower coarseness factor around pipe and top boundary in *Plaxis 2D*. The mesh can be seen in Figure 5.14.

5.2.2.3 Soil Parameters

Same values as Table 5.3 and Table 5.4 were used for water and ice phases, and soil general properties, respectively.

5.2.2.4 Constitutive Model Parameters

In Table 5.9, constitutive model's parameters can be seen. Pipeline for this experiment was 7 mm, a bit thicker, so the new pipline parameter can be seen in Table 5.10.

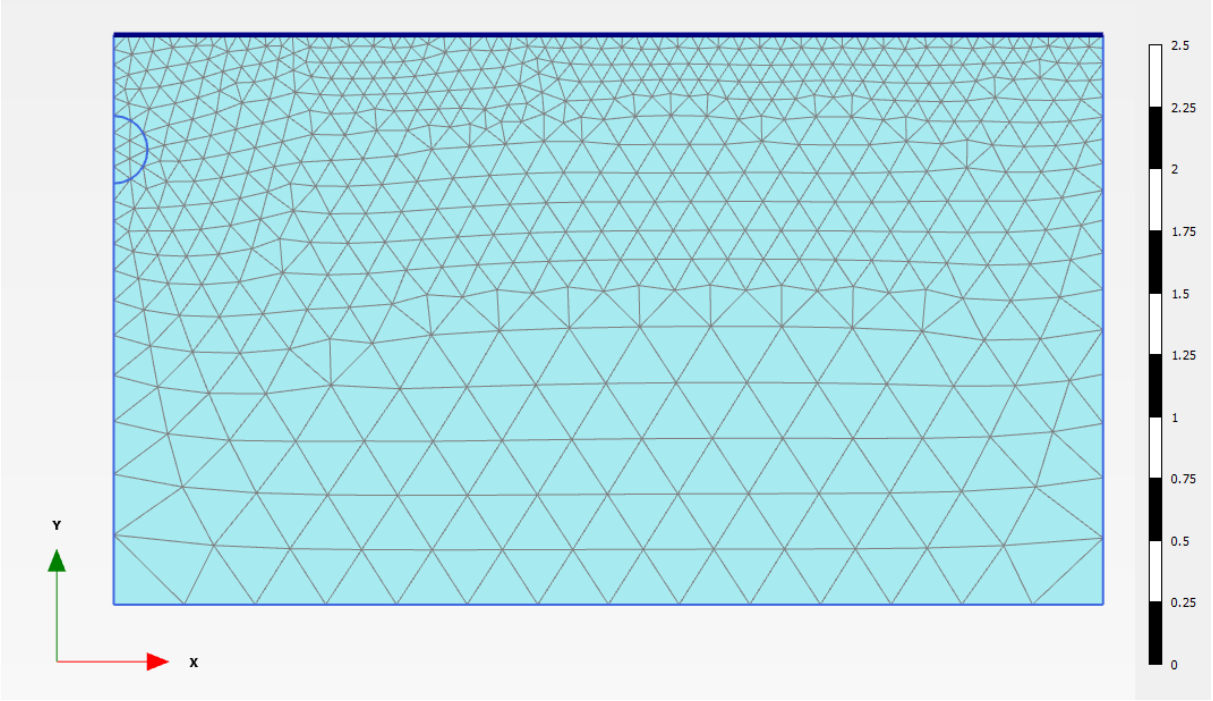

Figure 5.14: Mesh configuration of Caen experimental facility for second freezing cycle

Table 5.9: Caen BVP soil input frozen soil model's parameters

Parameters	Value	Parameters	Value
T_{ref} (K)	273.16	β (m^2/N)	0.08×10^{-6}
$E_{f,ref}$ (N/m^2)	50×10^6	λ_r (-)	0.3712
$E_{f,inc}$ (N/m^2/K)	10×10^6	ρ_r (N/m^2)	250×10^3
ν_f (-)	0.45	α (-)	9
G_0 (N/m^2)	4×10^6	T_{ref} (K)	273.16
κ_0 (-)	0.1	p_{ref} (N/m^2)	-395×10^6
p_c^* (N/m^2)	-40×10^3	m (-)	1
λ_0 (-)	0.45	p_{y0}^* (N/m^2)	-50×10^3
γ (-)	1	Y_{ref} (m)	0
k_t (-)	0.09	Δp_{y0}^* (N/m^2/m)	0
M (-)	1.2	e_0 (-)	0.66
λ_s (-)	0.85	$(S_{c,seg})_{in}$ (N/m^2)	600×10^3
κ_s (-)	5×10^{-3}	p_{atm} (N/m^2)	-100×10^3
r (-)	0.6	K_w (N/m^2)	10×10^6

Table 5.10: Pipeline Properties

Parameter	Value	Parameter	Value
Material Type	Elastic	EI (N m^2/m)	5717
EA_1 (N/m)	1.4×10^9	w (N/m/m)	340

5.2.2.5 Other Parameters

Other parameters, such a hydraulic parameters were chosen the same values as before.

5.2.2.6 Stages and Control Parameters

As said before, some stages with certain control parameters are needed for modeling. In Table 5.11, control parameters for this simulation and phases which were used can be seen. Just like before, in "Initial" stage, stresses are distributed by K0 procedure; then in "construction" phase, pipe is "excavated" and pipeline is activated; in "cooling" phase, ambient temperature and and pipe temperature is lowered to -5°C and -0.75°C, respectively. Next phase,"time effect", is comprised of 7 phases with same control parameters, but with following time intervals: 300×10^3 seconds, 500×10^3 seconds, 330×10^3 seconds, 200×10^3 seconds, 1.2×10^6 seconds, 7.8×10^6 seconds and 8.21×10^6 seconds. Then, in "2nd cooling", pipe temperature was lowered to -8.5°C and in the consecutive phase, "time effect", model was run for 41 days without any temperature changes.

5.2.2.7 Simulation Results

As mentioned, the only available data is the pipe movement (Carlson (1994)). After running the simulation, result for pipe movement can be seen in 5.15. It should be noted that data for thawing stage was available, unlike last case, but due to unknown errors and problems, it was not possible to simulate it. Hence, no simulation data is presented for thawing step.

Table 5.11: Control Parameters of Caen BVP simulation

	General			Deformation Control Parameters				Numerical Control Parameters		
	Calculation type	Thermal Calculation type	Time interval	Max steps	Tolerated Error	Max load fraction per step	over-relaxation factor	Max Steps	Tolerated Error	over-relaxation factor
Initial	K0 Procedure	Steady State Thermal	0	1000	0.01	-	1.2	-	-	-
construction	Fully coupled flow-deformation	Use previous temperature	36×10^3	1000	0.01	0.5	1.2	1000	5×10^{-3}	1.5
Cooling	Fully coupled flow-deformation	Use previous temperature	36×10^3	10000	0.02	0.01	0.8	10000	0.02	0.8
time effects	Fully coupled flow-deformation	Use previous temperature	various	10000	0.02	0.01	0.8	10000	0.01	0.8
2nd cooling	Fully coupled flow-deformation	Use previous temperature	3600	10000	0.02	0.01	0.8	10000	0.01	0.8
time effect	Fully coupled flow-deformation	Use previous temperature	3.539×10^6	10000	0.02	0.01	0.08	10000	0.01	0.8

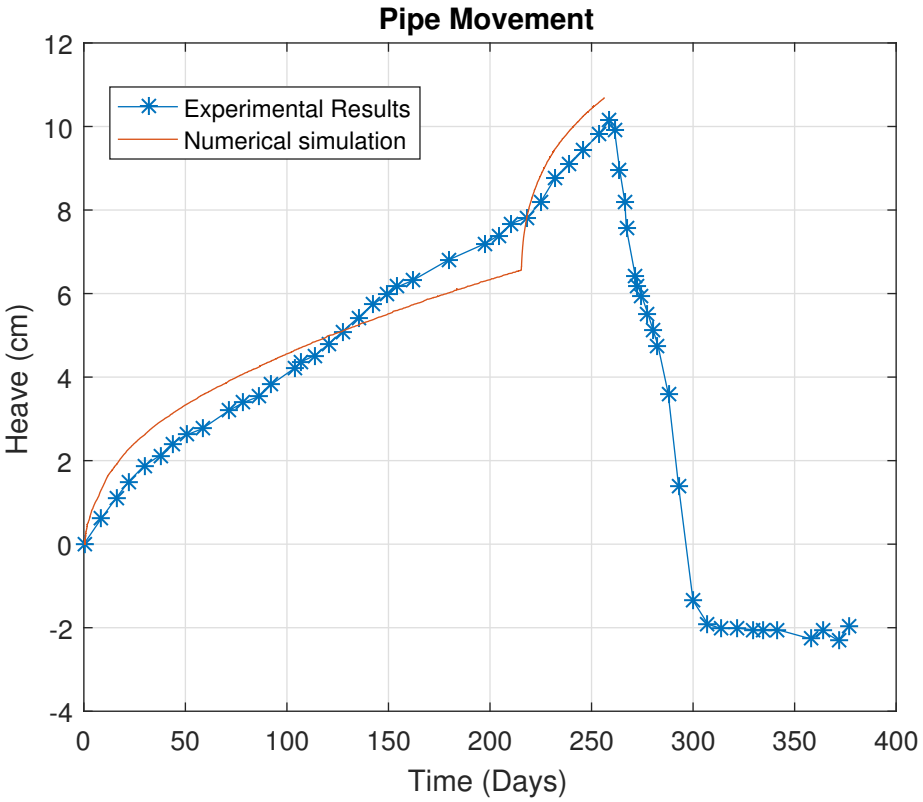

Figure 5.15: Pipe Movement

Chapter 6

Summary and Recommendations for Further Work

Here, a summary and discussion of the work will be presented.

6.1 Discussion

Generally, there has been a good correspondence between numerical simulation results and experimental results. In this chapter, main result will be discussed. It will be shown that this constitutive model is able to model frost heave, ice lens formation and cryogenic suction quite successfully.

6.1.1 Implemented Constitutive Model

Previously, Aukenthaler (2016) has verified and validated soundness of the model, in terms of if it will behave logically under thermal and mechanical loads. He shows that under different loading condition, model shows logical, coherent and good results. Next step after his work was to test the model under real boundary value conditions. Here in this thesis, two boundary value problem (BVP) was run. For both of them, as mentioned, a good corresponding between experimental results and simulation results was obtained.

The process of work was to firstly put in laboratory soil parameters in the model, then try to put logical values for other parameters, then through back-calculation, tune those parameters. Since these analyses are coupled THM simulation, where three sets of equation are being solved

at the same time, and there is a high level of non-linearity. Moreover, simulations were heavy, sensitive and time-consuming.

Even though some of the parameters were back calculated, unlike validation phase some of parameters have to stay fixed. This helped to improve the robustness of the model through some improvement in the code of model, which is written as a DLL file for *Plaxis*, by developer of the codes, S.A. Ghoreishian Amiri.

6.1.2 Boundary Value Problems

In the first example, where a 359-days freezing was conducted on the Caen silt, good correspondence between experimental result and numerical result was obtained. Firstly, as seen through Figures 5.8 to 5.11, which are heave data for 4 sites at the top, simulation shows good correspondence with experimental heave. Pipe movement, as seen in Figure 5.12, is a bit different; the pipe movement could have been increased by tuning some parameters, but then heave at 4 sites would start to show bad results, so it was decided to have heave at this level. In Appendix **??**, for all stages, the deformed mesh is shown, where it can be seen that at the top of center line of pipe, the heave is maximum and it is reduced as we move further away from pipe.

Temperature distribution for 50th day can be seen in Figure 5.13. It shows a good correspondence with measured 273.16 K isotherm line, like the work of Bekele (2016). For better representation of temperature and how it evolves during the simulation, reader can refer to Appendix B.3. Moreover, the ice content is increasing with temperature drop and its evolution can be seen in Appendix B.2. It can be seen that ice starts to form initially from both top boundary and pipe boundary and as time passes, it progresses further down. Also, suction of water into freezing area can be seen in Appendix B.7.

As said in Section 4.4, in this model, soil segregates as it freezes, and it can be seen in Appendix B.3, as temperature drops and ice starts to form, void ratio in frozen areas increases.

As said in Section 4.5 and shown in Figure 4.7, as soil freezes, soil unfrozen state preconsolidation pressure will decrease and its segregation threshold will increase. Evolution of these two parameters in freezing time can be seen in Appendix B.6 for former and Appendix B.5 for later.

In the second example, soil underwent two steps of freezing, one with lower pipe temperature, and then two steps of thawing. Unfortunately, the only available data for this one was the pipe movement. As seen in Figure 5.15, results of the freezing steps shows a good correspondence with experimental results. Due to unknown reasons, it was not possible to model the thawing part with correct results. Detailed result of this simulation, unlike last one which was

summarized in Appendix B, is not reported.

6.2 Summary and Conclusions

Elastoplastic Frozen Soil model is able to simulate water suction upon freezing, ice segregation, frost heave, and ice lens formation. By running two BVPs, it was shown that the model is able to simulate these phenomenons. Some changes in code was done to improve robustness of the code and model (S.A. Ghoreishian Amiri, personal communication, April 2017). The model is tested successfully for freezing processes, but it still has to be tested for thawing processes.

6.3 Recommendations for Further Work

Recommendation for further work can be categorized into three parts:

- short-term
  - Problem with simulation of thawing part should be found and to see thaw weakening and settlement.
  - An example other than chilled pipe has to be run to check robustness of the model (like Zhang and Kushwaha (1998))
- medium-term
  - Running a BVP with rate-dependant version
- long-term
  - Taking into account salinity and gaseous phase in the constitutive model

Appendix A

Acronyms

AGF Artificial Ground Freezing

BBM Barcelona Basic Model

BVP Boundary Value Problem

CSL Critical-State Line

FEA Finite Element Analysis

FEM Finite Element Methods

GSL Grain Segregation

ITL Ice Tension Line

LCL Loading Collapse

MCC Modified Cam-Clay

NTNU Norwegian University of Science and Technology

OWS Ottawa banding Sand

WLT glacial tilt from West Lebanon, New Hampshire

Appendix B

Result of Numerical Simulation

Simulation of First Group, Third Freezing Step

B.1 Heave

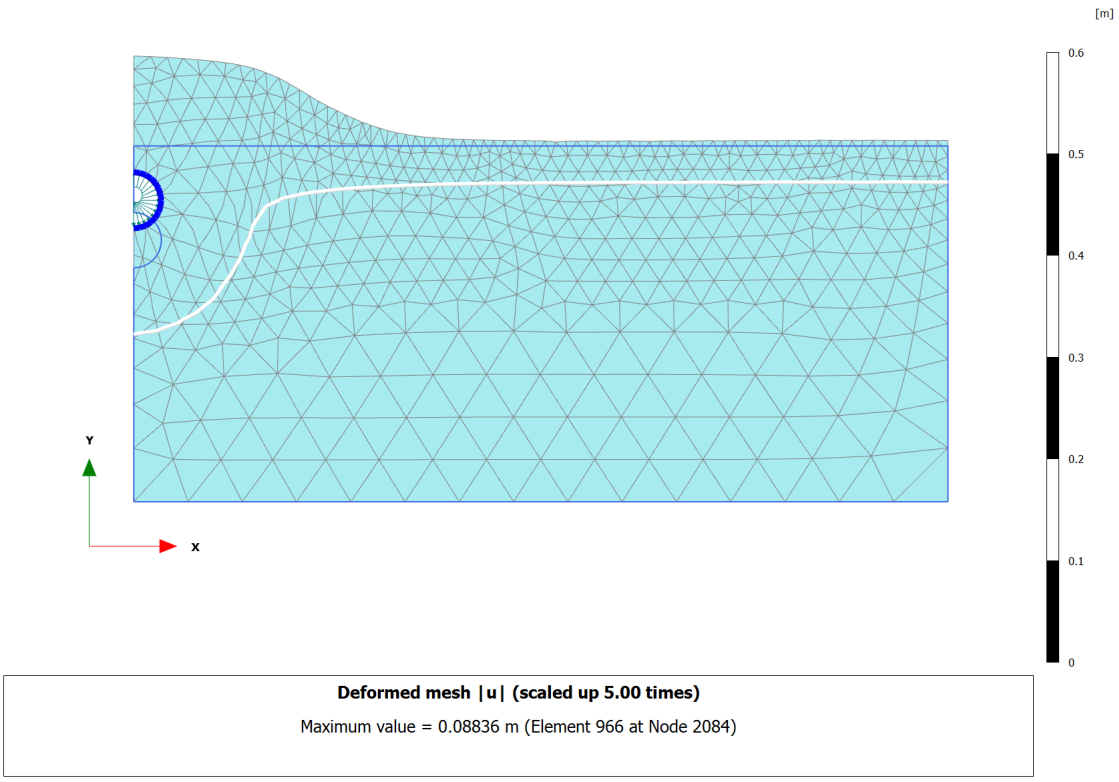

Figure B.1: Heave at the end of "1st Time effect" phase

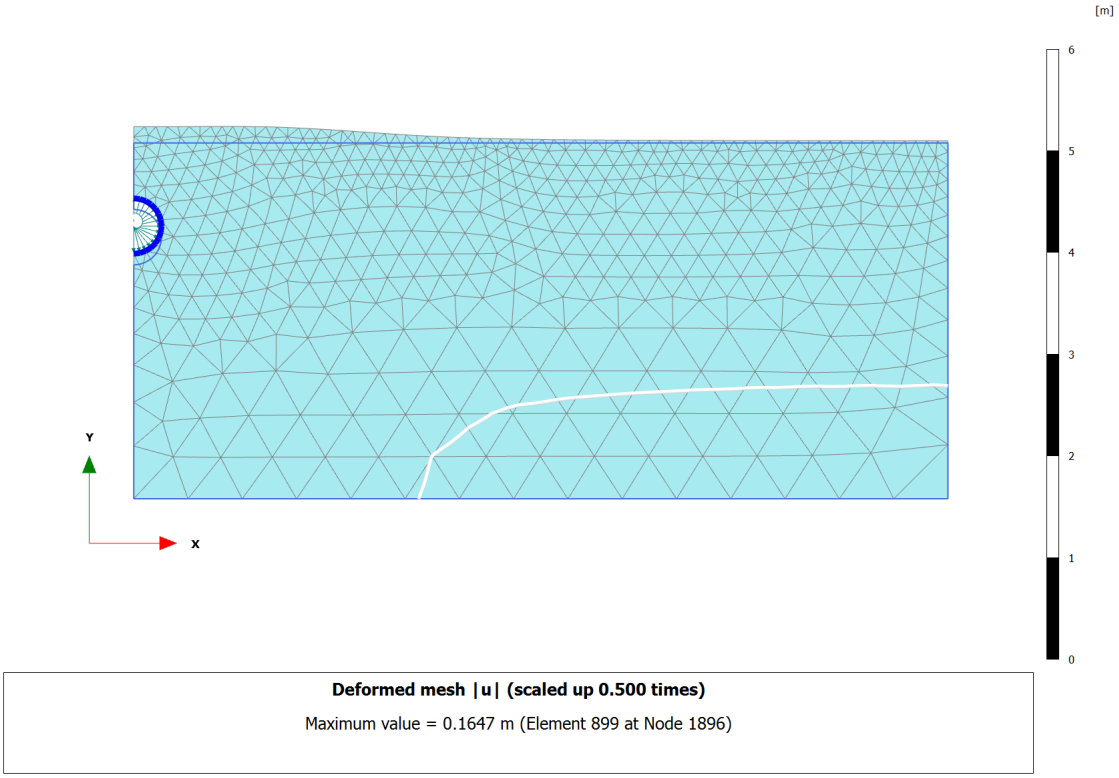

Figure B.2: Heave at the end of “3rd Time effect” phase

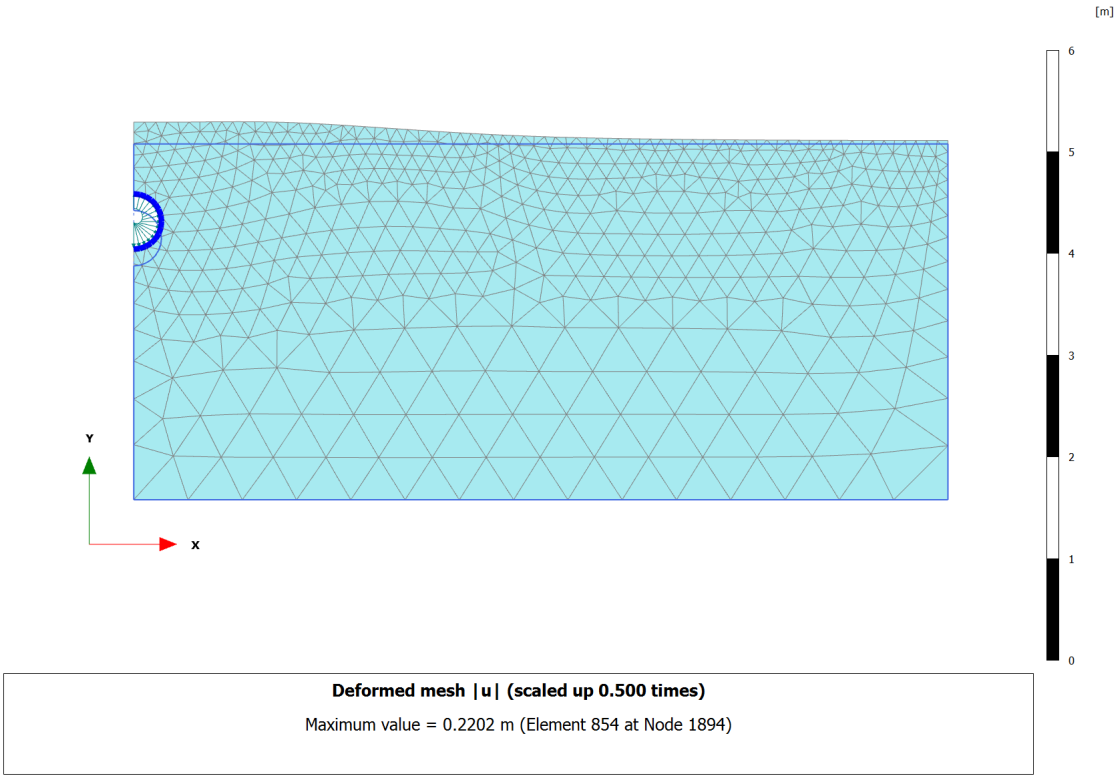

Figure B.3: Heave at the end of “5th Time effect” phase

B.2 Ice Saturation

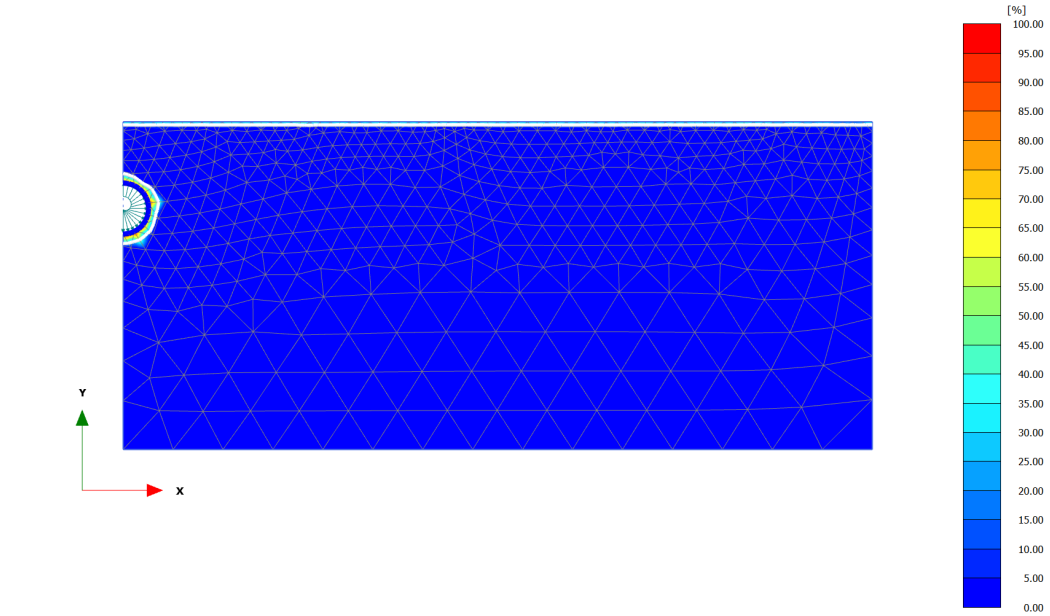

Figure B.4: ice content at the end of “cooling” phase

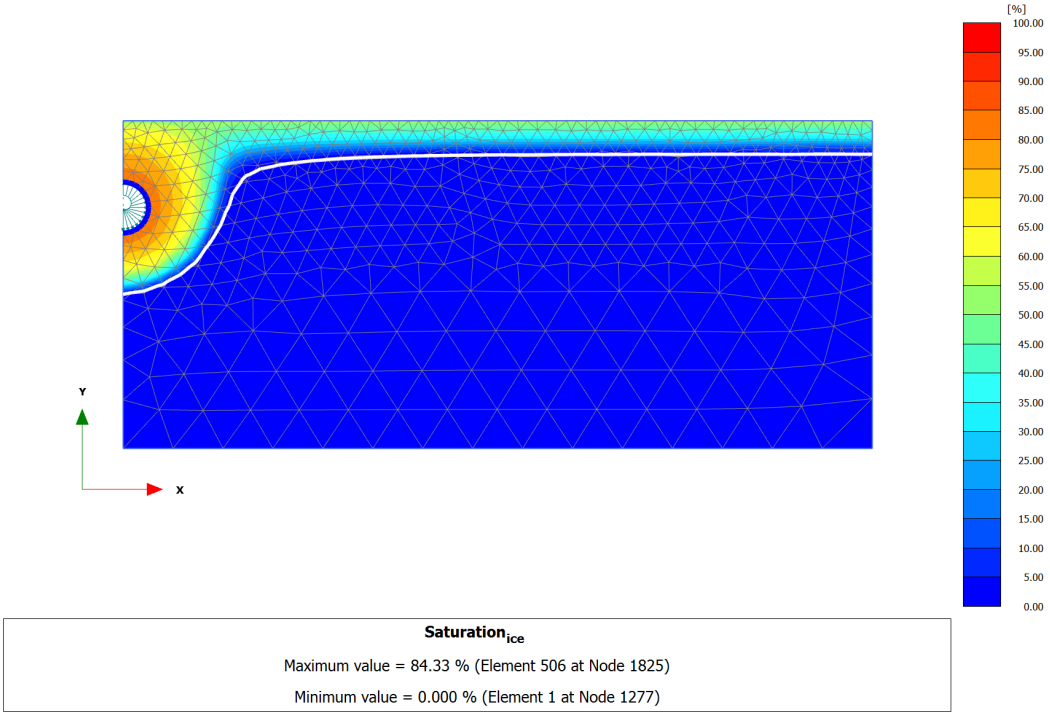

Figure B.5: ice content at the end of “2nd Time effect” phase

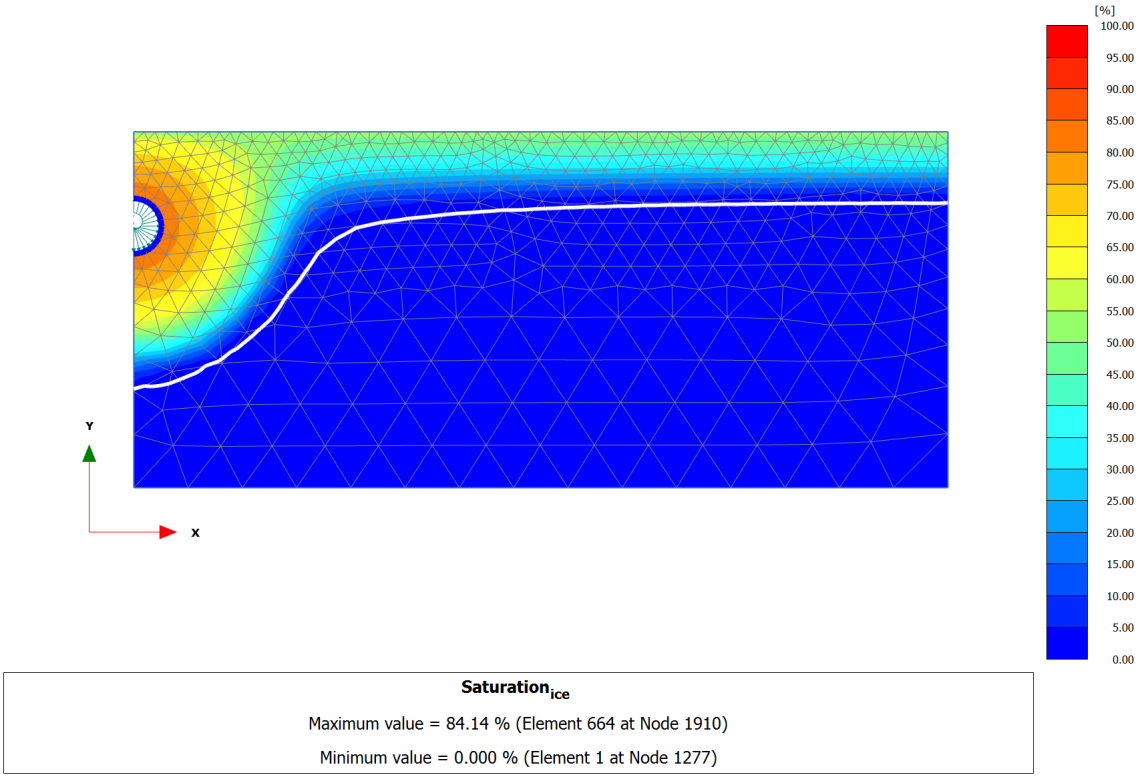

Figure B.6: ice content at the end of “3rd Time effect” phase

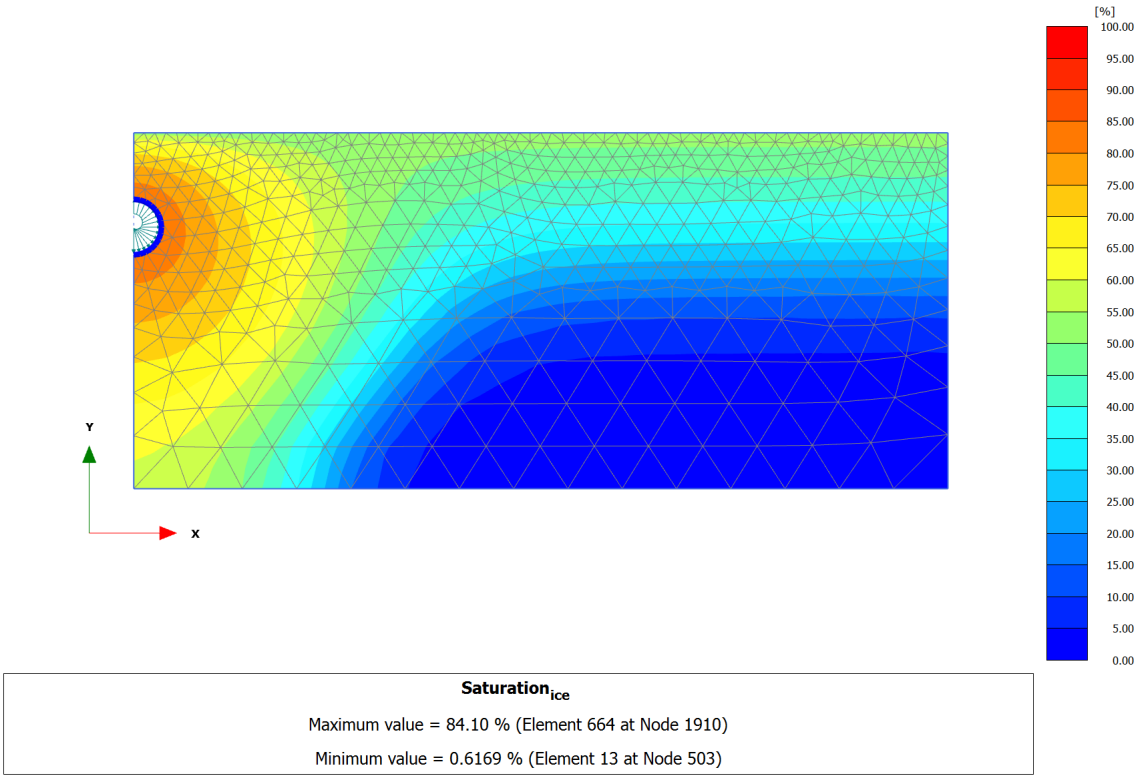

Figure B.7: ice content at the end of “5th Time effect” phase

B.3 Temperature Distribution

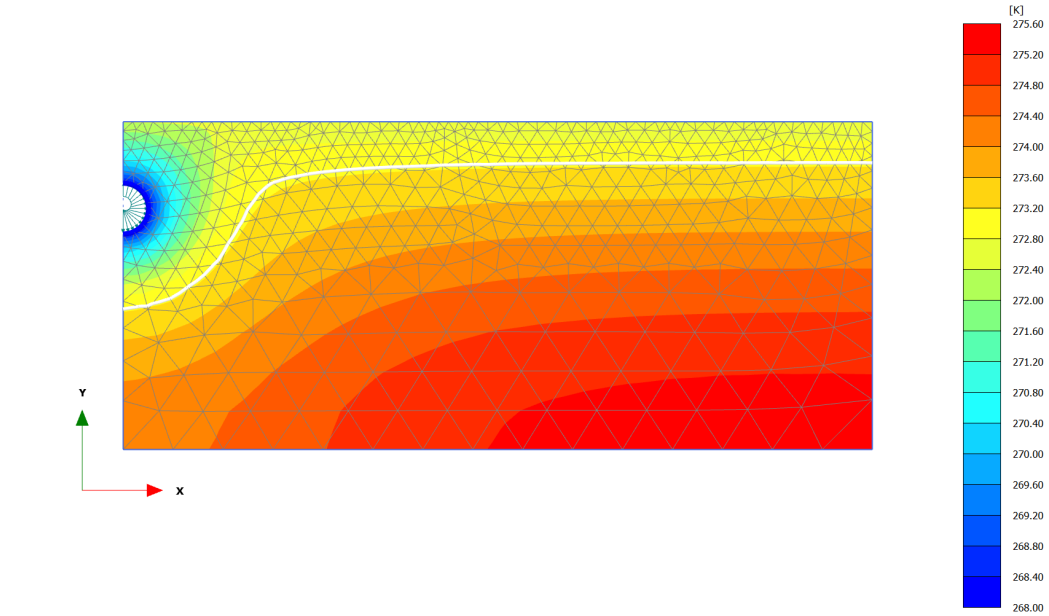

Figure B.8: Temperature distribution after 50 days

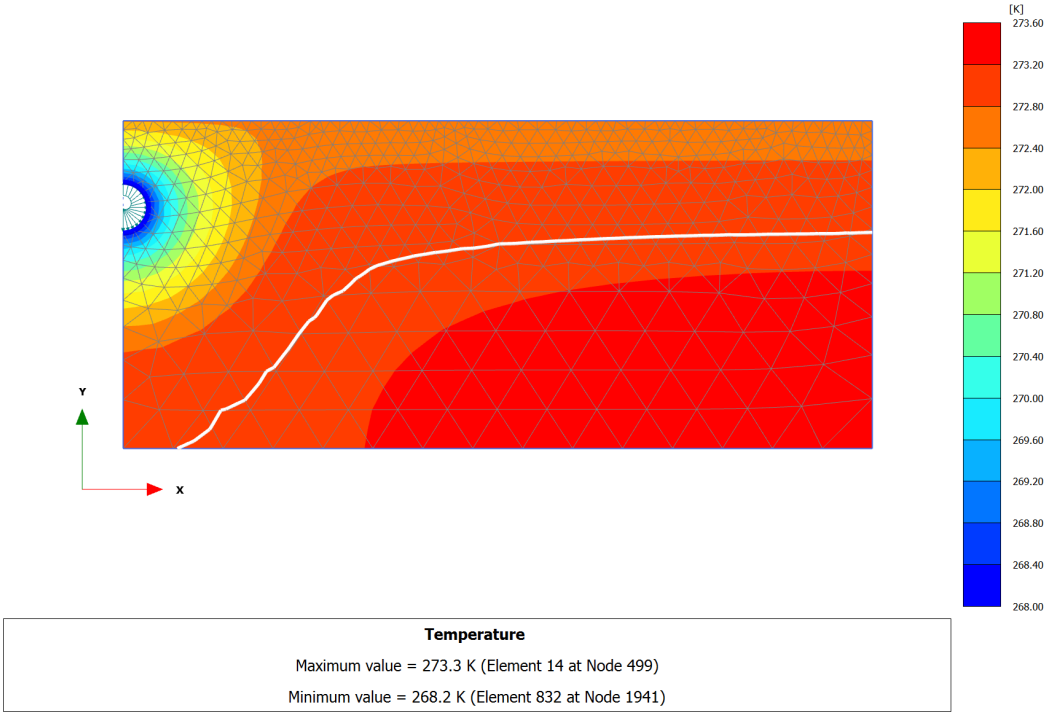

Figure B.9: Temperature distribution after 150 days

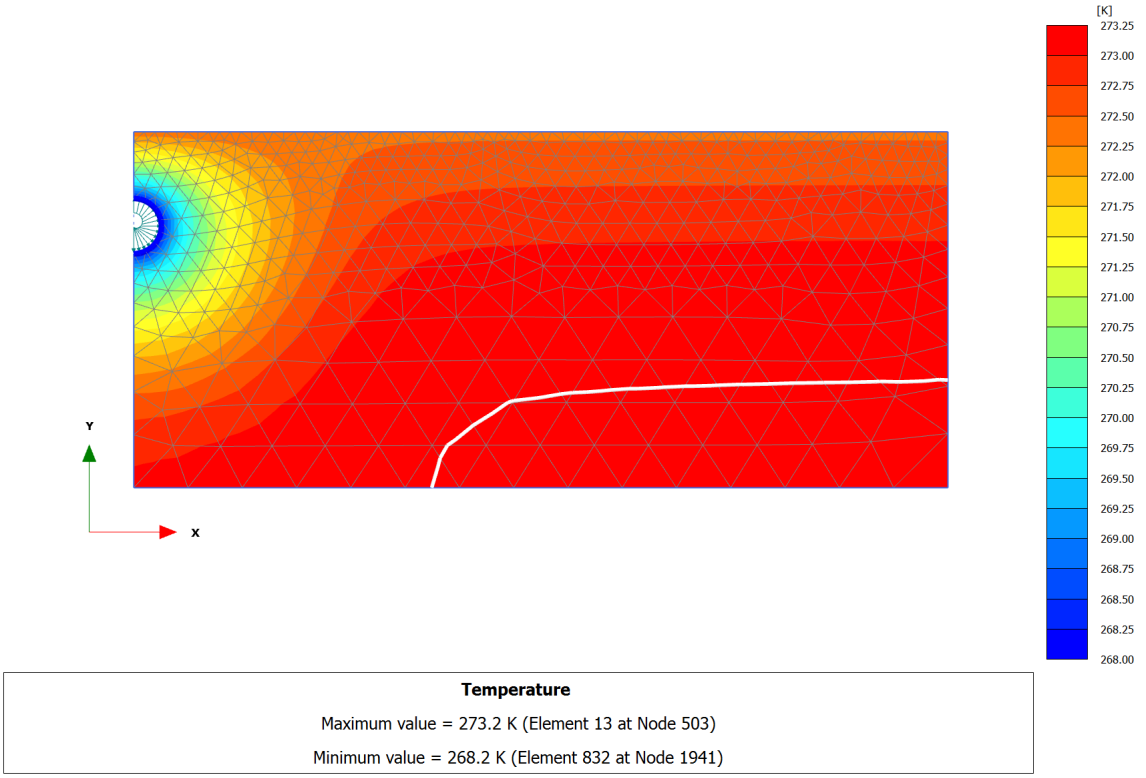

Figure B.10: Temperature distribution after 250 days

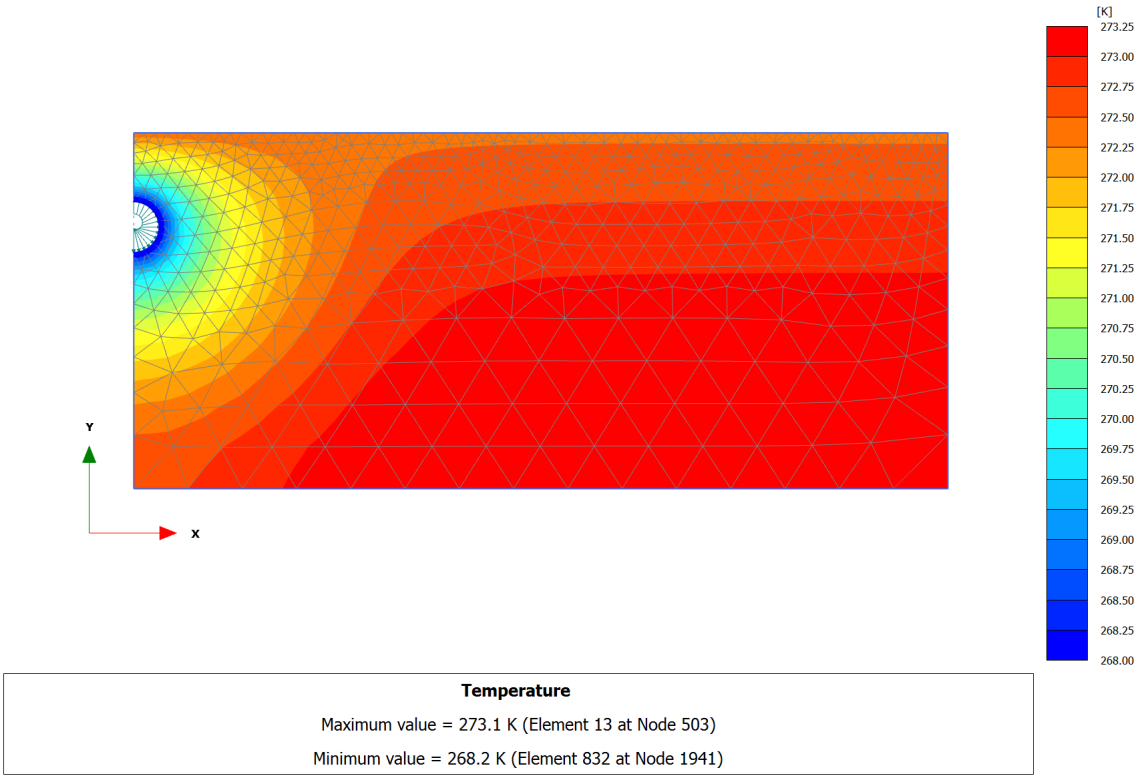

Figure B.11: Temperature distribution after 359 days

B.4 void ratio

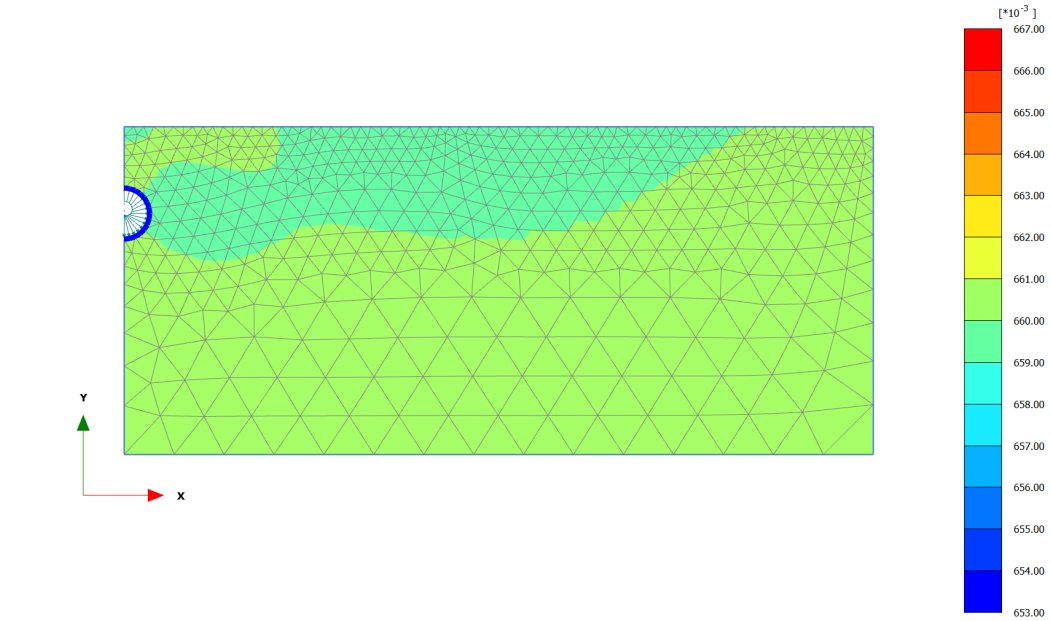

Figure B.12: Void ratio distribution in “construction” stage

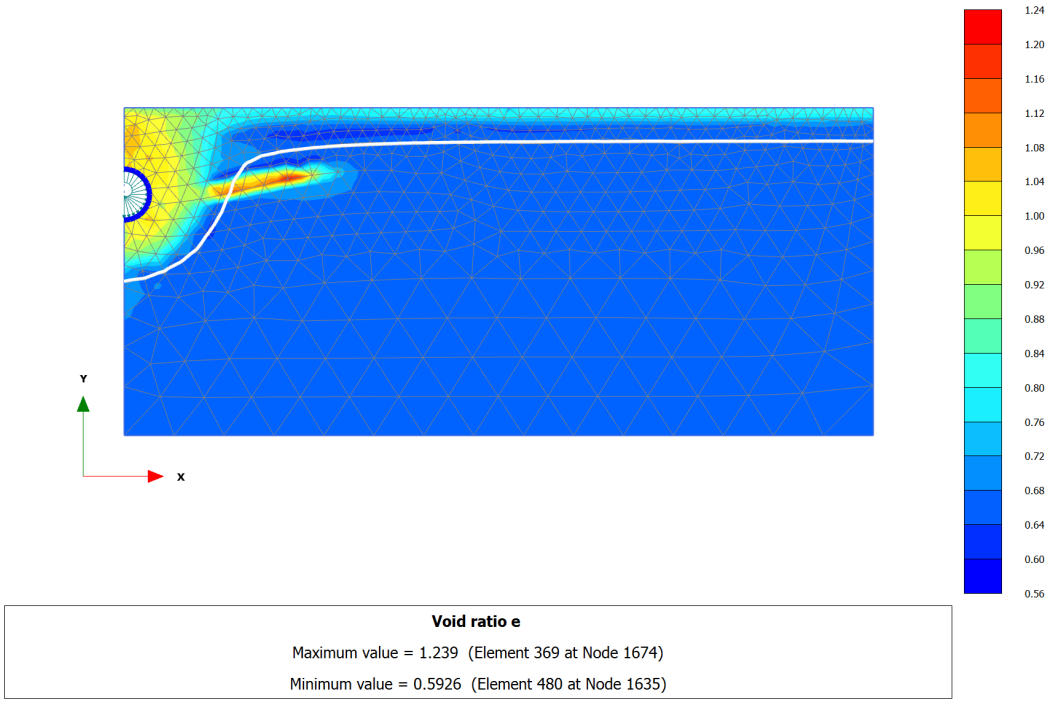

Figure B.13: Void ratio distribution in “1st time effect” stage

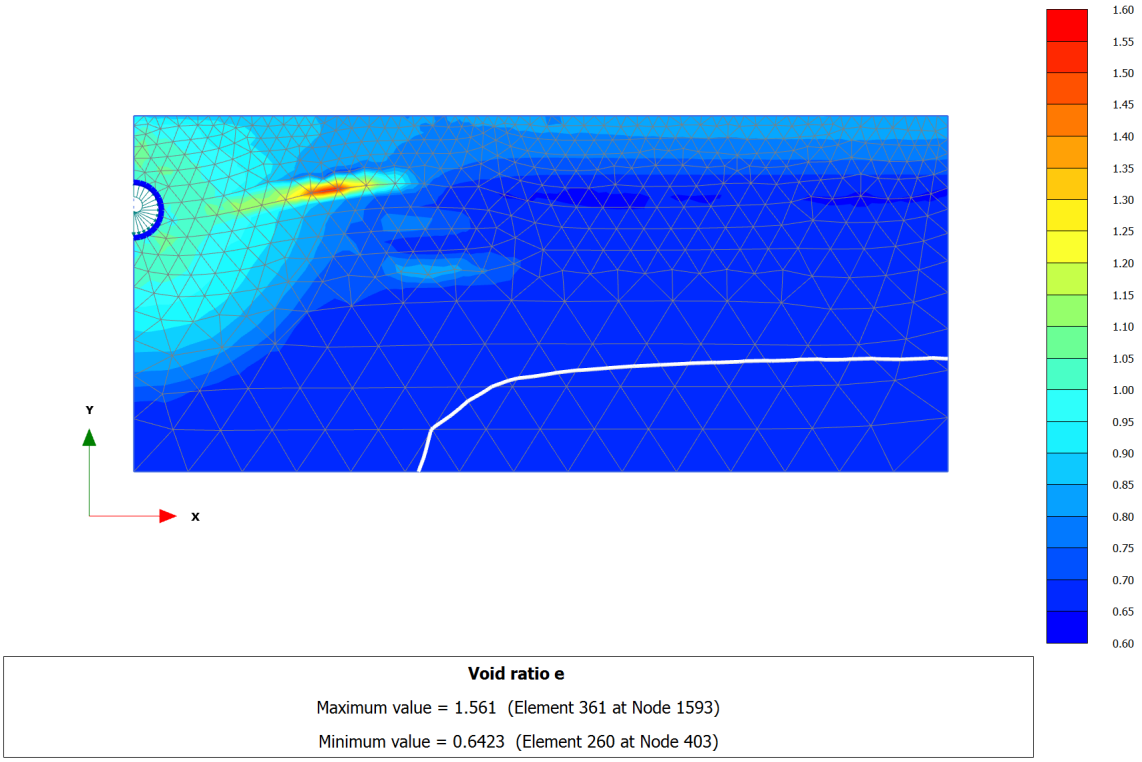

Figure B.14: Void ratio distribution in “3rd time effect” stage

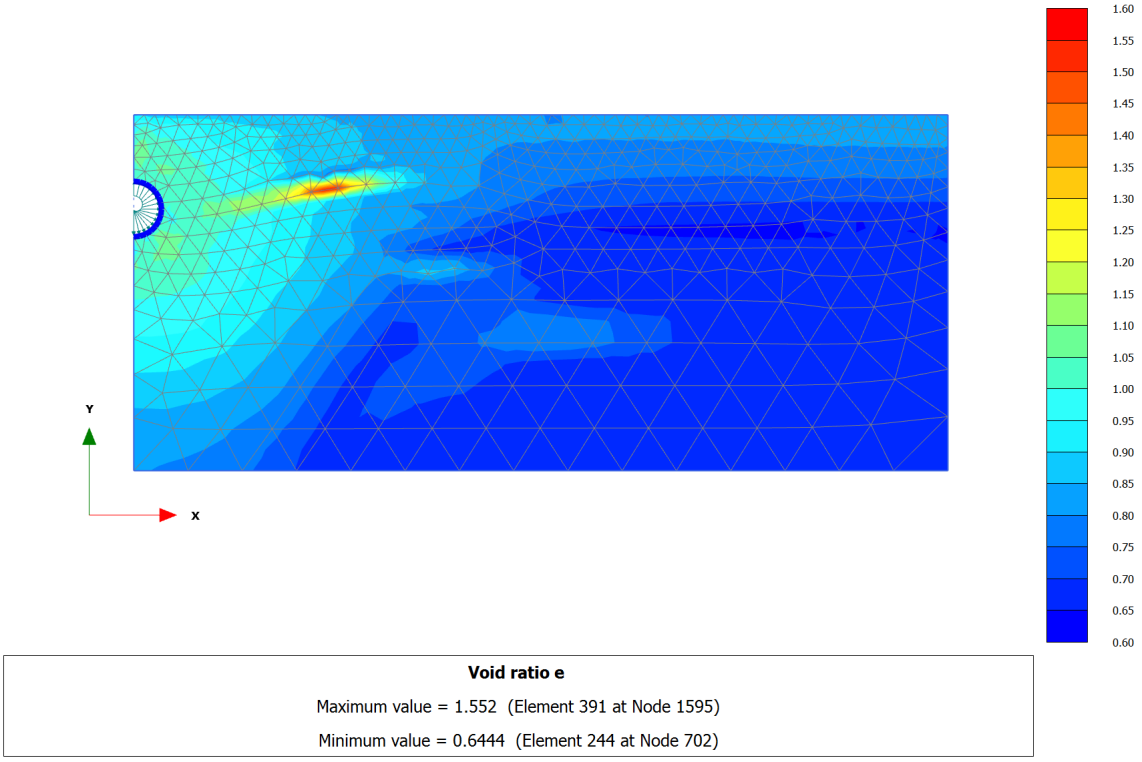

Figure B.15: Void ratio distribution in “5th time effect” stage

B.5 Segregation Threshold

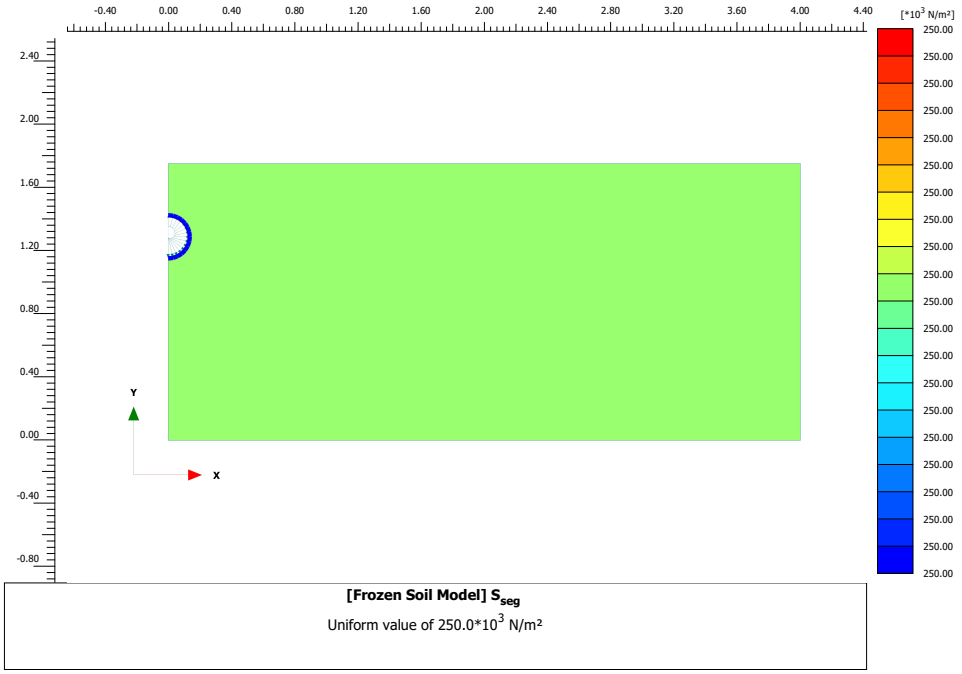

Figure B.16: Segregation threshold distribution in “construction” stage

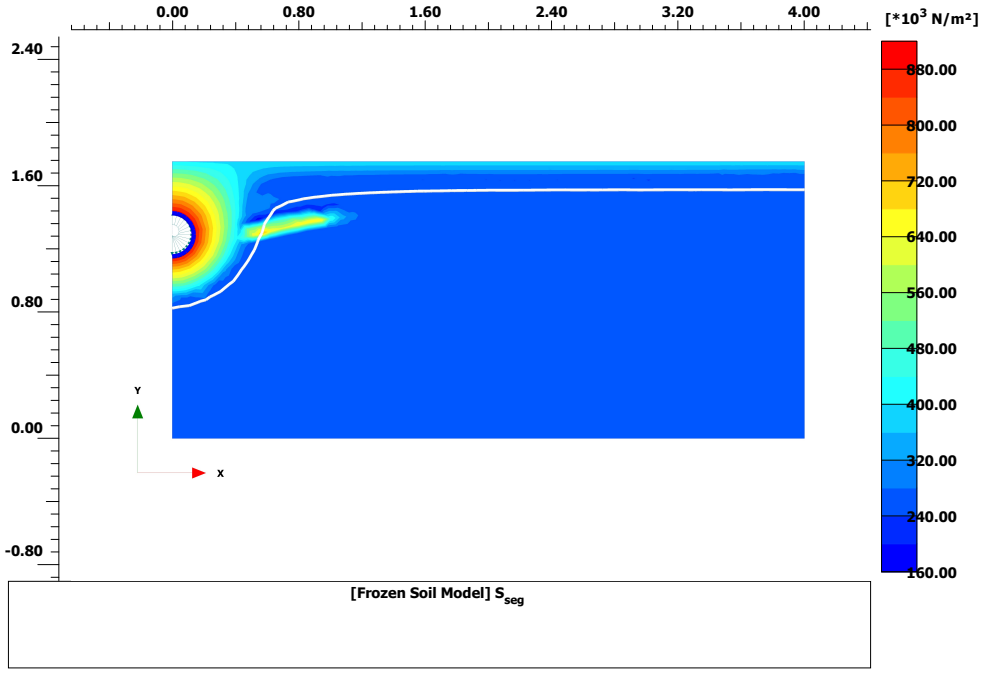

Figure B.17: Segregation threshold distribution in “1st time effect” stage

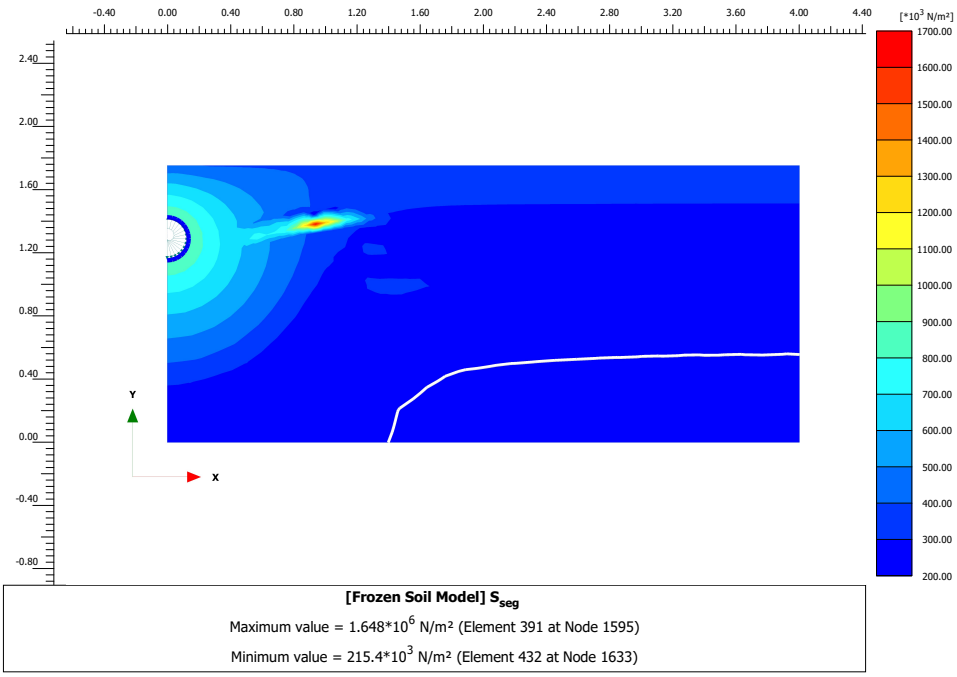

Figure B.18: Segregation threshold distribution in “3rd time effect” stage

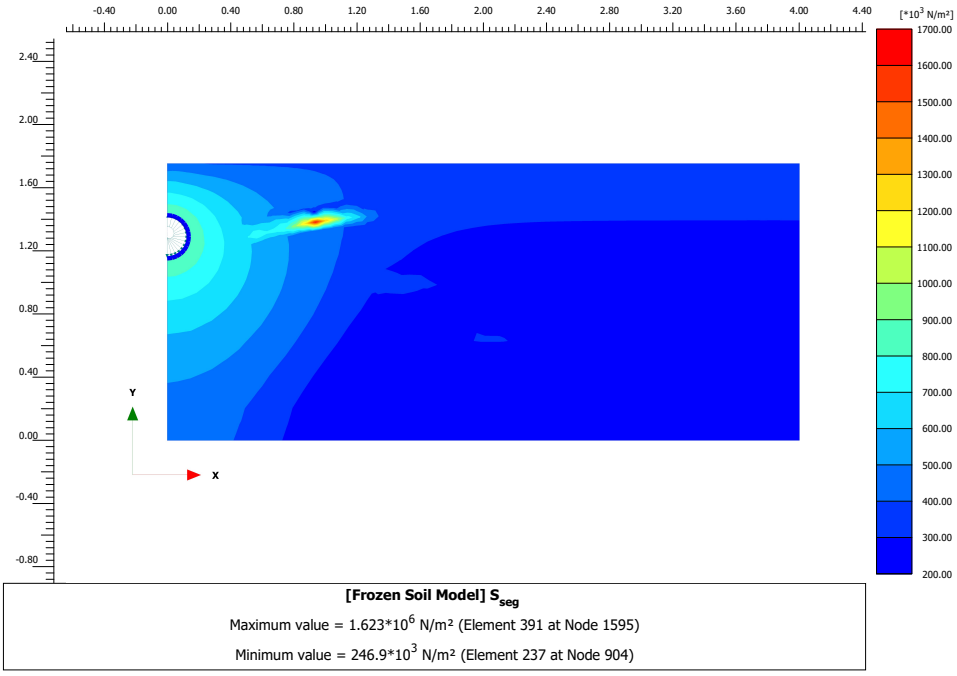

Figure B.19: Segregation threshold distribution in “5th time effect” stage

B.6 Unfrozen State Preconsolidation Pressure, p_{y0}

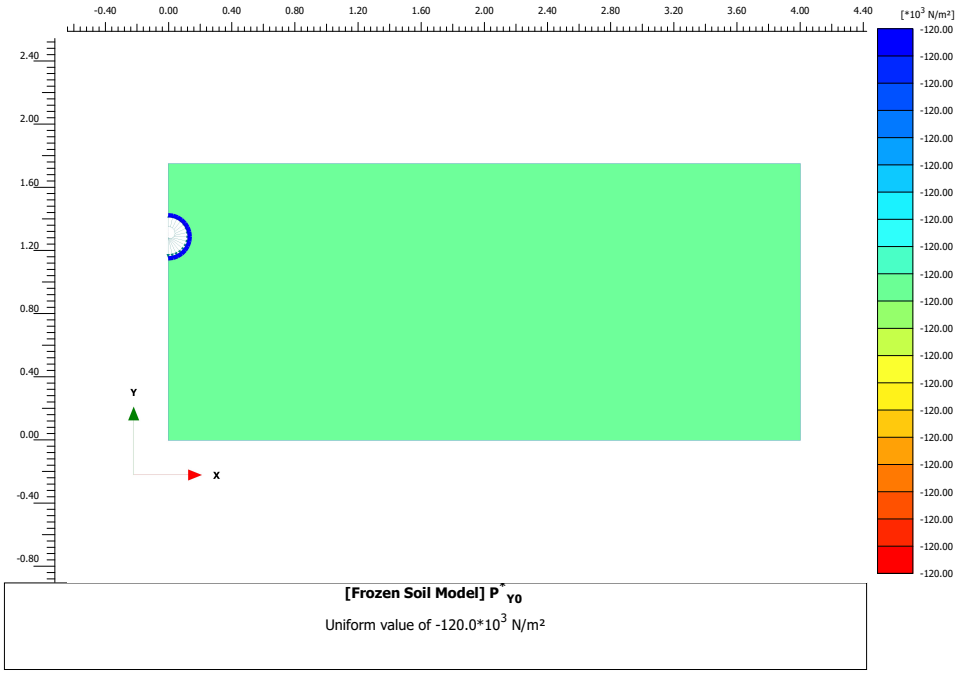

Figure B.20: Unfrozen State Preconsolidation Pressure distribution in “construction” stage

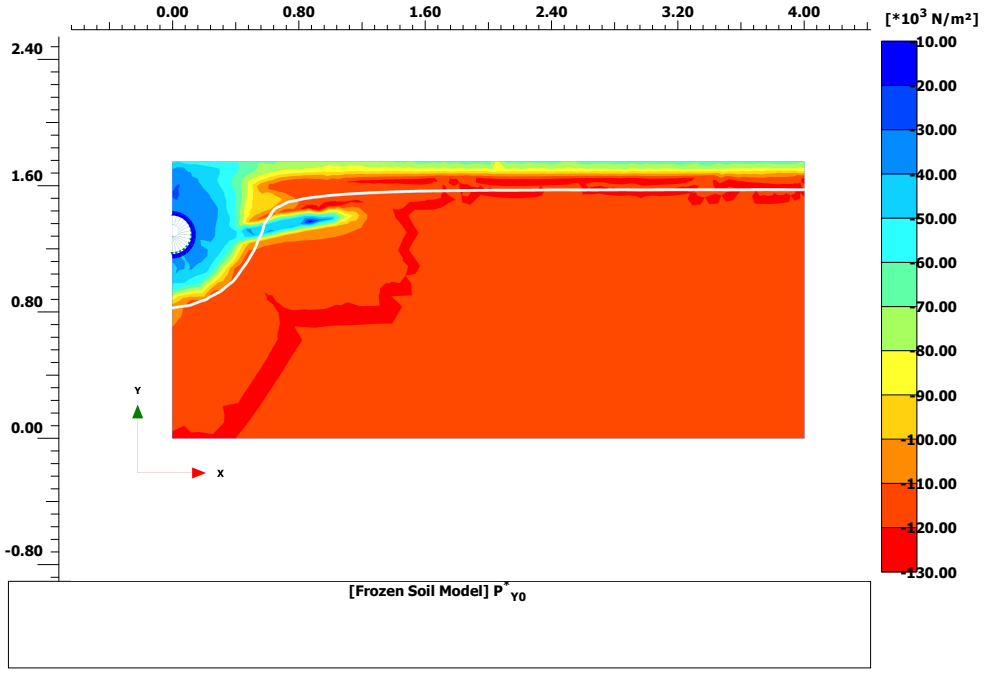

Figure B.21: Unfrozen State Preconsolidation Pressure distribution in “1st time effect” stage

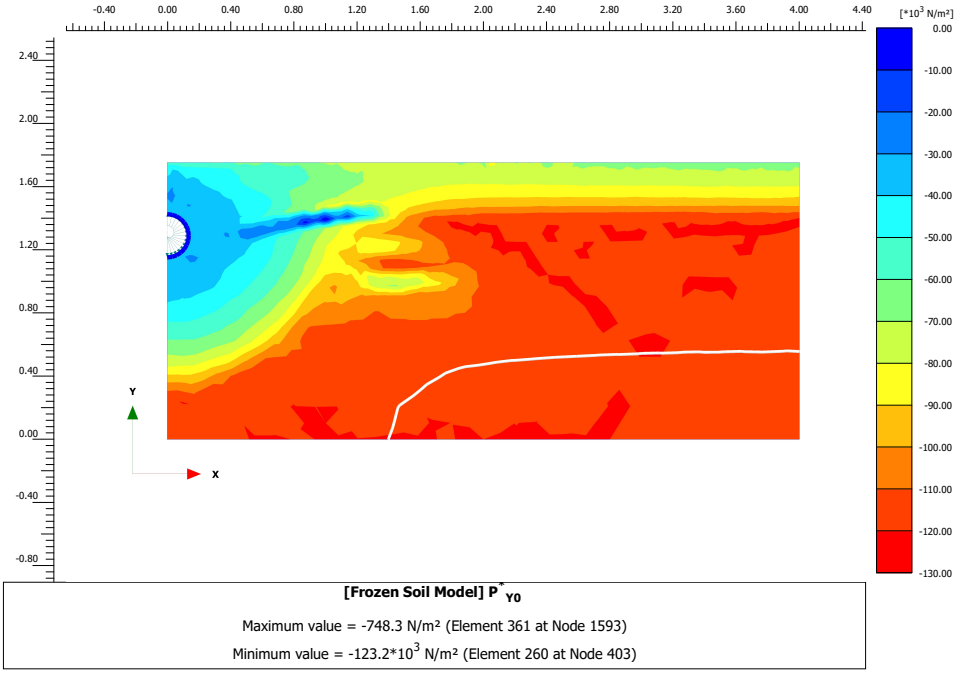

Figure B.22: Unfrozen State Preconsolidation Pressure in “3rd time effect” stage

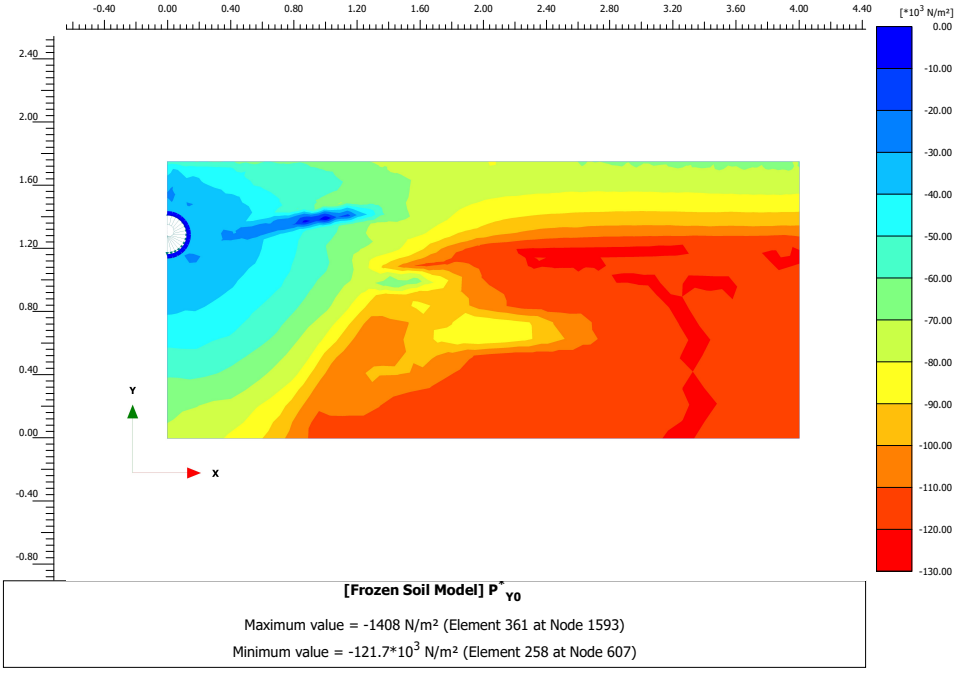

Figure B.23: Unfrozen State Preconsolidation Pressure distribution distribution in “5th time effect” stage

B.7 Ground Water Flow

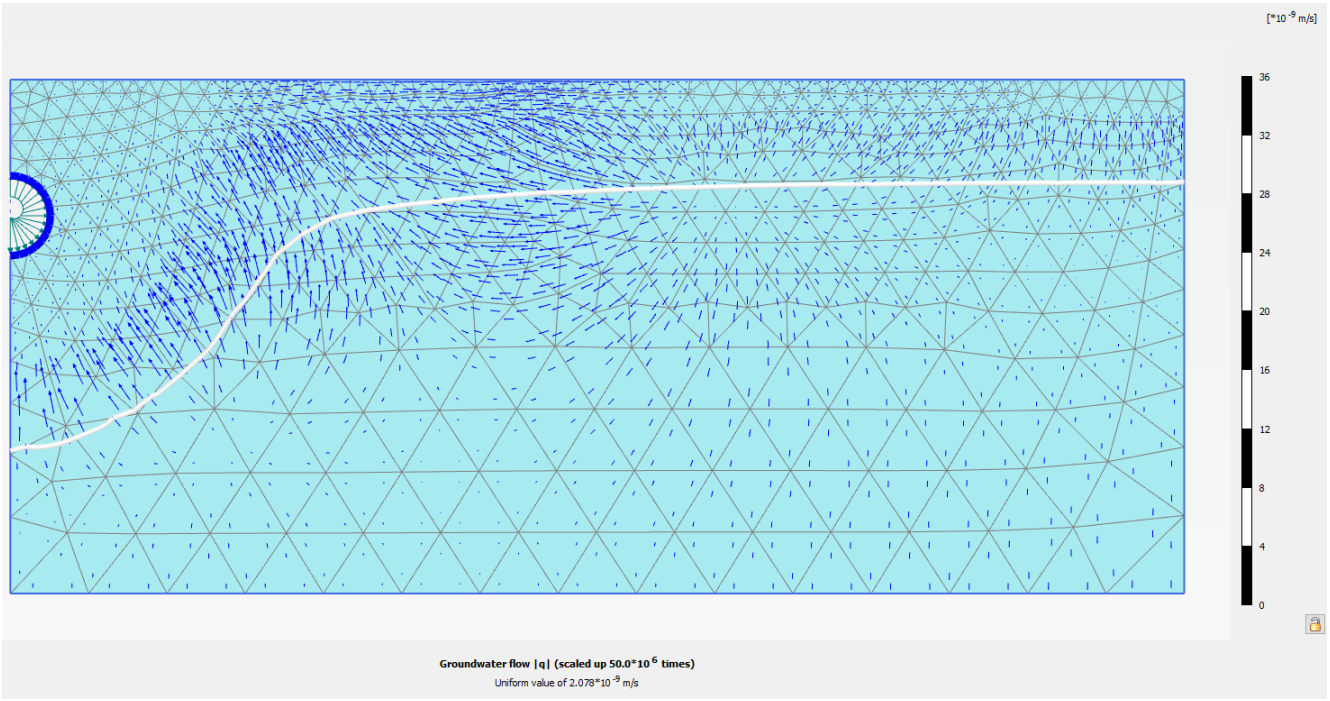

Figure B.24: Ground water flow in “2nd time effect” stage

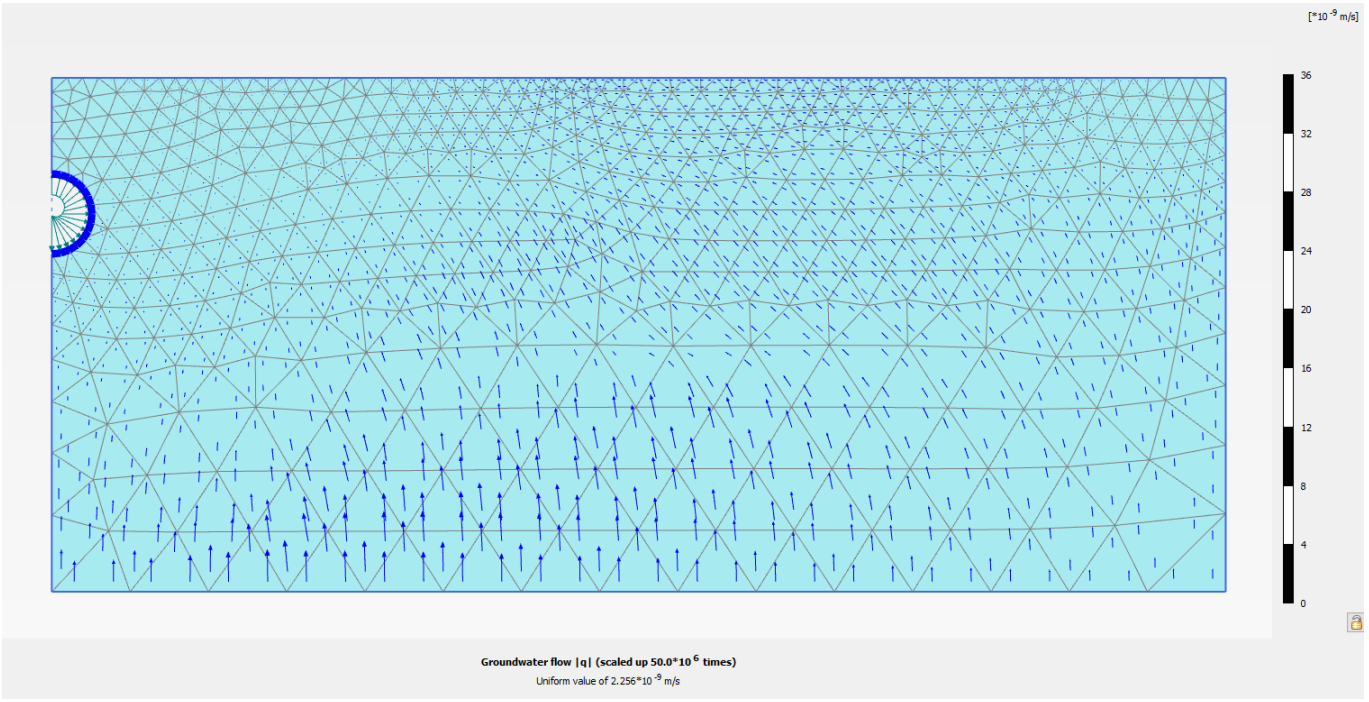

Figure B.25: Ground water flow in “4th time effect” stage

Bibliography

Alonso, E. E., Gens, A., and Josa, A. (1990). A constitutive model for partially saturated soils. *Géotechnique*, 40(3):405–430.

Andersland, O. and Ladanyi, B. (2004). *Frozen Ground Engineering*. Wiley.

Arenson, L. U. and Springman, S. M. (2005). Mathematical descriptions for the behaviour of ice-rich frozen soils at temperatures close to 0 °C. *Canadian Geotechnical Journal*, 42(2):431–442.

Aukenthaler, M. (2016). *The Frozen Unfrozen Barcelona Basic Model; A verification and validation of a new constitutive mode*. Msc thesis, Delft University of Technology.

Bekele, Y. (2016). *Isogeometric Analysis of Coupled Problems in Porous Media*. Phd thesis, Norwegian University of Science and Technology.

Boeckli, L., Brenning, A., Gruber, S., and Noetzli, J. (2012). Permafrost distribution in the european alps: calculation and evaluation of an index map and summary statistics. *The Cryosphere*, 6(4):807–820.

Bragg, R. A. and Andersland, O. B. (1981). Strain rate, temperature, and sample size effects on compression and tensile properties of frozen sand. *Engineering Geology*, 18(1):35–46.

Brinkgreve, R., Kumarswamy, S., and Swolfs, W. (2017). Plaxis 2D manual. Technical report.

Brown, J., Ferrians, O., Heginbottom, J., and Melnikov, E. (1997). International permafrost association circum-arctic map of permafrost and ground ice conditions, scale 1: 10,000,000, circum-pacific map series, no. *Map CP-45.(Digital version available:< http://www. geodata. soton. ac. uk/ipa/>)*.

Burt, T. P. and Williams, P. J. (1976). Hydraulic conductivity in frozen soils. *Earth Surface Processes*, 1(4):349–360.

Carlson, L. (1994). Database report for the caen frost heave test facility. Technical report.

Chamberlain, E., Groves, C., and Perham, R. (1972). The mechanical behaviour of frozen earth materials under high pressure triaxial test conditions. *Géotechnique*, 22(3):469–483.

Crosta, G. B., Chen, H., and Lee, C. F. (2004). Replay of the 1987 val pola landslide, italian alps. *Geomorphology*, 60(1–2):127–146.

Dallimore, S. (1985). *Observations and predictions of frost heave around a chilled pipeline*. Msc thesis, Carleton University.

DiMillio, A. (1999). A quarter century of geotechnical research.

Dore, G. and Zubeck, H. (2008). *Cold Regions Pavement Engineering*. CMcGraw-Hill Education.

Dudeja, D. (2011). *Thaw Weakening*, pages 1155–1156. Springer Netherlands, Dordrecht.

Ghoreishian Amiri, S., Grimstad, G., and Kadivar, M. (2016a). An elastic-viscoplastic model for saturated frozen soils. *European Journal of Environmental and Civil Engineering*, pages 1–17.

Ghoreishian Amiri, S. A., Grimstad, G., Aukenthaler, M., Panagoulias, S., Brinkgreve, R., and Haxaire, A. (2016b). Frozen and unfrozen soil model. Technical report.

Ghoreishian Amiri, S. A., Grimstad, G., Kadivar, M., and Nordal, S. (2016c). Constitutive model for rate-independent behavior of saturated frozen soils. *Canadian Geotechnical Journal*, 53(10):1646–1657.

Gisnås, K., Etzelmüller, B., Lussana, C., Hjort, J., Sannel, A. B. K., Isaksen, K., Westermann, S., Kuhry, P., Christiansen, H. H., Frampton, A., and Åkerman, J. Permafrost map for norway, sweden and finland. *Permafrost and Periglacial Processes*, pages n/a–n/a.

Harris, C. (2005). *Climate Change, Mountain Permafrost Degradation and Geotechnical Hazard*, pages 215–224. Springer Netherlands, Dordrecht.

Ladanyi, B. (1972). An engineering theory of creep of frozen soils. *Canadian Geotechnical Journal*, 9(1):63–80.

Lai, Y., Li, S., Qi, J., Gao, Z., and Chang, X. (2008). Strength distributions of warm frozen clay and its stochastic damage constitutive model. *Cold Regions Science and Technology*, 53(2):200–215.

Li, N., Chen, F., Xu, B., and Swoboda, G. (2008). Theoretical modeling framework for an unsaturated freezing soil. *Cold Regions Science and Technology*, 54(1):19–35.

Nicolsky, D. J., Romanovsky, V. E., Tipenko, G. S., and Walker, D. A. (2008). Modeling biogeophysical interactions in nonsorted circles in the low arctic. *Journal of Geophysical Research: Biogeosciences*, 113(G3):n/a–n/a.

Nishimura, S., Gens, A., Olivella, S., and Jardine, R. J. (2009). Thm-coupled finite element analysis of frozen soil: formulation and application. *Géotechnique*, 59(3):159–171.

Nixon, J. F. (1991). Discrete ice lens theory for frost heave in soils. *Canadian Geotechnical Journal*, 28(6):843–859.

Noetzli, J., Hoelze, M., and HabeAEBERLI, W. (2003). Mountain permafrost and recent alpine rock-fall events: a gis-based approach to determine critical factors. pages 827–832.

Nordal, S. (2016). *Geotechnical Engieering, Advanced Course [Class Handout]*. Geotechnical division, NTNU.

Parameswaran, V. and Jones, S. (1981). Triaxial testing of frozen sand. *Journal of Glaciology*, 27(95):147-155.

Peppin, S. S. L. and Style, R. W. (2013). The physics of frost heave and ice-lens growth. *Vadose Zone Journal*, 12(1).

Petrovic, J. J. (2003). Review mechanical properties of ice and snow. *Journal of Materials Science*, 38(1):1–6.

Selvadurai, A. P. S., Hu, J., and Konuk, I. (1999). Computational modelling of frost heave induced soil–pipeline interaction: II. modelling of experiments at the caen test facility. *Cold Regions Science and Technology*, 29(3):229–257.

Selvadurai, A. P. S. and Suvorov, A. P. (2016). *Thermo-Poroelasticity and Geomechanics*. Cambridge University Press.

Sinitsyn, A. O. and Løset, S. (2011). Strength of frozen saline silt under triaxial compression with high strain rate. *Soil Mechanics and Foundation Engineering*, 48(5):196–202.

Smith, M. W. and Patterson, D. E. (1989). Detailed observations on the nature of frost heaving at a field scale. *Canadian Geotechnical Journal*, 26(2):306–312.

Taber, S. (1929). Frost heaving. *Journal of Geology*, 37(5):428–461.

Taber, S. (1930). The mechanics of frost heaving. *Journal of Geology*, 38(4):303–317.

Thomas, H. R., Cleall, P., Li, Y.-C., Harris, C., and Kern-Luetschg, M. (2009). Modelling of cryogenic processes in permafrost and seasonally frozen soils. *Géotechnique*, 59(3):173–184.

Tin, T., Sovacool, B. K., Blake, D., Magill, P., El Naggar, S., Lidstrom, S., Ishizawa, K., and Berte, J. (2010). Energy efficiency and renewable energy under extreme conditions: Case studies from antarctica. *Renewable Energy*, 35(8):1715–1723.

Wettlaufer, J. and M. Grae Worster, M. (2006). Premelting dynamics. *Annual Review of Fluid Mechanics*, 38:427–452.

Williams, P. J., Riseborough, D. W., and Smith, M. W. The france-canada joint study of deformation of an experimental pipe line by differential frost heave.

Williams, P. J., Riseborough, D. W., and Smith, M. W. (1993). The france-canada joint study of deformation of an experimental pipe line by differential frost heave. *International Journal of Offshore and Polar Engineering*, 3(1):56–60.

Xie, Q., Zhu, Z., and Kang, G. (2014). Dynamic stress–strain behavior of frozen soil: Experiments and modeling. *Cold Regions Science and Technology*, 106–107:153–160.

Xie, S.-b., Jian-jun, Q., Yuan-ming, L., Zhi-wei, Z., and Xiang-tian, X. (2015). Effects of freeze-thaw cycles on soil mechanical and physical properties in the qinghai-tibet plateau. *Journal of Mountain Science*, 12(4):999–1009.

Yamamoto, Y. and Springman, S. M. (2014). Axial compression stress path tests on artificial frozen soil samples in a triaxial device at temperatures just below 0 °C. *Canadian Geotechnical Journal*, 51(10):1178–1195.

Yoshikawa, K. and Overduin, P. P. (2005). Comparing unfrozen water content measurements of frozen soil using recently developed commercial sensors. *Cold Regions Science and Technology*, 42(3):250–256.

Youssef, H. (1986). Mechanical properties and behaviour of frozen soils. page 299-322.

Yuanming, L., Yugui, Y., Xiaoxiao, C., and Shuangyang, L. (2010). Strength criterion and elastoplastic constitutive model of frozen silt in generalized plastic mechanics. *International Journal of Plasticity*, 26(10):1461–1484.

Zhang, T., Barry, R., Knowles, K., Ling, F., and Armstrong, R. (2003). Distribution of seasonally and perennially frozen ground in the northern hemisphere. pages 1289–1294.

Zhang, Y. and Michalowski, R. L. (2015). Thermal-hydro-mechanical analysis of frost heave and thaw settlement. *Journal of Geotechnical and Geoenvironmental Engineering*, 141(7).

Zhang, Z. X. and Kushwaha, R. L. (1998). Modeling soil freeze-thaw and ice effect on canal bank. *Canadian Geotechnical Journal*, 35(4):655–665.

Zhou, M. (2014). *Computational simulation of freezing: Multiphase modeling and strength upscaling*. Phd thesis, Ruhr University Bochum.

Zhu, Z., Ning, J., and Ma, W. (2010). A constitutive model of frozen soil with damage and numerical simulation for the coupled problem. *Science China Physics, Mechanics and Astronomy*, 53(4):699–711.

Zienkiewicz, O., Taylor, R., and Zhu, J. (2005). *The Finite Element Method: Its Basis and Fundamentals*. Elsevier Science.